STRUCTURAL BIOLOGY

ISSN 2059-7983

Received 18 September 2018
Accepted 12 December 2018

Edited by V. T. Forsyth, Institut Laue–Langevin, France, and Keele University, UK

Keywords: neutron scattering; biological systems; structure and dynamics

Neutron scattering in the biological sciences: progress and prospects

Rana Ashkar,[a] Hassina Z. Bilheux,[b] Heliosa Bordallo,[c] Robert Briber,[d] David J. E. Callaway,[e] Xiaolin Cheng,[f] Xiang-Qiang Chu,[g] Joseph E. Curtis,[h] Mark Dadmun,[i] Paul Fenimore,[j] David Fushman,[k] Frank Gabel,[l] Kushol Gupta,[m] Frederick Herberle,[b] Frank Heinrich,[h,n] Liang Hong,[o] John Katsaras,[p,q] Zvi Kelman,[r] Eugenia Kharlampieva,[s] Gerald R. Kneller,[t] Andrey Kovalevsky,[u] Susan Krueger,[h] Paul Langan,[b] Raquel Lieberman,[v] Yun Liu,[h] Mathias Losche,[n] Edward Lyman,[w] Yimin Mao,[h] John Marino,[r] Carla Mattos,[x] Flora Meilleur,[b,y] Peter Moody,[z] Jonathan D. Nickels,[aa] William B. O'Dell,[r] Hugh O'Neill,[b] Ursula Perez-Salas,[bb] Judith Peters,[cc] Loukas Petridis,[dd] Alexei P. Sokolov,[i] Christopher Stanley,[b] Norman Wagner,[ee] Michael Weinrich,[h] Kevin Weiss,[b] Troy Wymore,[gg] Yang Zhang[hh] and Jeremy C. Smith[ff]*

[a]Department of Physics, Virginia Polytechnic Institute and State University, 850 West Campus Drive, Blacksburg, VA 24061, USA, [b]Neutron Sciences Directorate, Oak Ridge National Laboratory, 1 Bethel Valley Road, Oak Ridge, TN 37831, USA, [c]Niels Bohr Institute, 2100 Copenhagen, Denmark, [d]Materials Science and Engineeering, University of Maryland, 1109 Chemical and Nuclear Engineering Building, College Park, MD 20742, USA, [e]Department of Chemistry and Biochemistry, The City College of New York, 160 Convent Avenue, New York, NY 10031, USA, [f]Department of Medicinal Chemistry and Pharmacognosy, Ohio State University College of Pharmacy, 642 Riffe Building, Columbus, OH 43210, USA, [g]Graduate School of China Academy of Engineering Physics, Beijing, 100193, People's Republic of China, [h]NIST Center for Neutron Research, National Institutes of Standard and Technology, 100 Bureau Drive, Mail Stop 6102, Gaithersburg, MD 20899, USA, [i]Department of Chemistry, University of Tennessee Knoxville, Knoxville, TN 37996, USA, [j]Los Alamos National Laboratory, Los Alamos, NM 87545, USA, [k]Department of Chemistry and Biochemistry, Center for Biomolecular Structure and Organization, University of Maryland, College Park, MD 20742, USA, [l]Institut Laue–Langevin, Université Grenoble Alpes, CEA, CNRS, IBS, 38042 Grenoble, France, [m]Department of Biochemistry and Biophysics, Perelman School of Medicine at the University of Pennsylvania, Philadelphia, PA 19104, USA, [n]Department of Physics, Carnegie Mellon University, Pittsburgh, Pennsylvania, USA, [o]Department of Physics and Astronomy, Institute of Natural Sciences, Shanghai Jiao Tong University, Shanghai 200240, People's Republic of China, [p]Neutron Scattering Science Division, Oak Ridge National Laboratory, Oak Ridge, TN 37831, USA, [q]Canadian Neutron Beam Centre, National Research Council, Chalk River, Ontario, Canada, [r]Institute for Bioscience and Biotechnology Research, National Institute of Standards and Technology and the University of Maryland, Rockville, MD 20850, USA, [s]Department of Chemistry, University of Alabama at Birmingham, 901 14th Street South, Birmingham, AL 35294, USA, [t]Centre de Biophysique Moléculaire, CNRS, Université d'Orléans, Chateau de la Source, Avenue du Parc Floral, Orléans, France, [u]Biology and Soft Matter Division, Oak Ridge National Laboratory, Oak Ridge, TN 37831, USA, [v]School of Chemistry and Biochemistry, Georgia Institute of Technology, Atlanta, Georgia, USA, [w]Department of Physics and Astrophysics, University of Delaware, Newark, DE 19716, USA, [x]Department of Chemistry and Chemical Biology, Northeastern University, Boston, Massachusetts, USA, [y]Department of Molecular and Structural Biochemistry, North Carolina State University, Raleigh, NC 27695, USA, [z]Leicester Institute of Structural and Chemical Biology, Department of Molecular and Cell Biology, University of Leicester, Leicester LE1 9HN, England, [aa]Department of Chemical and Environmental Engineering, University of Cincinnati, Cincinnati, OH 45221, USA, [bb]University of Illinois Chicago, Chicago, Illinois, USA, [cc]Institut Laue–Langevin, Université Grenoble Alpes, LiPhy, Grenoble, France, [dd]UT/ORNL Center for Molecular Biophysics, Oak Ridge National Laboratory Biosciences Division, 1 Bethel Valley Road, Oak Ridge, TN 37831, USA, [ee]Center for Neutron Science, Department of Chemical and Biomolecular Engineering, University of Delaware, Newark, DE 19716, USA, [ff]Department of Biochemistry, Cellular and Molecular Biology, University of Tennessee Knoxville, Knoxville, TN 37996, USA, [gg]Department of Chemistry, University of Michigan, Ann Arbor, MI 48109, USA, and [hh]Department of Nuclear, Plasma and Radiological Engineering, Department of Materials Science and Engineering, Department of Electrical and Computer Engineering, Beckman Institute for Advanced Science and Technology, University of Illinois at Urbana-Champaign, Urbana, IL 61801, USA. *Correspondence e-mail: smithjc@ornl.gov

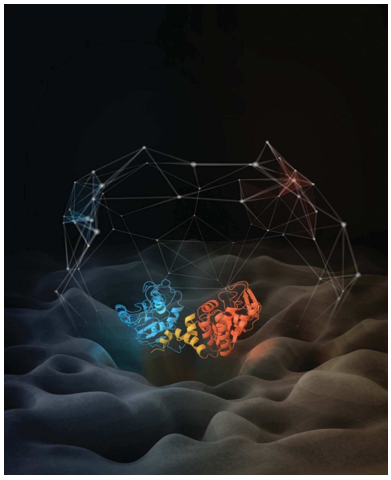

The scattering of neutrons can be used to provide information on the structure and dynamics of biological systems on multiple length and time scales. Pursuant to a National Science Foundation-funded workshop in February 2018, recent developments in this field are reviewed here, as well as future prospects that can be expected given recent advances in sources, instrumentation and computational power and methods. Crystallography, solution scattering, dynamics, membranes, labeling and imaging are examined. For the extraction of maximum information, the incorporation of judicious specific deuterium labeling, the integration of several types of experiment, and interpretation using high-performance computer simulation models are often found to be particularly powerful.

1. Introduction

Gaining a predictive understanding of the behavior of complex biological systems is one of the greatest scientific challenges that we will face over the next decades (Alberts, 2011). This involves determining the assembly and the function of, and the cooperation between, system components, which are often hierarchical biological complexes, in three dimensions and as a function of time. These processes are governed by known physical laws, but constitute a poorly understood branch of complex systems science. The required information must be derived through characterizing the structural biology of the component molecules, how they interact with each other, how these interactions affect the properties of the individual molecules and how these interactions change in space and time.

These are exciting times for structural biology research, with the availability of an expanding armory of powerful experimental tools that allow the characterization of the structure and dynamics of biological molecules and their complexes over increasing ranges of length and time. Clearly, no single experimental method covers the ranges of length and time scales that are required to address all crucial problems in structural biology. X-ray crystallography and small-angle scattering, nuclear magnetic resonance (NMR) spectroscopy, mass spectrometry, fluorescence resonance energy transfer (FRET), electron paramagnetic resonance (EPR) spectroscopy, and two-dimensional and three-dimensional electron microscopy (EM) are examples of common techniques that provide essential structural and dynamic information on biological materials and processes. At the same time, these techniques have important limitations and therefore there is a need to combine them in order to provide the information needed to understand complex biological systems.

Recent worldwide research and development activities have sown the seeds for the deepened application of neutron scattering as a tool in biological research that provides elusive, unique information about complex biological systems that is unobtainable using the tools listed above. With no charge, neutrons cause little radiation damage and are highly penetrating, enabling the use of complex sample environments. Neutrons are ideal for studying the multiscale phenomena intrinsic to biological processes: important biological processes occur over broad ranges of length and time scales, and therefore their examination requires the development of an integrated suite of multi-length and multi-time-scale experiments, all welded to computational methods. Crystallography, small-angle scattering, diffraction, reflectometry and imaging beamlines are ideal for studying the structure of biological matter on atomic to micrometre length scales (and, for imaging, beyond). Moreover, neutrons have energies similar to atomic motions, and therefore, uniquely, neutron spectroscopic beamlines characterize self and collective motions on subpicosecond to microsecond time scales. Neutrons also permit time-resolved studies of kinetic pathways, disordered structure and flexibility, correlated motions and local dynamics, membrane structure and dynamics, and their associated processes.

A particularly desirable property of neutrons for biology has to do with hydrogen (H), which is the most abundant element in biological systems. Photons and electrons interact with the atomic electric field. With just one electron, hydrogen is at the limit of visibility to X-rays. Neutrons, on the other hand, interact with nuclei, and protons have a relatively strong and negative scattering length (Sears, 1992). The isotope deuterium (D) has an even stronger scattering length, which is positive. This different sensitivity of neutrons to hydrogen and deuterium allows an enhanced visibility of specific parts of complex biological systems through isotopic substitution. These properties are the foundation by which neutron scattering can be used to obtain precise information on the location and dynamics of hydrogen at the atomic level, as well as truly unique information on large, dynamic, multi-domain complexes on longer length and time scales. The use of contrast matching and variation through careful deuteration and labeling is crucial to reveal the structure of intricate and multi-component complexes. Neutron techniques are most effective with well controlled deuteration of samples, and thus infrastructure that offers methods to deliver the deuteration and labeling of materials is an essential component of neutron work.

The application of neutrons to biology has traditionally focused on studying the structure and dynamics of relatively small well known proteins, model membrane systems and simple binary complexes. Recently, however, more complex biological systems have been examined. This has been made possible owing to significant progress by researchers from across the world in bridging technical gaps, not only in neutron scattering instrumentation but also in molecular and cell biology, in deuterium labeling and in computational technologies. Together with increased neutron flux on the available beamlines, the development of innovative techniques for polarizing neutron beams and H atoms in samples has enhanced scattering power. It is now possible to dynamically control scattering contrast, and this, coupled with the development of new instrumentation, allows simultaneous access to broad regions of time and space. There has also been better integration of high-performance computing techniques with neutron scattering experiments, and computational tools are being developed that allow the combination of experimental data from multiple complementary techniques to generate more complete models of complex biological systems.

Recent progress in this area has also benefited from the shared expertise and resources arising from the co-location of neutron sources throughout the world with other types of synergistic advanced user research facilities. Examples include the co-location of the ISIS Neutron and Muon Source with the Diamond Light Source in the UK, the Institut Laue–Langevin (ILL) reactor neutron source with the European Synchrotron Radiation Facility (ESRF) in Grenoble, France, the Japan Proton Accelerator Research Complex (J-PARC) spallation neutron source with the Japan Atomic Energy Research Institute (JAERI) reactor neutron source in Tokai-mura, Japan, and the MAX-IV synchrotron-radiation source with the future European Spallation Source (ESS) in Lund,

Sweden. US involvement in developing new approaches in this effort has been greatly facilitated by the co-location of the High Flux Isotope Reactor (HFIR) reactor neutron source and the Spallation Neutron Source (SNS) with the Oak Ridge Leadership Computing Facility (OLCF) high-performance computer user facility and associated expertise at Oak Ridge National Laboratory (ORNL).

Coupling supercomputing to neutron measurements provides pathways to develop crucial complementary techniques that are needed to understand and analyze neutron scattering results. Spanning the accessible time and length scales of neutron techniques (such as from crystallography to USANS or from vibrational spectroscopy to spin echo) requires petaflop and exaflop machines. Particularly when allied with high-performance computing, neutrons provide unique information for the biological sciences, key to which is their sensitivity to the position and dynamics of protons.

A few examples of classic historical papers on neutron scattering in biology include the determination of the catalytic base in trypsin (Kossiakoff & Spencer, 1980), the determination of the structure of cellulose (Nishiyama *et al.*, 2002), the measurement of protein hydration shells in solution (Svergun *et al.*, 1998), the discovery of a dynamical transition in a protein (Doster *et al.*, 1989) and the measurement of the softness of a protein (Zaccai, 2000). The present article, which stems from a workshop of 43 scientists that was held in Alexandria, Virginia on 22–25 February 2018, sponsored by the National Science Foundation (NSF), summarizes more recent advances, many of which have not been around long enough for their impact to be fully appreciated. We also discuss the prospects of neutron scattering in the biological sciences and, furthermore, the article also serves as an introduction for researchers curious as to whether neutron scattering can, or should, play a role in their present or future studies.

The workshop was divided into breakout groups on crystallography, dynamics, solution structures, membranes and labeling/imaging, and these groups report here separately on their themes in heterogeneous styles. Although such a broad remit can never be comprehensive, we discuss many significant steps that have recently been taken and ideas for the future.

2. Crystallography

2.1. Overview

H atoms are central to enzyme chemistry as, ultimately, reaction rates and chemistry are dependent upon coordinated changes in the local electrostatics, hydrogen-bonding interactions and protonation states of catalytic residues along the reaction coordinate. Therefore, understanding enzyme chemistry at the atomic level requires the visualization of H atoms in active sites, cofactors, substrates, water molecules and remote residues. This information, although decisive for deriving many biological mechanisms, is challenging to obtain.

X-ray crystallography is currently still the primary tool in structural biology, although the resulting structures represent only a small fraction of existing proteins. These structures tend to be of relatively small proteins or their complexes. Currently, there are about 146 000 X-ray crystal structures of proteins in the Protein Data Bank (PDB). However, H atoms are exceedingly difficult to locate in X-ray structures, and cryo-EM has not yet reached the required resolution.

Hydrogen positions are often inferred from the positions of other atoms derived by X-ray crystallography, and hydrogens bound to carbon, in particular, can sometimes be placed. However, this is often not the case in the biologically active sites of macromolecules, where the presence and position of hydrogen is crucial to the enzymatic mechanism. The pK_a of any ionizable group can be significantly influenced by the local electrostatic field generated at the site by the protein. When X-ray crystallographic data are available to ultrahigh resolution, some H atoms may be visible or their positions may be inferred from precise geometrical parameter analyses (Neumann & Tittmann, 2014), and the combination of atomic-resolution X-ray crystallographic data with quantum-chemical or charge-density analysis can then provide a further level of detail on the chemical profile of the enzyme (Jelsch *et al.*, 2000; Liebschner *et al.*, 2009; Zarychta *et al.*, 2015). However, even when such ultrahigh-resolution data can be obtained, a significant fraction (typically >50%) of more mobile or labile H atoms remain difficult to discern, leaving specific questions concerning catalytic mechanisms unanswered.

The difficulty of locating H atoms using X-ray crystallography can be circumvented by neutron protein crystallography (Schröder *et al.*, 2018; Meilleur, Myles *et al.*, 2006; Blakeley, 2009). This is because whereas X-rays scatter from electrons, neutrons scatter from nuclei, with the result that the coherent neutron scattering lengths of hydrogen (H) and the hydrogen isotope deuterium (D) are similar in magnitude to those of carbon (C), nitrogen (N) and oxygen (O) (Fig. 1; Sears, 1992). A complication of neutron protein crystallography is that the scattering length of hydrogen is negative, whereas those of C, N and O are positive, which gives rise to density cancelation in lower resolution Fourier maps that can hamper interpretation and analysis. In contrast, deuterium has a positive neutron scattering length and thus gives a clear positive peak in nuclear density maps. While the visibility of H atoms requires neutron crystallographic data at a resolution of

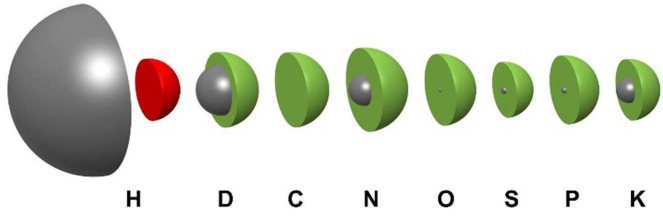

Figure 1
Incoherent neutron scattering cross-sections and coherent neutron scattering lengths for selected elements. Relative incoherent scattering cross-sections are represented by the left hemispheres and relative coherent scattering lengths are represented by the right hemispheres. The red hemisphere for hydrogen indicates the negative sign of its scattering length, while the others shown in green are positive. Incoherent cross-sections and coherent scattering lengths are not represented on the same scale. Reprinted from O'Dell *et al.* (2016) with permission.

2.0 Å or better, D atoms are readily visible in crystallographic structures identical to their hydrogenated counterparts (Di Costanzo *et al.*, 2007; Fisher & Helliwell, 2008; Hazemann *et al.*, 2005; Meilleur *et al.*, 2005; Artero *et al.*, 2005) at typical resolutions of 2.5 Å or better.

About 140 neutron crystal structures have been solved. This number is very small relative to the X-ray output, and this difference is owing in part to the relatively large crystals that must be grown for neutron work (<0.5 mm^3). However, the number of PDB depositions does not reflect the impact of the technique. The neutron crystal structures of even a few enzymes, showing the protonation states of side chains and water molecules involved in catalysis, have brought out issues and pointed to invalid assumptions that are often made when using X-ray crystal structures to infer catalytic mechanisms. Arguably, neutron crystal structures provide the most detailed data from which to model enzyme reaction mechanisms with quantum-chemical techniques.

The identicality of hydrogenated and deuterated structures has the caveat that the bond distances are slightly different, and this needs to be accounted for in the refinement of the highest resolution neutron macromolecular crystallography (nMX) structures. Overall, there is now a wide range of fields of structural science research in biology, chemistry and biochemistry in which individual nMX structures have resolved issues that have been left unresolved by other probes, such as X-rays, electron microscopy or NMR. This aspect is a vital contribution of neutrons as a probe.

2.2. Hydrogen/deuterium isotopic substitution

The greater magnitude of the coherent scattering length of deuterium (6.671 fm) compared with that of hydrogen (−3.741 fm) results in a larger $\sum|\mathbf{F}|$ and therefore greater average reflection intensities. Simultaneously, the sixfold decrease in the incoherent scattering length of deuterium (3.99 fm) compared with that of hydrogen (25.27 fm) dramatically reduces the isotropic background intensity. The gain in signal and reduction in noise upon perdeuteration allow data sets to be collected from smaller crystals (<0.5 mm^3) or with reduced total exposure times (<10 days) (Hazemann *et al.*, 2005; Munshi *et al.*, 2012; Cuypers *et al.*, 2013; Haupt *et al.*, 2014; Tomanicek *et al.*, 2013; Kita & Morimoto, 2016). Furthermore, the coherent scattering length of deuterium is positive, as are those of common atoms found in proteins, while the coherent scattering length of hydrogen is negative (Fig. 1). At the typical resolutions (1.9–2.3 Å) obtained for neutron protein crystallographic data, deuterium substitution improves the analysis of nuclear density maps by minimizing the number of sites where the negative coherent scattering length of H atoms leads to density cancelation.

2.3. H/D exchange

Bulk solvent, ordered water molecules and H atoms bound to protein O, N or acidic C atoms such as histidine $C^{\varepsilon1}$ (*i.e.* titratable H atoms; Niimura *et al.*, 2003) can all be replaced with deuterium by preparing all reagents in deuterium oxide (D_2O) either during or after complete crystal growth. The majority (>80%) of the neutron protein crystal structures currently deposited in the PDB have been solved from protein samples that have undergone H/D exchange during crystallization or upon complete crystal growth either by soaking in D_2O or via vapor exchange.

Understanding the kinetics of hydrogen exchange in protein structures is itself of fundamental interest (Englander *et al.*, 1996), particularly concerning accessibility and dynamics. H/D exchange is a quantifiable parameter that neutron structures provide by observation of the H/D-exchange level at the backbone amides. The results can be compared with similar quantities derived by NMR, validating the methods, and both are complementary to mass spectrometry.

2.4. Perdeuteration

Titratable H atoms represent approximatively 25% of the total H atoms of any protein. To exchange the remaining 75% attached to C atoms, proteins need to be perdeuterated during synthesis. The expression of perdeuterated proteins in fully deuterium-labeled growth media has yielded less than ∼20% of the PDB depositions of neutron protein crystal structures, but remains the gold standard for the field.

Since essentially all neutron crystallographic work is carried out using D_2O-based solvent buffers, a particular concern for these experiments is the possibility of H_2O back-exchange across reservoir or capillary sealants. This may limit the quality of neutron scattering-length density (SLD) maps and of the associated analysis. Therefore, a systematic method of exploiting infrared spectroscopy for the analysis of back-exchange phenomena in the reservoirs used for crystal growth has been proposed (Yee *et al.*, 2017).

2.5. Crystal growth

The diffracted intensity in Bragg reflections in a single-crystal experiment can be written as

$$I \propto \frac{I_0 \times |F|^2 \times V \times \lambda^2}{v_0^2}, \qquad (1)$$

where I, I_0, $|F|$, V, λ and v_0 are the diffracted intensity, the incident beam intensity, the structure-factor magnitude, the volume of the crystal irradiated by the beam, the incident wavelength and the volume of the unit cell, respectively (Schultz *et al.*, 2005). Neutron beam fluxes are inherently many orders of magnitude weaker than synchrotron X-ray beams (Meilleur, Myles *et al.*, 2006). Therefore, neutron crystallography requires crystals that are at least three orders of magnitude larger than crystals suitable for X-ray crystallography because, as shown in (1), the diffracted intensity is directly proportional to the incident beam intensity. Vapor diffusion using large-volume sitting drops is the most-used setup to grow large crystals. Large crystals suitable for neutron diffraction have also been grown using batch and slow liquid–liquid diffusion methods. The typical crystal volumes needed by researchers for nMX are in the near to 1 mm^3 range. The several interrelated parameters in (1), including crystal

volume, that have been found to be necessary in practice for nMX have been plotted by Blakeley (2009). The different methods that are typically used to grow large crystals have been reviewed by O'Dell *et al.* (2016).

2.6. Instrumentation, data collection and processing

Instrumentation worldwide is optimized for data-collection rates and unit-cell sizes. For example, current instrumentation capabilities at ORNL include the single-crystal diffractometer IMAGINE (Meilleur *et al.*, 2013), which uses the quasi-Laue configuration to optimize the data-collection efficiency, while at the Spallation Neutron Source the time-of-flight macromolecular neutron diffractometer MaNDi can perform crystallography on crystals with large unit cells (up to 250 Å).

Quasi-Laue instruments accept a defined, broad range of incident neutron wavelengths ($\Delta\lambda/\lambda_{mid} \simeq 25$–$60\%$) that greatly increases the number of stimulated reflections at each crystal setting relative to the monochromatic mode (Wilkinson & Lehmann, 1991). The broad-wavelength bandpass is therefore a more effective use of the neutrons available from the reactor source, and the configuration also avoids the need for a monochromatic crystal upstream of the sample that would inevitably have less than 100% reflection efficiency at any selected wavelength. The quasi-Laue technique represents a compromise on the amount of observed incoherent background: it is more than that observed with monochromatic radiation but less than that observed with truly 'white-beam' radiation. While the monochromatic geometry produces data sets of higher quality compared with the quasi-Laue geometry (either for X-rays or neutrons), for neutron protein crystallography the quasi-Laue configuration has the unique advantage of allowing smaller crystals and/or shorter exposure times to be used (Helliwell, 1997).

Within one project, basically identical samples have produced basically identical diffraction resolution limits but with much shorter exposure times at the quasi-Laue instrument. The monochromatic instrument wins, however, with the achieved nMX data completeness. The white-beam Laue data would have poorer data quality than either quasi-Laue or monochromatic data, but this has not so far been implemented for reactor-source nMX (but could be in order to rapidly measure the lower diffraction resolution data to improve nMX Laue data completeness).

Unlike reactor sources, accelerator-driven spallation sources provide neutrons in discrete pulses, and this time structure permits the use of a time-of-flight (TOF) Laue mode for macromolecular diffractometers. A relatively large wavelength range can be accepted by the instrument to maximize the number of stimulated reflections. The detectors record the position, intensity and time of incidence for each scattered neutron from each pulse in a single event mode. The neutron time of flight can then be converted to the corresponding wavelength, and the observed quasi-Laue diffraction pattern can be 'binned' or separated into reflections and background for each incident wavelength. TOF methods therefore provide both the increased number of reflections of the quasi-Laue mode and the reduced background of the monochromatic mode.

Diffraction data from reactor-based instruments can be indexed and integrated using the software packages developed for X-ray crystallography with appropriate modifications to account for the detector geometry of the instrument. The software packages used include *LAUEGEN* (Campbell *et al.*, 1998; Helliwell *et al.*, 1989), *d*TREK* (Pflugrath, 1999; Langan & Greene, 2004) and *DENZO* (Otwinowski & Minor, 1997). Handling the additional TOF information recorded by spallation-source instruments requires the development of dedicated data-reduction packages (Ohhara *et al.*, 2009; Schultz *et al.*, 2014). Unlike monochromatic data, polychromatic data sets (either for X-rays or neutrons) must be wavelength-normalized to account for the spectral shape of the incident beam. The software used to wavelength-normalize data is also adapted from X-ray Laue crystallography software packages (Arzt *et al.*, 1999; Campbell *et al.*, 1998). Data scaling is then performed with routine protein crystallography software such as *SCALEPACK* (Otwinowski & Minor, 1997) or *SCALA* (Winn *et al.*, 2011). New phasing methods are being developed, such as the use of anomalous dispersion to determine the experimental phases of protein crystal structures, providing a new tool for structural biologists (Cuypers *et al.*, 2016).

2.7. Structure refinement

Structure refinement is carried out against neutron data alone or simultaneously against both X-ray and neutron data. The latter protocol, which can be performed using *nCNS* and *PHENIX*, is referred to as joint refinement or X/N refinement (Wlodawer & Hendrickson, 1982). An alternative approach to joint refinement is to refine the positions of the 'heavy atoms' against the X-ray data and to then keep the positions of these atoms fixed while refining the positions of the H and D atoms against the neutron data (Habash *et al.*, 1997, 2000). The number of parameters to be refined for a neutron structure is considerably greater than for an X-ray structure: the number of atoms is nearly doubled and ∼25% of the hydrogen positions require H/D-occupancy refinement. However, typical neutron data sets contain fewer unique reflections than their X-ray counterparts because of their lower completeness and resolution. Refining a model against both X-ray and neutron data significantly increases the data-to-parameter ratio and reduces the risk of 'overfitting' the available data during refinement (Adams *et al.*, 2009). Joint refinement is widely used for neutron structure refinement against data collected from partially deuterated proteins at resolutions of >2.2 Å. At these moderate resolutions, cancelations of neutron density for CH, CH_2 and CH_3 groups may obscure the direct modeling of side chains (Adams *et al.*, 2009; Afonine *et al.*, 2010).

Currently, there are three refinement programs that can refine neutron protein diffraction data: *CNSsolve* (Brünger *et al.*, 1998; Mustyakimov & Langan, 2007), *phenix.refine* (Adams *et al.*, 2009, 2011; Afonine *et al.*, 2010) and *SHELXL* (Sheldrick, 2015; Gruene *et al.*, 2014). The *phenix.refine*

module of the *PHENIX* software package (Adams *et al.*, 2011) is capable of refining X-ray, neutron and joint X-ray/neutron data (Afonine *et al.*, 2010). The familiarity of *phenix.refine* to the crystallographic community has made it the most used package for neutron structure refinement. *Crystallography and NMR System* (*CNS*) was originally developed as an online server to aid structure determination from solution NMR and X-ray crystallographic data (Brunger, 2007; Brünger *et al.*, 1998). A neutron diffraction patch, termed *nCNS*, can be added to *CNS* to perform refinement of neutron or joint X-ray/neutron data with *CNSsolve* (Adams *et al.*, 2009; Mustyakimov & Langan, 2007). *nCNS* has been used for 19 deposited neutron structures. *SHELXL* has been used to refine neutron structures of crambin (Chen *et al.*, 2012), xylose isomerase (Katz *et al.*, 2006; Kovalevsky *et al.*, 2008), dihydrofolate reductase (Bennett *et al.*, 2006) and endothiapepsin (Coates *et al.*, 2001). Recently, Gruene *et al.* (2014) modified *SHELXL* to include specific instructions for neutron macromolecule structure refinement.

2.8. Complementary techniques

Neutron crystallography is complemented by techniques such as X-ray crystallography, NMR, EPR, X-ray absorption spectroscopy, extended X-ray absorption fine structure (EXAFS) and enzyme-kinetics measurements (Table 1). Integrative/hybrid approaches resulting from a combination of several techniques are becoming increasingly important in structural biology. Cryo-EM, which is undergoing exponential development at the moment, is exciting but comes with its own challenges, some of which can be overcome by neutron diffraction techniques. One of the greatest limitations of cryo-EM is that it is difficult to collect data for macromolecules smaller than about 100 kDa. In this sense, cryo-EM and X-ray crystallography are highly complementary techniques. Both can be enhanced by neutron diffraction data, each in their own way.

2.9. Current applications in neutron crystallography

Current applications are summarized in Table 2.

2.9.1. Enzyme chemistry. Neutron protein crystallography is particularly valuable for its ability to decipher the chemistry carried out by enzymes. Although there are a relatively small number of neutron crystal structures, each one has the potential to provide insight into a whole family of proteins. Serine proteases benefited from neutron crystallography in elucidating how the protease catalytic triad worked a long time ago. The N-terminal nucleophile mechanism, as found, for example, in the proteasome, was deduced from the X-ray structure of penicillin acylase, but a neutron crystal structure would have fully revealed the role of water in mediating proton transfer unambiguously (McVey *et al.*, 2001). Another example is the protonation of the γ-phosphate of GppNHp in Ras, which puts in question the protonation states of GTP in all GTPases owing to the conserved nature of the nucleotide-binding pocket in the entire superfamily (Fig. 2).

Table 1
Techniques complementary to neutron crystallography.

Technique	Complementary area
NMR	Protonation-state determination
MS, NMR, solid-state NMR	H/D exchange: dynamics, binding
EPR, single-crystal spectroscopy	Redox chemistry, metal-center oxidation state
QM/MM	Catalytic mechanism
Serial femtosecond crystallography	Redox chemistry, radiation damage

Neutron crystallography provides nondestructive and proton-resolved structures in the assembly and mechanisms of biomolecules, which is further strengthened by combining these results with X-ray studies and quantum-chemical and molecular-dynamics calculations. Examples of studies that have exploited the power of neutrons to provide the direct location of protons or ions include the identification of the Fe^{IV}–OH intermediate species as a reactive intermediate in a heme peroxidase using neutron crystallography, EPR and single-crystal X-ray fluorescence (Kwon *et al.*, 2016), and the location of captured protons in HIV-1 protease before and after a two-proton transfer between the catalytic residues and a bound clinical drug using neutron crystallography (Fig. 3). These latter results were combined with quantum-mechanics/molecular-mechanics (QM/MM) calculations to elucidate the low-pH requirement of this process, as the assembly is only stable when four surface residues are protonated (Gerlits *et al.*, 2016). This demonstrates a long-range electrostatic influence on local proton-transfer processes. Likewise, neutron and X-ray crystallography combined with quantum calculations uncovered previously unknown details of the ligand binding and the catalytic mechanism of a vitamin B_6-dependent aspartate aminotransferase (AAT; Dajnowicz *et al.*, 2017) and

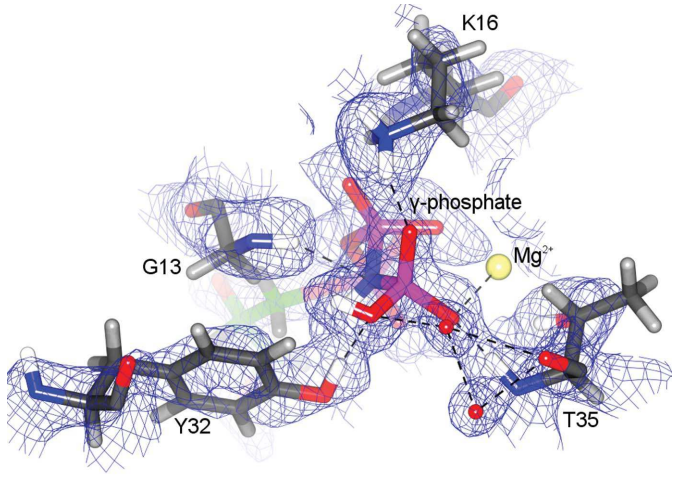

Figure 2
H-Ras in complex with the GTP analog GppNHp (PDB entry 4rsg; Knihtila *et al.*, 2015). Unexpectedly, clear neutron scattering-length density could be observed for a protonated (^{2}H) γ-phosphate in the $2F_o - F_c$ map. The D atoms of the nucleophilic water (hydrogen-bonded to the γ-phosphate and Thr35) are not visible in the density map, suggesting rotational freedom. Ligand C atoms are shown in green. ^{1}H atoms are shown in light gray, while atoms that have undergone exchange to ^{2}H are shown in white. The blue mesh represents a neutron SLD $2F_o - F_c$ map contoured at σ = 1.0. Reproduced from Schröder *et al.* (2018).

Table 2
Current applications of neutron protein crystallography.

Application	Example (2015–2018)
Protonation states to elucidate enzymatic mechanism	Xylose isomerase (Meilleur, Snell *et al.*, 2006), chlorite dismutase (Schaffner *et al.*, 2017), T4 lysozyme (Hiromoto *et al.*, 2017), phosphoactive yellow protein (Yonezawa *et al.*, 2017), RAS (Knihtila *et al.*, 2015), Cel45A (Nakamura *et al.*, 2015), phycocyanobilin:ferredoxin oxidoreductase (Unno *et al.*, 2015)
Protein–ligand interaction/protein–drug complex	Galectin 3C (Manzoni *et al.*, 2018), xylose isomerase (Munshi *et al.*, 2014), PKG (Gerlits *et al.*, 2018), β-lactamase (Langan *et al.*, 2018), trypsin (Schiebel *et al.*, 2017), GCN5-related *N*-acetyltransferase (Kumar *et al.*, 2018), pyridoxal 5′-phosphate enzyme (Dajnowicz *et al.*, 2017), concanavalin A (Gerlits, Coates *et al.*, 2017), MTAN (Banco *et al.*, 2016), farnesyl pyrophosphate synthase (Yokoyama *et al.*, 2015)
Titration (pH studies)	HIV (Gerlits *et al.*, 2016), RAS (Knihtila, 2016), xylanase (Wan *et al.*, 2015)
Hydration and water binding at the active site of enzymes	Carbonic anhydrase (Kovalevsky *et al.*, 2018), RAS (Knihtila *et al.*, 2015), H-FABP (Howard *et al.*, 2016), carbohydrate-binding module (Fisher *et al.*, 2015), hydronium ion identification (Kovalevsky *et al.*, 2011)
Metalloprotein/redox chemistry	Lytic polysaccharide monooxygenase (Bacik *et al.*, 2017; O'Dell *et al.*, 2017), cholesterol oxidase (Golden *et al.*, 2017), ascorbate peroxidase (Kwon *et al.*, 2016), cytochrome *c* peroxidase (Kwon *et al.*, 2016)
Room ('physiological') temperature structures†	HIV (Gerlits, Keen *et al.*, 2017)

† Most neutron crystallographic data are collected at room temperature. Here, we list proteins for which neutron diffraction at room temperature revealed structural artifacts in the cryo X-ray structure owing to the low temperature.

of the role of second-shell residues in the mechanism of lytic polysaccharide monooxygenase (O'Dell *et al.*, 2017; Fig. 4).

2.9.2. Redox enzymes. In marked contrast to X-rays and electrons, which are highly reducing, ionizing radiations, the thermal neutrons (<25 meV, $\lambda > 0.5$ Å) used in structural studies of biological molecules do not cause direct, measurable radiation damage to samples. One very useful consequence of this is that the oxidation states of metal centers or redox cofactors (such as in flavoenzymes) are not altered during neutron crystallographic data collection, so that the protonation, geometric and electronic coordination environments can be correctly assigned to the known redox state of the center (Bodenheimer *et al.*, 2017; O'Dell *et al.*, 2017; Golden *et al.*, 2017; Casadei *et al.*, 2014). The lack of radiation damage also means that neutron crystallography can be used to determine structures at physiological temperatures, avoiding the artifacts that might be induced by the rapid flash-cooling to 100 K usually used for X-ray work (and the eponymously named cryo-EM; Gerlits, Keen *et al.*, 2017; Deacon *et al.*, 1997).

2.9.3. Roles of water. Water, as the universal solvent in which proteins evolved, plays direct roles in protein structure,

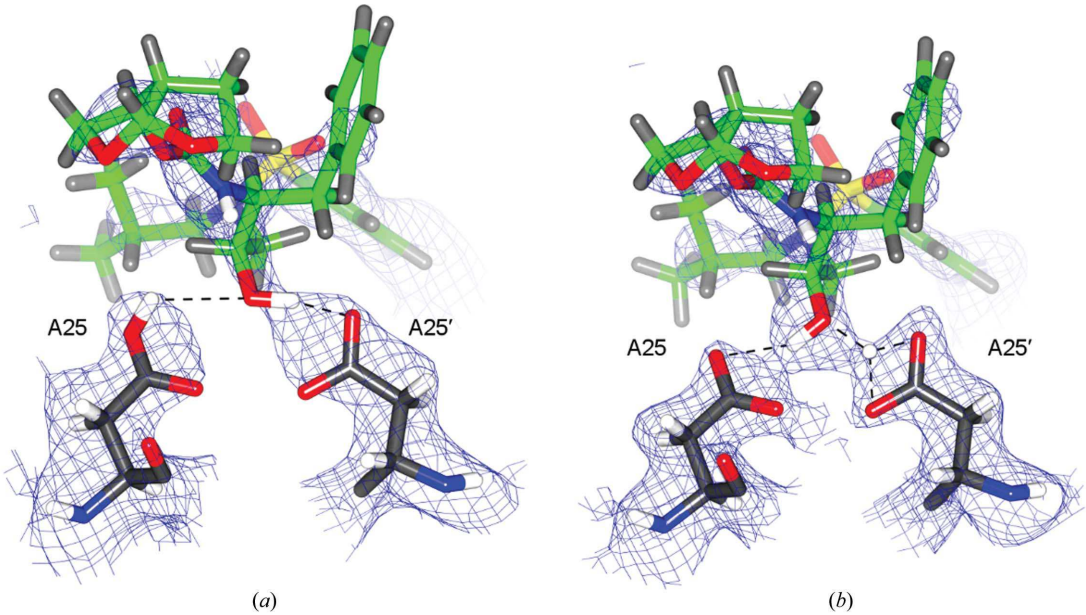

Figure 3
HIV-1 protease in complex with the clinical drug darunavir (PDB entries 5e5j and 5e5k; Gerlits *et al.*, 2016). Upon homodimerization, the catalytic site contains two closely positioned aspartic acid residues. (*a*) At pH 4.3, darunavir accepts a hydrogen bond from Ala25 and donates a hydrogen bond to Ala25′. (*b*) At pH 6.0, the two hydrogens undergo a transfer reaction in the catalytic site, which was captured for the first time by neutron crystallography. C atoms belonging to darunavir are colored green. ^{1}H atoms are shown in light gray, while atoms that have undergone exchange to ^{2}H are shown in white. The blue mesh represents neutron SLD $2F_o - F_c$ maps contoured at $\sigma = 1.0$. Reproduced from Schröder *et al.* (2018).

folding, dynamics and function (Smith *et al.*, 2004). Neutron protein crystallography describes water molecules at the atomic level, including the positions of the H atoms, thus providing correct water orientations. This is information that structural biologists cannot obtain from X-ray crystallography or NMR alone. One of the major problems of computational approaches in predicting how ligands will bind is the placement of water molecules in the binding pockets. Understanding the details of how water molecules interact with the protein and ligands is a major stumbling block that can be overcome by neutron crystallography. Studies of carbonic anhydrase are a good example (Fisher *et al.*, 2010). The thermodynamic consequences of ligand binding are an important aspect of drug design. Displacing an ordered water molecule in a binding pocket upon the binding of a ligand is associated with a favorable entropic change. Thus, neutron crystallography, by revealing both the location and the orientation of water molecules, can inform computational high-throughput screening approaches by revealing the hydrogen-bond network of water molecules present in a ligand-free binding pocket (Aggarwal *et al.*, 2016). Neutrons can also contribute to understanding the thermodynamics of ligand binding in a different way, by determining the vibrational free-energy change upon binding using dynamic neutron scattering (Balog *et al.*, 2004). Neutron crystallographic protein–ligand interaction studies are also important for obtaining the protonation and tautomerization states of the drugs themselves.

Neutron protein crystallography can determine the role of water in enzymatic mechanisms. The basis for calculations relies on guesswork if the positions of H atoms are unknown. The neutron structure of the small GTPase H-Ras illustrates the importance of understanding water dynamics and interactions at the active site of the enzyme (Knihtila *et al.*, 2015). The so-called nucleophilic water molecule at the active site of H-Ras is in a pocket where it can interact with various hydrogen-bonding donor or acceptor atoms. Yet, the D atoms of this crystallographic water molecule cannot be modeled in the neutron structure, suggesting rotational freedom. This information can inform computational chemists and serve as a basis for understanding the reaction mechanism.

Neutron crystallography reveals changes in protonation states in titration studies. Assumptions of side-chain protonation states are generally made based on the pK_a in water, but the pK_a of a side chain in an active site can be shifted considerably by the local environment (Bashford & Karplus, 1990). Only neutron protein crystallography allows their direct observation. Titration can be performed on the same or different crystals for data collection at different pH values. It is also possible to measure the pH of the 100 µl drop in which the crystals are sitting (Gerlits *et al.*, 2016). Furthermore, neutron crystallography allows the visualization of the structure at room temperature, which is more reflective of *in vivo* thermodynamic protonation states than at cryogenic temperatures.

2.9.4. Roles of water: evolutionary aspects. Natural enzymes have been optimized through evolution: a colossal experiment in the diversification of protein structure–function relationships carried out over enormous stretches of time. Aspects of this amazing process can be recapitulated with ancestral sequence reconstruction (ASR), which infers the common ancestral sequences of enzymes that existed over millions and sometimes billions of years ago (Harms & Thornton, 2013; Merkl & Sterner, 2016). ASR can provide unprecedented insight into the entire realm (active-site and outer sphere residues) of sequence changes sufficient for the emergence of novel enzyme function and thus directly addresses context-dependent effects. Lack of this evolutionary context is arguably a severe hindrance to the rational (re)design of enzymes. An example of this effect is often manifested when engineers change an active-site residue without altering the 'second-sphere' residues to support such a change, abolishing functionality in the process. Yet, to take full advantage of ASR for enzyme engineering, changes in sequences need to be understood in the context of substrate binding, catalytic activity and, especially, protonation states, as provided by neutron crystallography. This insight can in turn provide a set of governing principles to guide subsequent enzyme-engineering efforts.

2.9.5. Computational chemistry and neutron protein crystallography. Much of enzyme chemistry is accomplished through the transfer of protons. Neutron crystallography can

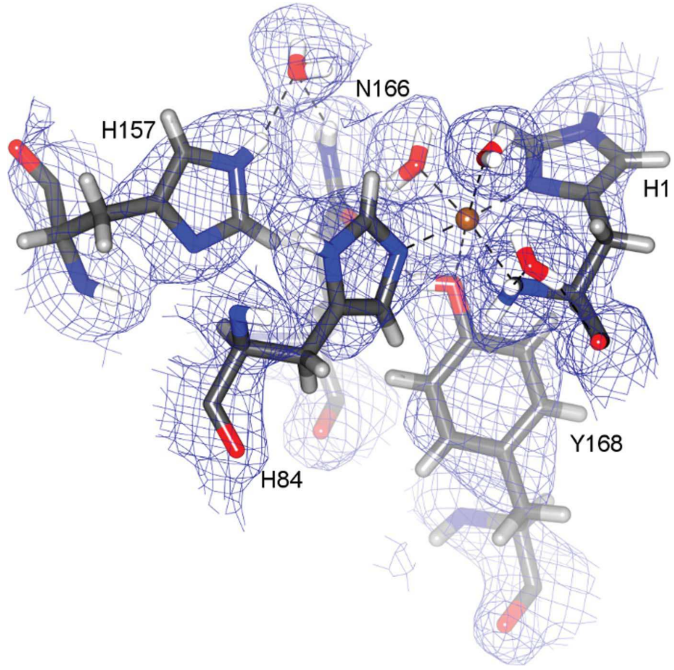

Figure 4
Active site of *Nc*LPMO9D in the enzymatic resting state (PDB entry 5tki; O'Dell *et al.*, 2017). The conformation and tautomeric state of the singly protonated His157 revealed by neutron protein crystallography was confirmed to stabilize molecular oxygen (not shown) near the active site of LPMO by quantum-chemical calculations. The H1 backbone amide N and carbonyl O atoms form hydrogen bonds to the 'pocket' water molecule, which has been hypothesized to participate in substrate interactions. ^{1}H atoms are shown in light gray, while atoms that have undergone exchange to ^{2}H are shown in white. The Cu atom is shown in brown. The blue mesh represents a neutron SLD $2F_o - F_c$ map contoured at σ = 1.0. Reproduced from Schröder *et al.* (2018).

provide accurate proton positions for stable states along reaction pathways. However, crystallography cannot directly capture transition states. To do so requires the calculation of reaction mechanisms and their associated energetics using computational techniques starting from the neutron-derived stable states. Technology has developed in this computational area, leading to the 2013 Nobel Prize in Chemistry (Smith & Roux, 2013), but correct calculations require accurate starting models from verified experimental knowledge as input to the calculations. One of the main challenges in computational enzymology, and in enzymology in general, is assigning protonation/tautomeric states to protein residues, substrates and/or cofactors and tracking these subsequent proton dynamics throughout the catalytic cycle. Neutron crystallography provides these data as input restraints for computational calculations of complete reaction mechanisms.

In theory, several computational methodologies exist for predicting the protonation/tautomerization states, ranging from completely empirical to quantum-mechanical (Alongi & Shields, 2010). QM/MM methods treat the reacting volume with quantum-chemical methods and the surrounding protein with molecular mechanics. Other approaches include implicit solvent models such as the Poisson–Boltzmann and Generalized Born models (Knight & Brooks, 2011). Constant-pH simulations facilitate the assignment of all titratable sites and consider the effect of conformational fluctuations (Goh *et al.*, 2014). These simulations are often performed with an implicit solvent model, but methods that include explicit solvent have also been developed. Alternatively, hybrid QM/MM methods can be used to determine the pK_a of an isolated site using free-energy perturbation methods (Guogui *et al.*, 2003). In contrast to other methods, QM/MM methods can be generally applied to practically any model of interest. Neutron crystallography provides a critical data set for testing and refining all these methods which, in general, are in error by at least one pK_a unit in the best circumstances (Fisher *et al.*, 2009).

The strength of QM/MM methods for the investigation of enzyme mechanisms is well established, but also requires expert knowledge of the model in several critical aspects to achieve insightful results (Dixit *et al.*, 2016; Lu *et al.*, 2016; Quesne *et al.*, 2016). Arguably the most critical aspects of constructing an accurate model are the choice of QM method and the assignment of the QM/MM boundary. When extensively sampling or exploring several different mechanistic hypotheses, a computationally efficient and relatively accurate method is desired. Currently, DFTB3 appears to be a reasonable choice for these explorations and for several enzymes when transition metals are not present (copper being an exception; Gaus *et al.*, 2012). DFTB3, and perhaps also PM6, are computationally efficient methods that can provide relatively accurate free-energy profiles for many enzymatic reactions (Christensen *et al.*, 2016). Density functional theory (DFT) methods that fall under the category of generalized gradient approximation (GGA) can be more accurate and more general (covering transition metals). With high-performance computing (HPC), DFT–GGA methods can represent a QM region of 50–200 atoms in free-energy simulations (Wymore *et al.*, 2014). The accuracy of the lower-level methods can be examined by employing more accurate approximation to coupled cluster methods applicable to large systems [DLPNO-CCSD(T)], alhough in this case only the potential energy of the model can be calculated, and these single-point energy calculations can span a few days of computation (Liakos & Neese, 2015). Thus, with an accurate starting model provided by neutron crystallography and a multiscale modeling approach, the free-energy profile for an enzyme mechanism can be elucidated along with a rationale of why other reaction pathways are not applicable.

2.10. Future applications

The impact of neutron protein crystallography in the fundamental understanding of biochemistry and its translation into biological function, including allosteric regulation, and the definition of proton-transfer pathways will continue to grow in the near future. Neutron crystallographic structures will aid in elucidating grand challenges in biology, such as specificity, cooperativity and allostery. Most diffraction instruments are now equipped with cryogenic sample environments, allowing the structures of unstable intermediates along reaction pathways to be solved (Li *et al.*, 2017; Kwon *et al.*, 2018). Deciphering protein chemistry will benefit from synergetic approaches combining QM/MM/MD and neutron and X-ray crystallography experiments. The most recent instruments enable data collection from crystals with unit cells of up to 250 Å (Coates *et al.*, 2015; Azadmanesh *et al.*, 2017). Within the next few years, systems which crystallize with large unit cells, such as protein–protein or protein–nucleic acid complexes, will become amenable to neutron crystallography, allowing overlap with cryo-EM studies of the same complexes and thereby allowing radiation-damage-free structures to be determined using neutrons, rather than electrons, as the probe.

With the development of the next generation of instruments and the construction of new neutron sources, even the solution of the challenging neutron structures of membrane proteins, including ion channels and aquaporins, will become possible (Coates & Robertson, 2017; Kurihara *et al.*, 2018). Protonation states and water hydrogen-bonding networks in channels and pumps will therefore be able to be experimentally determined. The new instruments and sources will also enable the study of systems that do not diffract X-rays to high resolution (<1.8 Å), such as nucleic acid enzymes. Of special interest are the application of neutron protein crystallography to allosteric networks and pump–probe neutron crystallography.

2.10.1. Allosteric networks. The mechanistic pathways of allosteric communication across proteins can be mediated by amino-acid side chains and water molecules within the structure. Knowing the protonation states of the side chains and the orientations of water molecules involved in allosteric networks will significantly contribute to the fundamental understanding of allostery and thus protein function. Again, some aspects of this understanding may be generalized to proteins other than those for which neutron crystal structures have been determined, helping to generate hypotheses that

can be tested both experimentally and by computational methods.

2.10.2. Pump–probe neutron crystallography. In neutron structures at room temperature it is possible to capture unusual hydrogen bonds with shared protons that may be very important for catalysis, as well as conformational states that disappear in cryotemperature X-ray crystallography. Pump–probe crystallography is therefore likely to be helpful in observing proton transfer with neutron crystallography. An obstacle is the relatively long time that is needed for data collection, so that in the near term studies are likely to be focused on long-lived metastable states. For example, photo-induced proton-transfer complexes can have very long lifetimes in photo-switchable GFP derivatives, which can be studied with neutron diffraction at room temperature or at cryotemperatures (Langan *et al.*, 2016). Neutron protein crystallography can also help to discover unusual structures that cannot be predicted by computational techniques without first performing the experiment. There are exciting possibilities for complementarity with pump–probed X-ray free-electron laser experiments that can provide room-temperature (heavy-atom) structures of very short-lived intermediates. We expect, however, that the unique role that nMX has, and will continue to have, in resolving chemical mechanism issues that X-rays, electrons and NMR cannot definitively solve will continue to be paramount.

3. Dynamic neutron scattering

3.1. Overview

Dynamic neutron scattering differs from other spectroscopies in that it is not only time-resolved but is also space-resolved. In other words, it provides information both on the time dependence of the motion detected, as do other spectroscopies, and on spatial cross-correlations and self-correlations of atomic motions via the dependence on the momentum transfer $\hbar q$. Various instruments have provided physics-based insights into the dynamics of biological systems of different levels of complexity on a large range of space and time scales (picoseconds to microseconds and 1–10 Å). This allows structural information on proteins to be correlated with their dynamics, such as proteins in different functional states and membranes. Recently, work has been extended to crowding and confinement as well as to live cells.

Incoherent inelastic (INS) and quasi-elastic scattering (QENS) give information on the self-correlations of atomic motions. As the incoherent cross-section of hydrogen is far larger than those of other biological elements, the signal from H-atom dynamics can be highlighted. A typical sample of a protein with exchanged hydrogens in a D_2O-hydrated powder will give information on the global dynamics as experienced by the unchangeable H atoms (Shrestha *et al.*, 2015).

Furthermore, it is possible that changes in dynamics can be probed *in situ* by employing mutants of the system under study lacking some of the components for comparison or through time separation in scattering experiments (Martinez *et al.*, 2016). The evolution of dynamics of living cells under different external conditions can be monitored by neutron scattering techniques, taking advantage of the many possible sample environments (Stingaciu *et al.*, 2016; Mamontov, 2017, 2018). QENS has mostly been used to probe picosecond and nanosecond motions in biomacromolecular systems (Shrestha *et al.*, 2016). Neutron spin echo (NSE) probes motions on longer time scales of up to ∼100 ns, mostly using coherent scattering. NSE has a storied history in polymer physics (Richter *et al.*, 1988) and is now being applied to biological systems (Bu *et al.*, 2005). QENS and NSE probe the stochastic dynamics which govern transport and relaxation processes on the nanosecond time scale.

Dynamic neutron scattering can be used to measure the average mean-square displacement in a protein, and this has been extensively used to probe the temperature-dependent dynamical transition that proteins undergo (Smith *et al.*, 2018; Doster *et al.*, 1989; Zaccai, 2000), which resembles the liquid–glass transition. Inelastic scattering can measure vibrational modes, and dispersion relations can be measured using triple-axis instruments (Goupil-Lamy *et al.*, 1997).

3.2. Perspectives for experimental work

3.2.1. Internal protein dynamics and allostery. Large protein molecules often consist of multiple domains, each of which may have a specific functional role, for example ligand-binding domain, catalytic domain *etc*. Studying the relative motions between selected domains is of great importance in understanding the enzymatic mechanism of these biomacromolecules (Yang *et al.*, 2010; Boura *et al.*, 2011). One can use NSE to experimentally study the relative motion between any two selected domains in a protein complex by deuteration of the rest of the complex, which is contrast-matched by the D_2O buffer (Farago *et al.*, 2010). Also, selective labeling of amino-acid residues suspected to play important roles in allosteric dynamics is a useful tool that has yet to be fully explored.

3.2.2. Intrinsically disordered proteins (IDPs). Intrinsically disordered proteins, and proteins with large intrinsically disordered regions (>30 residues), constitute about one third of all eukaryotic proteins (Ward *et al.*, 2004) and play important roles in intracellular signaling and regulation (Wright & Dyson, 2015). The lack of ordered three-dimensional structure gives IDPs the flexibility to adopt different structures when binding to different targets. Some IDPs remain unstructured even after binding to a target, and such dynamical complexes will mediate crosstalk when forming the ternary complex with other binding partners. The dynamics of IDPs, for example transitions between different structural states and conformational changes on binding to different targets, is crucial for their function in intracellular signaling and regulation (Dhindsa *et al.*, 2014). There is a need to develop neutron scattering methods to study the internal dynamics of IDPs, and these methods may lean heavily on the success of neutron scattering in polymer physics (Schirò *et al.*, 2015).

3.2.3. Solvation, hydration and hydrogen bonds. A challenge remains to understand the role of water and hydration

bonds in a plethora of biological systems and processes such as solvation and hydration. Water is never present as a pure substance; it often contains chemicals, ions, particulates and biological organisms. The co-understanding of the properties of water at the interfaces of these 'impurities' and the role and effect of water on their behavior presents an enormous opportunity to the neutron scattering community as a result of isotopic labeling, matching time and length scales, and accessibility to complex sample environments enabled by the high penetration of neutrons. These advantages enable detailed understanding of the water motions within the hydration shell of proteins in terms of the number of water molecules perturbed, the degree to which water motions are impacted, and the spatial extent of the perturbation (Perticaroli *et al.*, 2017).

Protein dynamics depends critically on solvent and hydration dynamics near the protein surface (Fenimore *et al.*, 2002). The motions underlying protein allostery have been clearly demonstrated in many systems and their 'slaving' by solvent dynamics has been shown (Frauenfelder *et al.*, 2009). The rates of many functional protein processes follow the rates of processes in the hydration shell, and here again neutron spectroscopy can determine the amplitude and energy landscape of the water motions, and with D/H contrast can separate the selected contributions (Mamontov & Chu, 2012; Chu *et al.*, 2012). This theme is also closely facilitated by recently developed statistical and quantum-mechanical theory-driven computational methods. Using classical simulation methods researchers have begun to perform efficient simulations on time scales of seconds, and of even longer with advanced rare-event sampling methods and autonomous multiscale methods (Paul *et al.*, 2017), as well as analysis based on convoluted neural networks, which have already revolutionized many engineering fields. Additionally, based on first-principles methods, one can now explicitly treat the nuclear quantum effect using methods such as path integrals. Synergistically integrated neutron scattering experiments and atomistic computations have the potential to provide a truly transformative understanding of processes such as solvation and hydration and the role of water and hydrogen bonds in biological systems and at interfaces (Tarek & Tobias, 2002).

3.2.4. Interactions of biomolecules with (in)organic surfaces. Smart hybrid materials, designed by combining biomolecules with (in)organic surfaces, are an innovative alternative for obtaining materials with unusual properties and have been applied in areas spanning from biotechnology to regenerative medicine and nanomedicine (Cobo *et al.*, 2015). A simple way to view such systems is to imagine that inorganic fillers, such as clays, COFs and MOFs, are added to biological systems (drugs, amino acids or proteins) and the selected functionality is triggered. To move forward, it is critical to reach an understanding of how intercalation (confinement) affects the structure–dynamics relationship (property) of the guest (active) compounds. Spectroscopy using neutrons combined with molecular modeling is a relatively unique approach (Dhindsa *et al.*, 2016) and can complement NMR studies. Isotopic difference neutron diffraction and Monte Carlo computer simulation can allow quantification of the interactions between the biomolecules and the cage surfaces, bringing unique insight for the development of novel functional biomaterials.

3.2.5. Drug screening and efficacy. The existing theoretical approach for drug screening overly emphasizes the enthalpic contribution to protein–ligand binding owing to the lack of knowledge of the entropic contribution and particularly the entropic contribution from water. Neutron scattering can quantitatively characterize the flexibility of protein and surface water simultaneously before and after binding (Balog *et al.*, 2004; Miao *et al.*, 2012). This will help to improve the existing theoretical framework to derive accurate binding free energies by including entropic terms. Another potential contribution is related to the question of how changes in the structure and dynamics of membranes are affected by interaction with hydrophobic drugs.

3.2.6. Biological membranes. Molecular motions in biological membranes are another area where neutron scattering contributes uniquely. Lipid bilayers exhibit dynamics on a range of time and length scales, ranging from dispersion, which has been detected with neutrons (Rheinstädter *et al.*, 2006), to molecular diffusion and rotation (Armstrong *et al.*, 2014), to collective thermal undulations and thickness fluctuations (Woodka *et al.*, 2012). These motions can provide crucial insight into specific properties such as the bending modulus or the lateral diffusion rates of individual lipids. For example, neutron scattering can observe the changes in local motions owing to the partitioning of small-molecule drugs into the hydrophobic region of the lipid bilayer (Sharma *et al.*, 2017; Barrett *et al.*, 2012; Fitter *et al.*, 2006). Neutron scattering is particularly adept at probing the long-wavelength collective undulations of lipid membranes, which are related to the bending modulus. Such observations can be combined with contrast-matching strategies to determine the mechanical properties of distinct phases within the plane of the membrane (Nickels *et al.*, 2017). These experiments are important for the development of physical models of lipid-raft formation in biomembranes.

3.2.7. Dynamics and transport of biological macromolecules under crowded conditions: dynamic neutron scattering. A new application of dynamic neutron scattering is to macromolecules in confined and crowded volumes. Many biological molecules are either self-crowded or function in a crowded environment. Typical examples include molecules in the cellular environment, proteins in lipid membranes (Stachowiak *et al.*, 2012) and the concentrated protein solutions commonly used in the pharmaceutical industry (Harris *et al.*, 2004). Crowding impacts the stability (Roberts, 2014), aggregation and transport properties of proteins and other biomolecules in concentrated solutions (Roosen-Runge *et al.*, 2011; Curtis, Nanda *et al.*, 2012; Nanda *et al.*, 2010; Liu *et al.*, 2010). Predicting protein stability is one of the central issues for the whole pharmaceutical industry and is also very important for understanding the pathogenesis of some diseases. However, how concentration affects protein stability remains elusive. Irreversible aggregation has long been

investigated owing to its relevance to human diseases. Recently, reversible aggregation, which typically occurs at high concentrations, has also attracted interest owing to its relevance to drug delivery and the manufacturing processes of therapeutic proteins. Understanding the transport effects of individual molecules in crowded solutions has been studied by optical tools that are mostly related to long-term diffusive behaviors (Bancaud *et al.*, 2009). However, short-term and local dynamical behaviors are difficult to probe using optical tools.

Another important aspect is to understand how crowded biological systems respond to environmental changes. Indeed, macromolecular crowding is a crucial component that is needed to understand the energetics and kinetics of biological processes in living systems (Erlkamp *et al.*, 2015; Stingaciu *et al.*, 2016; Mamontov, 2017, 2018) and is a prerequisite for the design of industrially relevant enzymatic reactions (Gao *et al.*, 2017). One interesting example is the study of the protective effects of osmolytes (or other co-solutes) in living cells against hostile conditions for life (Al-Ayoubi *et al.*, 2017). Osmolytes are known to accumulate in extremophiles, and the modification of molecular dynamics in their presence under various external conditions is of special interest for understanding adaptation mechanisms to a specific environment.

3.2.8. Living-cell systems. Functionality in living cells is determined by numerous and strictly coordinated pathways and mechanisms that are mostly mediated by water, which can be directly probed using neutron spectroscopy on a wide range of time and length scales. This approach is useful to probe water dynamics in cellular systems (Natali *et al.*, 2013), which is found to be highly influenced by the molecular environment. Quasi-elastic neutron scattering (QENS; Tehei *et al.*, 2007) and neutron spin echo (NSE) have recently been successfully applied to probe water mobility in cells (Tehei *et al.*, 2007), but also, remarkably, proteome flexibility (Martinez *et al.*, 2016) and membrane properties without modification of the system (Nickels *et al.*, 2017). Furthermore, NSE significantly expands the accessible time scale of neutron spectroscopy to include more dynamical processes and, even if the technique has not yet been fully explored, it is reasonable to foresee that it will become an important tool for future studies of living systems. Another interesting advantage of neutron spectroscopy is the possibility of using a variety of special sample-environment setups allowing cells to be investigated under various external conditions, under external stresses (Vauclare *et al.*, 2015) or close to their natural conditions, which are not necessarily those on the surface of the Earth (see Fig. 5). Finally, the combination of the averaged view accessible by neutrons with other complementary techniques such as site-specific NMR spectroscopy, dynamic light scattering or imaging is highly recommended as it adds understanding to these extremely complex systems.

3.2.9. Quantum-mechanical phenomena. Since Erwin Schrödinger wrote *What Is Life?* in 1944 (Schrödinger, 1944) there has been a significant discussion in the literature on the potential role of quantum effects in biological systems (Ball, 2011). There are several ways that potential quantum effects may appear. One of these is related to proton transfer, which is one of the major mechanisms for many biochemical reactions, such as photosynthesis (Wang *et al.*, 2006). Protons are the lightest atomic units, and their accurate description should include quantum effects. Tunneling is a potentially important effect for effective proton-transfer barriers in enzyme catalysis (Klinman & Kohen, 2013). Quantum effects may also be important for water dynamics (Gainaru *et al.*, 2014; Agapov *et al.*, 2015).

Neutron scattering provides a unique opportunity to look for quantum effects. This can start from analysis of the contribution of zero-point vibrations (a trivial quantum effect) to the total mean-squared displacements of H atoms; this analysis alone provides an estimate of how important quantum effects and corrections might be (Novikov & Sokolov, 2013). In addition, using hydrogen/deuterium substitution also allows an estimation of the role of quantum effects and tunneling in the dynamics of biological molecules and proton-transfer mechanisms. In the case of tunneling the dynamic effects depend exponentially on mass, thus leading to a large difference between the behavior of hydrogen and deuterium, while classical over-barrier relaxation has a weak dependence on this isotope substitution (Gainaru *et al.*, 2014). Also, the use of deep inelastic neutron scattering provides an analysis of proton momentum distribution (Reiter *et al.*, 2006). This enables analysis of the proton ground-state wavefunction that contains detailed information on possible quantum effects.

3.3. Instrumentation and technical perspectives

3.3.1. Deuteration. Sample deuteration is a powerful complement to neutron scattering methods in biology, not only for structure but also for dynamical techniques, and has arguably been underexploited for the latter. Neutron scattering from a fully deuterated protein is mostly coherent, resulting from interatomic motions, and this can be used to quantitatively characterize collective protein motions,

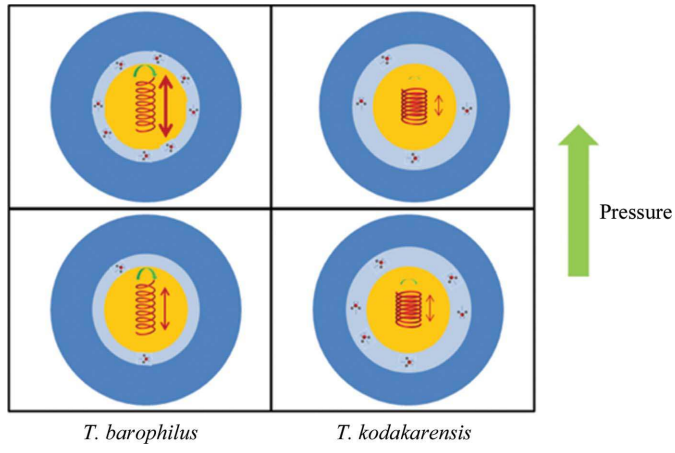

Figure 5
Sketch summarizing the effects of pressure on *Thermococcus barophilus* and *T. kodakarensis*. The dark blue surface represents bulk water and the light blue surface represents hydration water. The red spring characterizes the proteome and its contributions (translation and rotation) to dynamics (Martinez *et al.*, 2016).

furnishing the forms, time scales and spatial amplitudes of the dynamical modes simultaneously (Hong *et al.*, 2016; Nickels *et al.*, 2013; Perticaroli *et al.*, 2013). These collective motions are sometimes directly associated with the function of macromolecules, such as ligand-channel opening/closing and allosteric domain motions (Hong *et al.*, 2014, 2016).

Deuterated materials are also useful in reducing the incoherent contribution of specific biomolecules or specific biomolecular components. Selective isotopic labeling of specific amino acids (Wood *et al.*, 2013) or regions of the lipid membrane (König *et al.*, 1995; Nickels *et al.*, 2015) can be used to extract site-specific dynamical information from neutron scattering experiments. The hydrogen signal can be suppressed by deuteration. For example, the specific hydrogenation of an otherwise perdeuterated protein will highlight the dynamics of the hydrogenated segment. Also, using perdeuterated molecules in crowded solutions, it is possible to either hide or highlight certain classes of molecule to selectively probe the microscopic dynamics of specific components of a complex system. Another example of the use of deuteration is for solute molecules in the presence of water or other hydrogenated solvents. This approach has been used to isolate the motions of water in the hydration shell of numerous proteins (Zanotti *et al.*, 1999; Nickels *et al.*, 2012) and around lipid bilayers (Toppozini *et al.*, 2015).

3.3.2. Polarization analysis. The use of polarization analysis is an intriguing possibility for the future of neutron scattering in biology (Stuhrmann, 2004). The coherent and incoherent components of the scattering signal provide different but complementary information, which neutrons have the potential to resolve (Gaspar *et al.*, 2010). New developments for the application of dynamic nuclear polarization (Abragam & Goldman, 1978) in neutron protein crystallography offer the potential of measurements using the polarization of the sample to access coherent scattering in hydrogenated samples (Zhao *et al.*, 2013, 2016). Although its use in crystallography is for the future, polarization analysis is a vital part of inelastic neutron scattering, forming the fundamental principle of neutron spin echo (Mezei, 1972).

3.3.3. Neutron spin echo. The dynamic window accessible by neutron spin echo is comparable to the dynamics of functional motions in many biological systems, such as membranes and proteins. This technique therefore holds tremendous potential for determining functionally important motions. Therefore, there have been increasing efforts to study biologically relevant systems using NSE. However, the scarce availability of NSE beam time worldwide, coupled with the long data-collection times, limits the size of the NSE user community and is arguably the primary obstacle to the application of NSE by the biophysical community. The development of other complementary techniques, such as dynamic light scattering (DLS), at NSE beamlines would also expand the usefulness of the current instrumentation. The relative lack of theoretical development leads to a steep learning curve for inexperienced biological groups to use NSE. Thus, there is a need to develop suitable theories/models describing NSE for biological systems. Future development of NSE to extend to longer time scales would enable critical biological motions to be probed. More generally, the exploitation of coherent dynamic scattering holds much promise for characterizing correlated motions in proteins, and may well be paired with X-ray diffuse scattering in this regard (Meinhold *et al.*, 2007, 2008).

3.3.4. Combined approaches with other techniques. Dynamic neutron scattering can be usefully combined with many other techniques. Neutrons provide information on low-frequency collective motions that can be combined with less direct but local techniques. One example is NMR relaxation spectroscopy which, when combined with neutrons, provides both a global and a site-specific view of biomolecular dynamics (Miao *et al.*, 2012).

Also, single-molecule fluorescence resonance energy transfer (FRET) can furnish the relative fluctuations of two dye molecules which are labeled at selected positions of a protein molecule on time scales from milliseconds to hundreds of seconds (Roy *et al.*, 2008), without being affected by the whole-molecule translational and rotational diffusion. However, the dynamics derived from FRET collapse to one single distance devoid of three-dimensional information, whereas the latter can be obtained from NSE (Bu *et al.*, 2005). However, experimentally deriving protein internal dynamics from NSE is a considerable challenge as it requires the subtraction of the contribution resulting from the global motion from the overall neutron signals. Moreover, NSE signals tend to be weak and require long collection times (*e.g.* days). It may be possible to alleviate this problem with the aid of single-molecule FRET.

Dielectric spectroscopy is an important technique for studying multiscale relaxation and diffusion in complex systems that are often characterized by self-similarity and a vast range of accessible frequencies. Dielectric spectroscopy can be readily applied to detect relaxation frequencies, although their interpretation is sometimes difficult. This technique has been combined with QENS data from biomolecular systems (Kneller, 2005; Calandrini *et al.*, 2008). Recently, a high-pressure cell was developed which allows simultaneous neutron and dielectric spectroscopy measurements (Khodadadi *et al.*, 2008; Sanz *et al.*, 2018).

3.3.5. Theory, simulation and modeling: basic scattering theory. The theoretical background for the analysis of practically all neutron scattering experiments from biomolecular systems, including simulation-based approaches, is Van Hove's theory (Van Hove, 1954) in the classical limit, where atoms follow classical trajectories which can be either simulated by molecular-dynamics simulations or by probabilistic models. This very appealing approach is, however, an oversimplification which implies not only neglecting quantum effects in the scattering system but also recoil effects, which result from the impact of the scattered neutrons on the sample. There is no measurement without perturbation of the system under consideration, and it was Van Hove himself who showed in a rarely cited paper (Van Hove, 1958) that the imaginary part of the quantum Van Hove correlation function reflects the perturbation of the local atomic density owing to the

collision of the incident neutrons with the atoms in the sample. This perturbation is lost in the 'mathematical classical limit' $\hbar \rightarrow 0$, but it can be maintained in the 'physical classical limit', where $\hbar \rightarrow 0$ applies only to the description of the scattering system and the momentum transfer, $\hbar q$, stays finite (Kneller, 1994).

The basic question of what is measured in neutron scattering experiments has recently been brought up again by Frauenfelder *et al.* (2017) in the context of quasi-elastic neutron scattering experiments on proteins. The idea here is to use the concept of energy landscapes, which is adapted for complex systems such as proteins, and to describe neutron scattering in the light of Mössbauer spectroscopy. The approach is, however, not integrated into the framework of quantum scattering theory. This can be accomplished by describing incoherent neutron scattering as a particular form of Franck–Condon spectroscopy (Kneller, 2018) in which the incoming neutrons excite transitions on the 'energy landscape' of the scattering system, where the corresponding transition probabilities depend on the momentum transfer from the incoming neutrons to the scattering atoms. Much still needs to be performed, though, to develop routinely usable improved analysis methods of neutron scattering experiments, in which the neutron is an active probe capable of inducing changes in the scattering system.

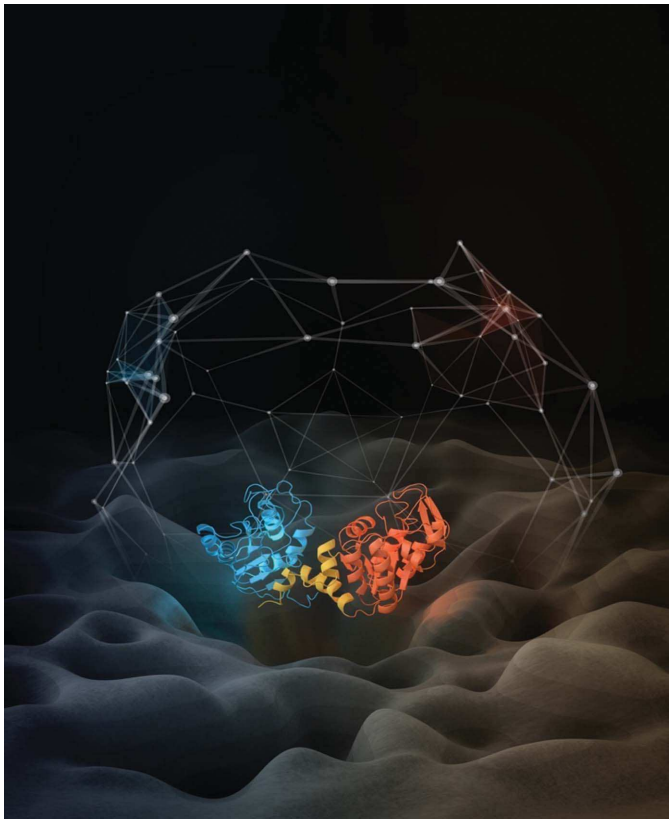

Figure 6
Depiction of a protein energy landscape. Protein energy landscapes can be quantitatively explored with dynamic neutron scattering. In this schematic image phosphoglycerate kinase is shown, together with an image of an energy landscape. Jumps between minima in the energy landscape can be represented by a transition matrix that can be drawn as a network. Image from https://www.scistyle.com.

3.3.6. Theory, simulation and modeling: trajectory-based modeling of neutron scattering spectra. Dynamic neutron scattering has heavily relied on theory, simulation and modeling for the interpretation of experimental results. Since the accessible time scales for most scattering experiments with thermal neutrons are similar to those accessible by molecular-dynamics (MD) simulations, and since both techniques probe the structure and dynamics of condensed-matter systems at the atomic level, MD simulations have been and remain a valuable tool in the analysis of neutron scattering experiments from complex systems, keeping in mind the limitations discussed in the previous paragraph. Corresponding software tools for linking MD and neutron scattering experiments, *i.e.* for calculating instrument-specific scattering functions from MD, have been developed (for example the *nMoldyn* package; Róg *et al.*, 2003; Hinsen *et al.*, 2012; http://dirac.cnrs-orleans.fr/plone/software/nmoldyn/) and *SASSENA* (https://github.com/benlabs/sassena; Lindner & Smith, 2012), including the aspect of 'virtual experiments' that is included in *MDANSE*, which was developed at the Institut Laue–Langevin in Grenoble (https://code.ill.fr/scientific-software/mdanse; Lindner *et al.*, 2013). MD simulations may also be used to 'gauge' Markov state models and characterize protein energy landscapes (Fig. 6). An important tool to develop the analysis of NSE data concerns the estimation of roto-translational diffusion tensors for proteins and macromolecules in general from the atomic positions and that average diffusion tensors can be computed from MD trajectories, taking into account internal flexibility (Chevrot *et al.*, 2013).

3.3.7. Theory, simulation and modeling: minimalist models. There is also a need for 'minimalist' models, which capture the dynamical properties of biomolecules at least semi-quantitatively (for example 'anomalous' diffusion in

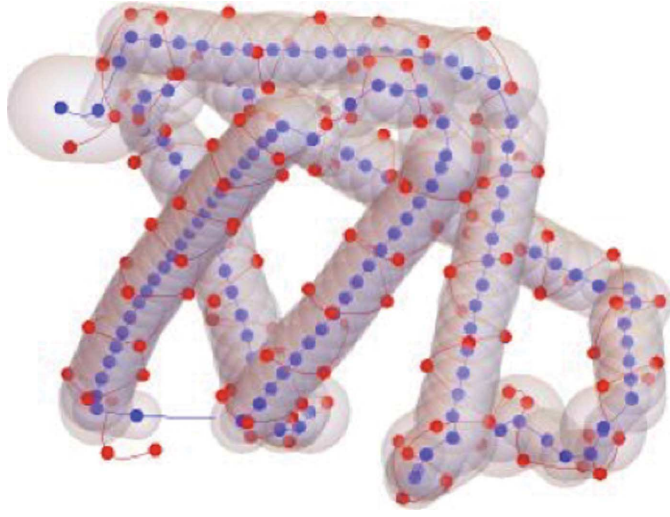

Figure 7
A minimalist, 'sausage' model of protein dynamics for myoglobin (PDB entry 1a6g; Vojtěchovský *et al.*, 1999). C^{α} atoms are in red; corresponding points on the protein axis are in blue. Details are given in Kneller & Hinsen (2015).

crowded media), but which can also be easily applied by biologists and biochemists and which grasp the essence of the information in experimental data with only a few parameters. QENS experiments are of particular concern here, since they give information about the atomic dynamics in the asymptotic diffusional regime and since the diffusional dynamics can be described by a few parameters only. In case of free diffusion these parameters are the (fractional) diffusion constant D_α and the fractional exponent α which describe the growth of the mean-square displacement of the diffusing particles with time (Hinsen & Kneller, 2016). The deviation of α from 1 describes anomalous diffusion, which is often seen in crowded samples ($0 < \alpha < 1$; otherwise known as 'subdiffusion'). In the case of space-limited diffusion, describing for example the internal atomic dynamics in proteins, models must describe the relaxation dynamics of the atomic position fluctuations and their mean amplitudes, which are reflected by the elastic incoherent structure factor (EISF). Here, the first steps in using minimalist models have been undertaken, using few-parameter models for the EISF (Meinhold *et al.*, 2008; Peters & Kneller, 2013; Vural *et al.*, 2015) and for the dynamics of the C^α dynamics in protein backbones (Kneller & Chevrot, 2012). The general idea here is to describe either relaxation times or amplitudes of atomic position fluctuations by *distributions*, which are characterized by a few parameters. Also, methods have been derived to supply the variance in the mean-square displacement (Yi *et al.*, 2012). These ideas can be pursued using very simple coarse-grained spatial models for biomolecules, such as the 'sausage model' for proteins which is depicted in Fig. 7 (Kneller & Hinsen, 2015) and which can be made into a dynamical model by giving the protein tube (visco)elastic properties.

4. Solution structures

4.1. Introduction

Small-angle scattering (SAS) is a long-established approach to the characterization of biological macromolecules in solution. In a model-independent fashion, fundamental parameters such as molecular volume, mass, composition and size can be determined with great precision. Combined with available atomic models from experiments or resources such as the PDB, these analyses can be extended to rigorously test structural hypotheses. Unlike high-resolution methods such as macromolecular crystallography (MX), nuclear magnetic resonance (NMR) and cryo-electron microscopy (cryo-EM), which all allow the *de novo* determination of atomic structure, SAS is a relatively low-resolution technique. However, SAS measurements are highly complementary and versatile, allowing precise control of the sample environment and experimental conditions in solution over a wide range of length scales. When neutron small-angle scattering (SANS) is applied, *contrast variation* is possible, allowing the unique opportunity to discern the relative positions and arrangements of components within functioning complexes as they exist within the large assembly, alongside the opportunity to learn about disordered and flexible regions of macromolecules that elude analysis by other methods. Frequently, SAS is applied as a component of a multi-faceted examination of biological macromolecules that includes several orthogonal techniques. Recent outstanding examples include the first ever direct detection of lipid rafts in a living organism, innovative work that used small-angle neutron scattering, contrast variation and specific deuteration through genetic manipulation to detect nanodomains in living *Bacillus subtilis* (Nickels *et al.*, 2017); the combined use of small-angle neutron scattering, deuterium labeling and contrast variation, temperature activation and fluorescence spectroscopy to obtain the time-resolved structural pathway of mechanical unfolding of a green fluorescent protein model substrate by the archaeal AAA+ PAN unfoldase on a subminute time scale (Ibrahim *et al.*, 2017); and domain-selective perdeuteration combined with contrast-matched small-angle neutron scattering, SAXS and computational modeling to precisely define relative domain arrangements on RNA during binding to a protein (Sonntag *et al.*, 2017).

4.2. Software

A major driver of the growth in the SAS technique (Fig. 8) has been the availability of user-friendly and robust software that allows the atomistic and coarse-grained molecular modeling of X-ray and neutron small-angle scattering data using available atomic information, alongside well over 146 000 entries in the PDB. The capabilities of current computer simulations provide a unique opportunity to model small-angle scattering data at the atomistic level, and to

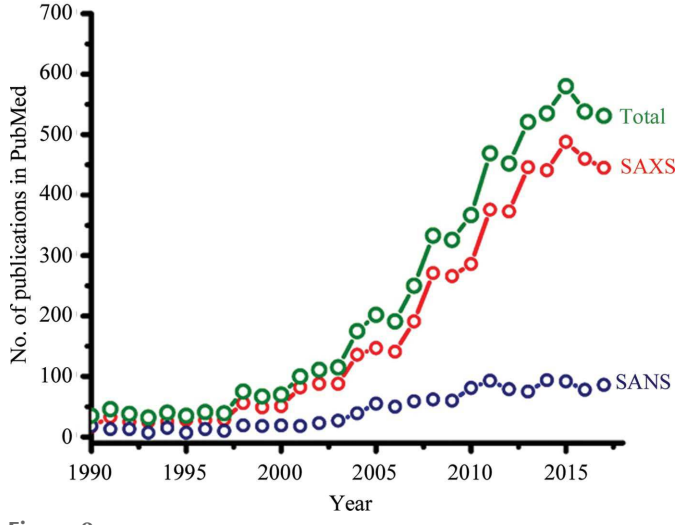

Figure 8
Small-angle scattering publications. Over the past 20 years SAS has arisen as a mainstay technique for investigators in several fields, including materials science and structural biology. The figure shows the number of publications that have applied SAS to macromolecules in PubMed (https://www.ncbi.nlm.nih.gov/pubmed/) by year. While the total number of publications employing this technique has grown considerably over the past two decades to 1–2 publications per day, most of this growth was realized using X-rays (SAXS); small-angle neutron scattering (SANS) has not grown commensurately, averaging closer to only 1–2 publications per week.

include other structural constraints ranging from molecular and atomistic energetics to crystallography, electron microscopy and NMR. Robust state-of-the-art molecular-simulation engines and molecular-dynamics and Monte Carlo (MC) force fields provide constraints to the solution structure inferred from the small-angle scattering data that incorporates the known physical chemistry of the system. Two related initiatives that have helped to drive this growth, especially within SANS, are CCP-SAS and *SASSIE*.

The most recent contributions under the CCP-SAS project (Perkins *et al.*, 2016) were to provide an open-source cloud-based software environment. This environment not only makes it clear how analyses are performed, but also permits experimental teams to understand complex chemical interactions and structural organizations, and is flexible enough to incorporate additional different experimental constraints into the modeling workflow.

SASSIE (Curtis, Raghunandan *et al.*, 2012) is designed to be modular in nature and to be used with any MD engine, force field, type of material or approach to solving the molecular structure. However, it is now primarily used for biological molecules and complexes using the CHARMM22 or CHARMM36 force fields. Carbohydrates and polymers can be accommodated if they conform to this framework. *SASSIE* includes MC simulation methods to create ensembles of biomolecular structures by sampling user-selected backbone dihedral angles to model experimental X-ray and neutron data. Without this advance, the generation of atomistic structures using modern force-field based simulations could take months or even be inaccessible.

The synergy of SANS and MD will be achieved by performing simulations of the same systems and by calculating SANS intensities directly from the simulation to compare with the experimental results. For large simulation trajectories, the computation of SANS intensities is itself an HPC problem. *SASSENA* (Lindner & Smith, 2012) is highly efficient software that runs in parallel on many thousands of cores, which speeds up the calculation of $I(Q)$ by orders of magnitude. It can calculate coherent and incoherent elastic neutron scattering functions from MD trajectories, properly considering the SLD of the atoms in the model. The limiting factor in its wider use is a lack of access to the HPC resources that are required to run the software.

Other software packages in which information from different methods is considered simultaneously during the structure-modeling process, *i.e.* the *Integrative Modeling Platform* (*IMP*; Russel *et al.*, 2012), have been helpful in the analysis of SAXS data. However, SANS data analysis that takes contrast variation into account is not well supported in these cases.

4.3. Sample-environment development

Arguably, the most versatile and powerful part of the SANS experiment is the sample environment: the ability to precisely control the conditions under which measurements are made, including temperature, pressure, flow and a multitude of other conditions. To continue the growth of SANS techniques, innovations are needed on this front, including the development of time-resolved measurements, interfacial measurements, methods to control pressure, temperature, shear flow and mixing, *in situ* lyophilization, and inline applications, such as multi-angle light scattering, UV–Vis measurements and inline size-exclusion chromatography. To address sample limitations, innovations in SANS with regard to small effective collimation (while maintaining flux and intensity) are needed. The needs of the experimentalist are also dictated by the questions being answered. For example, model-dependent versus model-independent questions dictate the needs for SAXS versus SANS, and many basic questions can be answered by SAXS.

4.4. Computation

Software-based analysis remains a key component of the SANS technique. While considerable progress and growth has been realized in recent years, there are several areas in which useful growth could be envisaged.

(i) Streamlined and automated data reduction (subtraction, merging). While SAXS beamlines have made considerable progress in throughput and automated data processing, similar innovations have not yet found their way to SANS stations. Such innovations increase the efficiency and throughput of the SAS experiment.

(ii) Access to high-performance computing. An atomistic representation is important for systems with flexible linkers, the conformation of which is a balance of entropic and enthalpic interactions that are influenced by hydration and are best captured when all atoms in the system are simulated. To achieve this, an accurate representation of the interactions occurring ('force field') and an adequate sampling of the configurational space of the biomolecules are required. States of single proteins can be modeled by atomistic MD, possibly in conjunction with enhanced sampling techniques. However, the computational cost of this approach is very large and access to HPC resources, such as the SUMMIT supercomputer at ORNL, is preferred.

(iii) Enhanced modeling software. While the number of software packages available for SAS analysis continues to grow, few options such as *SASSIE* are available in which contrast calculations and contrast-variation information are incorporated. Additionally, the continued growth of modules that incorporate many various sources of *a priori* information (*i.e.* NMR, FRET pairs, cryo-EM, chemical cross-linking) will benefit the approach.

(iv) Bridging SANS and electron microscopy. The cryo-EM revolution continues to impact structural biology on a broad scale and it is believed that cryo-tomography will similarly impact biological research in the coming years. While the SANS technique could provide valuable complementary information to these approaches, serving to enhance contrast and provide model validation, this potential will not be realized until more new software becomes available which

bridges this gap. Such development will require novel computational methods and experimental benchmarks.

4.5. Applications: basic research

Overall, SANS continues to provide a broad impact on public health and fundamental understanding of the processes of life. As mentioned previously, unlike X-rays, neutrons are penetrating and nondestructive, making them ideal not only for the study of higher order assemblies and biological macromolecules, but also for *in vivo* systems such as whole bacterial cells. A frontier in the application of SANS will be the continued *in situ*/*ex vivo*/*in vivo* application of the technique to the study of intact viruses, cellular organelles and cellular substructures. SANS has great utility in the study of protein structure, including aggregation in the context of neurological diseases such as Alzheimer's disease (Dante *et al.*, 2008; Yong *et al.*, 2002) and Parkinson's disease, phase separations and self-assembling systems. Moreover, SANS is uniquely well disposed to assess the structure of the solvent boundary of proteins alongside phenomena that change water activity, including macromolecular crowding (Curtis, Nanda *et al.*, 2012; Merzel & Smith, 2002).

SANS with contrast variation and selective deuteration is also well suited to the study of multisubunit protein complexes in solution. The strategic deuteration of one or more of the subunits can provide insight into the interactions between them (see Section 6). SANS with contrast variation is also ideal for the study of protein–nucleic acid assemblies as they exist in solution, as these two phases cannot be resolved using X-rays alone, which are heavily biased towards the higher density nucleic acid component. These composite particles include larger macromolecular assemblies such as chromatin, ribosomes and RNA splicing assemblies. SAS, including SANS, is well suited to assess and model the intrinsic disorder and flexibility found in over 40% of any eukaryotic proteome. Structural information about these regions of proteins is not accessible by techniques such as MX, NMR and cryo-EM.

4.6. Applications: translation

Together with basic research, SANS has become an invaluable tool in translational studies: the design and application of novel biomaterials and biologics. This includes product development, innovation, medicine and food/agriculture, all of which are areas of interest with regard to commerce and public health.

SANS has arisen as an invaluable approach to the characterization and development of biologics, most notably therapeutic antibodies. This includes the study of aggregation in concentrated formulations, aspects of preservation and delivery, surface interactions and adsorption, complexation with surfactants and polymers, and the correlation of solution properties with efficacy.

SANS with contrast variation has been applied to the study of new biomaterials with novel applications, including drug delivery (Nagata *et al.*, 2018; Cherhal *et al.*, 2015). These materials include liposomes, reverse micelles and programmable materials such as hydrogels and self-assembling peptides (Fernandez-Castanon *et al.*, 2016; Nagata *et al.*, 2018).

Most plant matter is composed of cellulose, hemicellulose and lignin. The conversion of this abundant matter to liquid fuels underlies key areas of research in the development of a new generation of biofuels. SANS is regularly applied to the study of the process methods that are being developed for these materials (Langan *et al.*, 2014; Smith *et al.*, 2015).

Research in agriculture applies SANS measurements to the study of foodstuffs such as milk and cheese (Ingham *et al.*, 2015).

4.7. Complementarity with cryo-EM

In a typical single-particle cryo-EM experiment, a protein solution is applied to grids, flash-frozen and imaged (Bai *et al.*, 2015). Owing to the relatively poor contrast of proteins embedded in ice, high-resolution structure determination requires the averaging of many thousands of particles. Many fields containing individual particles are imaged, followed by classification of the two-dimensional particle projections per orientation (and possibly conformation), class averaging and finally three-dimensional reconstruction. Variations on the technique also exist, such as cryoelectron tomography (cryo-ET; Beck & Baumeister, 2016). In this case, rather than relying on the natural distribution of particle orientations to obtain different angular projections for reconstruction, individual particle fields are instead imaged multiple times at a series of tilt angles. Three-dimensional reconstructions are performed individually using the (non-averaged) two-dimensional particle projections, followed by averaging of the three-dimensional reconstructions. This enables particles to be imaged and reconstructed in complex environments (for example dense protein mixtures, embedded in membranes or even in whole cells), whereas single-particle cryo-EM reconstruction would not be possible because of overlap with other structures in the projection images.

Cryo-EM has seen significant recent advances, with protein structures now frequently solved at resolutions of between 2 and 4 Å. These advances have been driven by hardware improvements such as direct electron detectors, by motion-correction methods and by improvements in computational reconstruction methods. One of the main remaining limitations to cryo-EM is its restriction to particle sizes that are large enough (and have sufficiently distinct features) to reliably align and average. The lower limit on particle size for robust structural determination remains in the range of hundreds of kilodaltons, although this will continue to decrease, particularly with recent hardware advances (such as the Volta phase plate) that can improve particle contrast (Khoshouei *et al.*, 2017).

Broadly speaking, compared with other structural techniques, the primary advantages of small-angle scattering (SAS) in biology are its applicability to systems under many solution conditions, to a wide range of particle sizes and to obtaining the bulk properties of flexible systems such as biopolymers, disordered proteins or flexible proteins. Because

cryo-EM also operates on 'solution-like' samples (albeit in vitreous ice), it has overlapping utility with SAS and is a better tool for certain problems (for example moderate- to high-resolution structural determination of large, rigid particles).

However, for many problems, particularly those involving dynamic systems or in controlled sample environments, SAS is a better (or complementary) tool. Unlike cryo-EM, SAS allows samples to be easily studied under the widest range of solution conditions and sample environments, including temperature ramps, flow, shear fields, illumination, high pressure, and electric and magnetic fields. SAS also allows the continuous monitoring of structural parameters as a function of time or sample conditions (for example to monitor folding/unfolding, conformation changes, polymerization, subunit assembly *etc.*). In addition, deuteration and contrast matching in SANS can allow these attributes to be studied for individual isolated components of a complex system that would be difficult or impossible to model in its entirety. Isotopically labeled/unlabeled mixtures can also be used to study the dynamics of mixing and exchange, for instance the exchange of lipids in membranes or proteins in assemblies. Finally, the bulk properties of flexible biopolymers, such as unfolded proteins, multidomain proteins with flexible linkers or protein–polymer conjugates, can be readily studied using SAS [which has long been used as a primary tool in polymer physics (Beaucage, 1996) and thus well developed and mature analysis methods are available for such systems]. Analyzing flexible proteins remains a challenge in cryo-EM, since large numbers of particles must be successfully classified and aligned even for static structures.

Owing to the distinct but overlapping use cases for SAS and cryo-EM, certain problems would be promising for joint treatment by both techniques. For instance, proteins with both rigid domains and flexible linkers could be analyzed jointly, with cryo-EM being used to determine the structures of the rigid domains, which could then be built into flexible models and refined against SAS data. In fact, one could envision this paradigm being used in many cases, with cryo-EM being used to build the static structural details of a model, while adjustable parameters or model details involving flexibility or dynamic processes are refined against SAS data (potentially as a function of sample environment and solution conditions). This type of joint analysis has been little-used, and an important area of future work could be the further development of computational tools to exploit the complementary information available through SAS and cryo-EM (Schroer & Svergun, 2018).

5. Membranes

5.1. Introduction

Through the isotopic substitution of H atoms in lipids, proteins and/or solvents, different moieties of a sample can be highlighted or muted and distinct regions in the biomolecule can be discerned. This property is crucial when determining lipid phase separation in membranes (Heberle *et al.*, 2013) and when studying membrane asymmetry (Heberle *et al.*, 2016; Doktorova *et al.*, 2018).

Neutrons are also well suited for capturing membrane dynamics, both at equilibrium and under external perturbations such as shear and flow, and providing length scale-dependent information on dynamical responses. Cold and thermal neutrons, because of their energies, are well suited to determining both single-atom dynamics (incoherent inelastic scattering) and the collective motions of atoms (coherent inelastic scattering). For example, although hydrogen, owing to its large incoherent cross-section (80.27 barns), is the largest contributor of any atom to the isotropic background signal in a static measurement, this feature is commonly used in studies of single-molecule dynamics. Moreover, replacing hydrogen by deuterium in the same sample enables the study of different collective motions, which can be used, for example, to determine the mechanical properties of membranes (for example the bending rigidity of asymmetric lipid bilayers with protiated and deuterated leaflets; Nickels *et al.*, 2015; Heberle *et al.*, 2016). Such data are also essential to parametrize force fields in order that simulations reproduce the dynamical response of simple membranes (Kučerka *et al.*, 2011). Understanding the dynamics of more complex samples that are intermediate in complexity between cells and model systems will then be achieved by combined simulation and scattering methods. All membrane-related biological functionality begins with individual molecular encounters on the bilayer. The dynamics of these encounters are therefore a crucial target of modeling approaches, such as MD simulation, which also retain the chemical accuracy needed to resolve lipid–protein and protein–protein interactions. To date, however, force fields have been parametrized to capture structural data for lipids, such as chain-order parameters, area per lipid and membrane thickness (Klauda *et al.*, 2010). In the future, the goals of MD simulation will become more focused on dynamical properties, for example the in-plane mobility of lipids and membrane proteins, the encountering of signaling partners, the mixing of membrane contents following vesicle fusion *etc.*, which demand the parametrization of force fields to reproduce membrane dynamical responses.

In summary, elastic and inelastic scattering techniques, when combined with computer simulations (for example molecular dynamics), new sample preparations of model membranes and the genetic and chemical manipulation of organisms to enable hydrogen and deuterium labeling (Nickels *et al.*, 2017), offer a unique opportunity to address some of the leading problems in biology. However, to fully make use of current neutron capabilities and to develop new ideas for the development of future instruments, the following need to be implemented: (i) synthetic lipid and protein deuteration and, in the case of proteins, segmental and post-translational deuteration, (ii) increased neutron flux on the sample, (iii) the development of data-analysis and modeling tools, (iv) the development of living model systems (*e.g. B. subtilis*) and (v) automated sample-handling capabilities.

5.2. Membrane-related biological challenges that benefit from neutron methodologies and *in silico* simulations

5.2.1. Membrane structure. Neutron scattering techniques, such as SANS and neutron reflectometry (NR), provide structural information on intrinsically disordered systems, such as membranes in their physiologically relevant states, on the nanometre scale. Biological membranes are two-dimensional fluid self-assembled structures whose structure and organization are central to many biological functions. For example, there is broad consensus that the spatial organization of lipids and proteins in biological membranes plays a critical role in the life of a cell and its functions (Coskun & Simons, 2011). Experimental evidence supports the notion that rafts (*i.e.* functional membrane domains) are involved in processes such as protein sorting, vesicular transport, viral entry and exit from cells, and cell signaling. Importantly, raft functionality may also involve the reversible coalescence and growth of small and transient domains into larger structures that act as platforms for organizing protein machinery. However, despite intense interest in the study of functional domains, the mechanisms responsible for lipid–protein interactions and domain-size transitions remain an open question (Heberle *et al.*, 2013).

SANS has proven to be a powerful technique for detecting and measuring the size of nanoscopic membrane domains in nanometre-sized unilamellar vesicles (ULVs) with lipid compositions that mimic the mammalian plasma membrane outer leaflet (Heberle *et al.*, 2013; Nickels *et al.*, 2015). Besides measuring the size of domains (Fig. 9), SANS has also been used to determine the bilayer thickness. Specifically, it was found that there is a direct correlation between domain size and the mismatch in bilayer thickness of the coexisting liquid-ordered (L_O) and liquid-disordered (L_D) lipid phases, suggesting a dominant role for line tension in controlling domain size (Heberle *et al.*, 2013).

Most recently, in a major advance, a novel isotopic labeling strategy was used in the Gram-positive bacterium *B. subtilis* to investigate the nanoscale structure and organization of its plasma membrane *in vivo* (Nickels *et al.*, 2017). Through genetic and chemical manipulation of the organism, the membrane of the cell was independently labeled with specific amounts of hydrogen and deuterium. Moreover, the creation of neutron contrast in the plane of the membrane using hydrogenated and deuterated fatty acids enabled the detection of lipid domains smaller than 40 nm, consistent with the notion of lipid rafts. This is the first direct detection of rafts in living systems. However, in the recent membrane work the quality of the data and/or the scope of the experiments were limited by the unavailability of deuterated material: deuterated lipids in the case of the model system and deuterated fatty acids for the *in vivo* study.

In addition to lateral heterogeneity, biological membranes exhibit compositional asymmetry between their two leaflets (Fig. 10), and this asymmetry is actively driven by the machinery of the cell (Ikeda *et al.*, 2006). Model studies

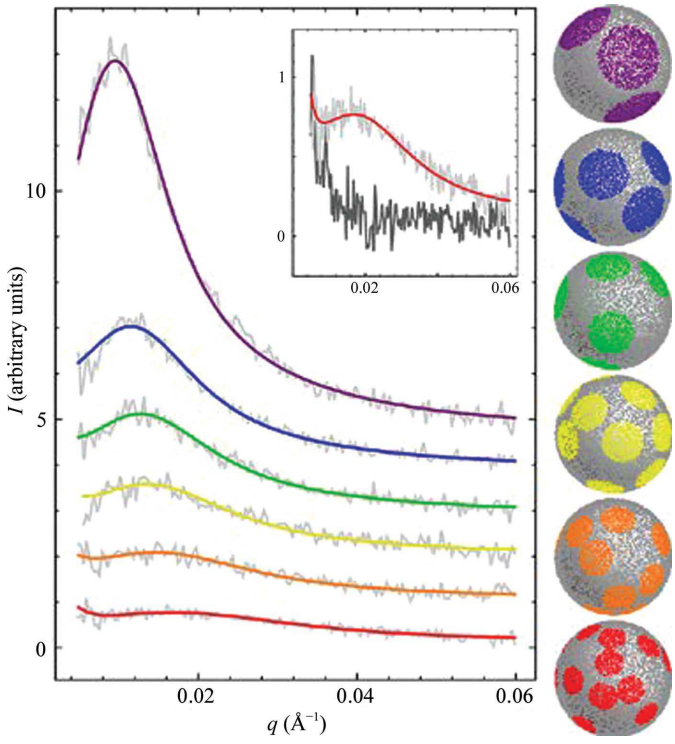

Figure 9
Monte Carlo fits to scattering data at 20°C. Left, scattering data (light gray lines) and best-fit curves (colored lines). Inset, the data and fit for samples at 20°C (light gray line) and 50°C (dark gray line) shown on an expanded scale. Right, examples of Monte Carlo vesicles from the best fit to the data of ULVs with different lipid compositions (Heberle *et al.*, 2013).

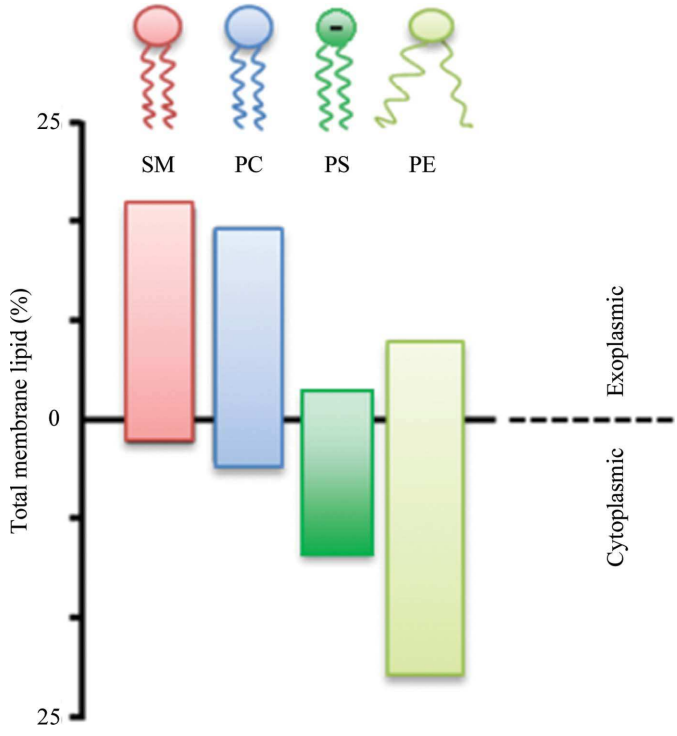

Figure 10
Distribution of lipids between the inner and outer leaflets of a mammalian plasma membrane.

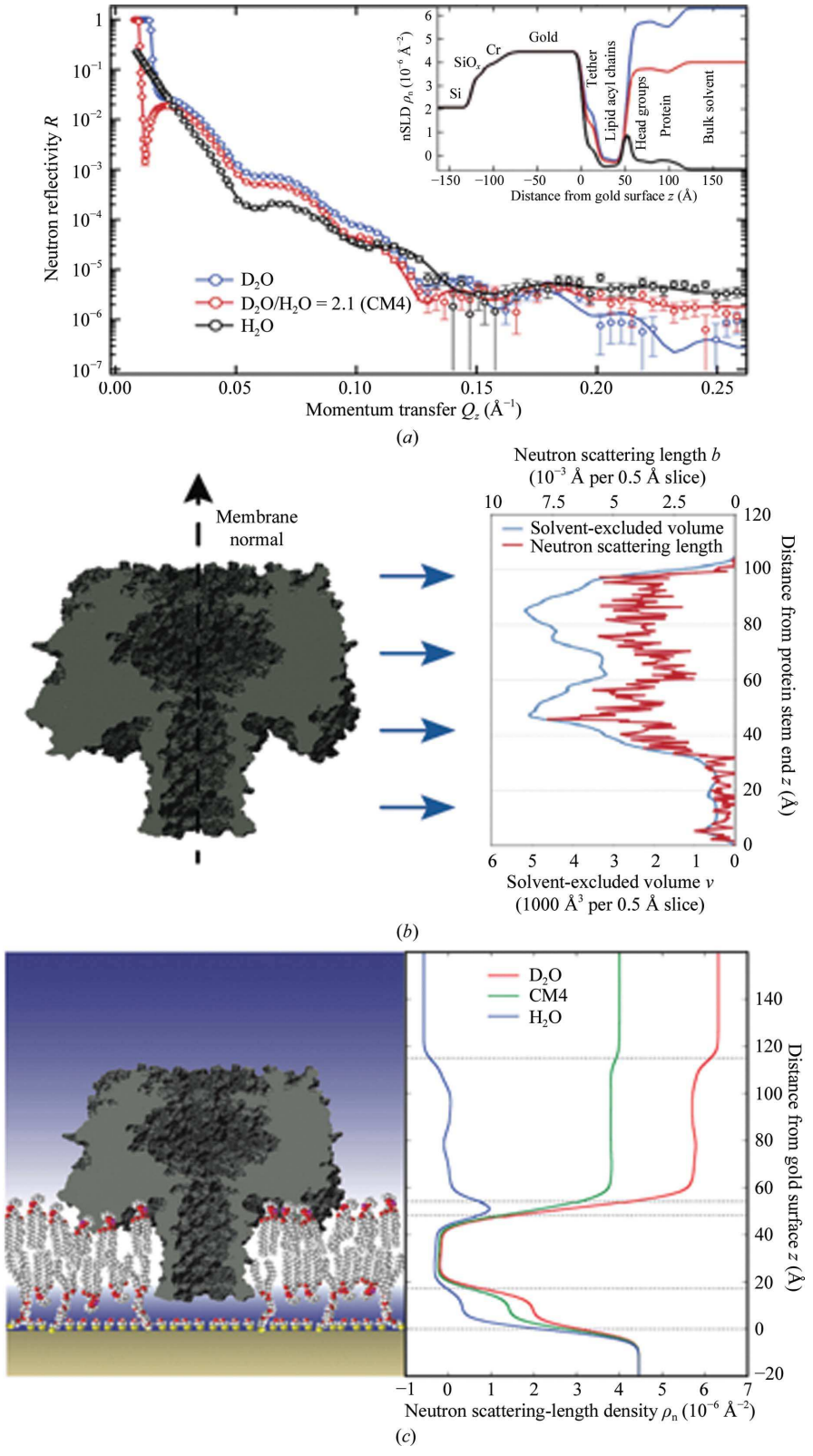

Figure 11
Determination of membrane-protein structures using NR. (*a*) Proteins embedded in a substrate-supported, in-plane fluid bilayer (lower left) are measured at various solvent contrasts. (*b*) Integrative modeling uses diverse sources of information, such as protein crystal structures, to model the NR data using rigid-body placement algorithms that determine the penetration depth and orientation of the protein in the membrane. (*c*) The final model that represents experimental data from NR at different contrasts, crystallographic, volumetric and chemical connectivity information, and thus describes the atomistic protein structure in the supported bilayer.

overwhelmingly still investigate symmetric membranes, despite concerns that they may overlook crucial aspects of membranes *in vivo*. Such membrane asymmetry is of high physiological relevance, directing transmembrane signaling events, including transmembrane transport processes that establish ion gradients. Recent SANS studies have been able to quantify the energetic cost of maintaining lipid-composition asymmetry in membranes (Wah *et al.*, 2017; Nakano *et al.*, 2007; Garg *et al.*, 2011; Breidigan *et al.*, 2017).

Advances towards the development of more realistic cell-membrane models have been hindered by the difficulty in preparing asymmetric vesicles (Heberle *et al.*, 2016) and the lack of tools and protocols for precisely quantifying their composition and degree of asymmetry. It is therefore not surprising that experimental data from asymmetric bilayers are scarce, and thus the effects of asymmetry on membrane structure and physical properties remain poorly understood. Today, there is much interest in the production of asymmetric membranes in a wide range of sample geometries, including supported and unsupported planar bilayers, and ULVs of various sizes. For example, SANS from isotopically asymmetric bilayers was used to determine the interaction between bilayer leaflets, and it was found that a disordered inner leaflet can partially fluidize ordered outer leaflet domains (Heberle *et al.*, 2016).

5.2.2. Structure of membrane-associated proteins. While the bilayer lipids provide the membrane with its organizational principles, it is generally accepted that proteins define its functional roles. In rare cases, single proteins provide specific functionality all on their own. However, most proteins work in concert with other proteins, either in homomeric or, more frequently, in heteromeric complexes. The association of proteins with fluid lipid bilayers can now be routinely studied by NR, and their conformational changes in response to external triggers (pH changes, voltage pulses or the addition of small-molecule ligands, partner proteins or nucleic acids) can be characterized on the molecular level,

including the effect that a protein can have on a lipid bilayer (Kent *et al.*, 2010; Jones *et al.*, 2012). It should also be pointed out that living cells have been interrogated by NR, specifically their adhesion properties on substrates (Junghans *et al.*, 2014).

The development of polymer-cushioned membranes (Majewski *et al.*, 1998; Wong *et al.*, 1999), and subsequently of substrate-supported membranes (McGillivray *et al.*, 2007) and novel molecular-modeling algorithms (Heinrich & Lösche, 2014; Shekhar *et al.*, 2011), have transformed NR (Fig. 11). Neutron scattering-length density (nSLD) profiles, determined by NR at various solvent contrasts using the same physical sample, with momentum transfers of up to Q_z = 0.25 Å^{-1}, are complemented with atomistic structure, volumetric and chemical information.

NR thus resolves the locations of proteins in membranes (McGillivray *et al.*, 2009; Shen *et al.*, 2014; Hoogerheide *et al.*, 2017) or lipid monolayers (Miller *et al.*, 2004, 2005) with ångstrom resolution and protein orientations to within a few degrees (Nanda *et al.*, 2010; Heinrich *et al.*, 2014). In addition, complementary studies using impedance spectroscopy (EIS), surface plasmon resonance (SPR) and fluorescence correlations (FCS) provide a comprehensive characterization of membrane quality, the thermodynamics of the proteins interacting with membranes and the dynamics of membranes and proteins. Using advanced deuteration schemes and integrative modeling of NR data, and together with the abovementioned complementary information, unique protein structures can be determined with ångstrom resolution, and the distribution of disordered protein segments can be characterized around the membrane surface or to the folded domains of the membrane-associated proteins.

Integration of such NR-derived protein–membrane profiles with large-scale MD simulations, which is currently under development in a collaboration between the NIST Center for Neutron Research (NCNR) and Oak Ridge National Laboratory (ORNL), is bringing the atomistic modeling of interfacial structures to a higher level of sophistication (Shenoy, Nanda *et al.*, 2012; Nanda *et al.*, 2015). Thus, differences between crystal structures and realistic structural ensembles in distinct environments become accessible, which can then be incorporated into three-dimensional models of protein–membrane complexes. With the selective deuteration of individual proteins or protein segments, membrane-associated protein complexes can be resolved (Yap *et al.*, 2015; Heinrich, 2016). Moreover, because of the robustness of the substrate-supported bilayer platform and the nondestructive nature of neutrons, using external stimuli one can sequentially track the conformational changes in membrane-associated proteins (Datta *et al.*, 2011). For example, recent work that determined the structural changes of a membrane-embedded voltage-gated protein channel as a function of applied membrane potential (Tronin *et al.*, 2014) highlights the potential of NR to characterize membrane-protein structures as a function of external triggers. To the best of our knowledge, no other structural biology technique has this capability. Recent application examples of the NR-based technologies described above include studies of the following.

(i) Cellular signaling events originating from membrane interfaces (Shenoy, Nanda *et al.*, 2012; Shenoy, Shekhar *et al.*, 2012).

(ii) The characterization of membrane-associated protein complexes and the structural determination of reaction partners within these complexes (McGillivray *et al.*, 2009; Yap *et al.*, 2015; Valincius *et al.*, 2008; Pfefferkorn *et al.*, 2012; Zimmermann *et al.*, 2017).

(iii) Molecular mechanisms that determine the morphogenesis of cellular organelles (Heinrich *et al.*, 2014).

(iv) The formation of capsid shells in nascent daughter particles of enveloped retrovirus (Nanda *et al.*, 2015; Datta *et al.*, 2011; Barros *et al.*, 2016; Eells *et al.*, 2017; O'Neil *et al.*, 2016).

5.2.3. Future developments. Sample throughput is a significant limitation of NR experiments. The CANDOR (Chromatic Analysis Neutron Diffractometer or Reflectometer) instrument, which is currently under construction at the NCNR, is one approach that has been taken to address this problem. CANDOR uses a broad neutron-wavelength band in the thermal spectrum of the cold source, instead of a single wavelength, which will boost the flux at the sample by two orders of magnitude and will be made available to the scientific community through the NSF-sponsored CHRNS program. Computer-controlled microfluidic sample handling is also needed to automate complex sample-manipulation schemes, enhancing the throughput of NR measurements. In addition, minimizing both the water reservoir adjacent to the membrane and the solid support structure will reduce incoherent scattering from the sample environment and dramatically increase the intrinsic resolution of the NR measurement. It has been shown that careful optimization of the sample environment can reduce the background to a level such that data can be recorded to momentum transfers as high as $Q_z \simeq$ 0.7 Å^{-1} (Krueger *et al.*, 2001), thus increasing the intrinsic resolution of NR measurements by a factor of three over what is performed currently.

5.2.4. Membrane dynamics. The energy resolution and accessible length/time scales of neutron spectroscopy enable

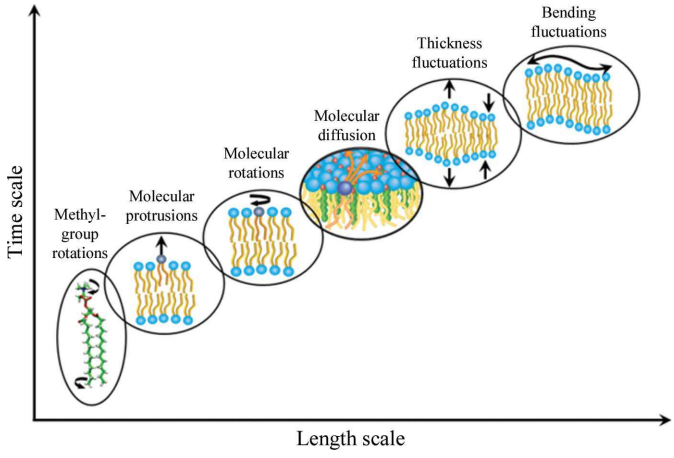

Figure 12
Hierarchical dynamical processes in membranes that can be studied with neutron scattering (provided by R. Ashkar).

studies of membrane dynamic phenomena such as molecular rotation and diffusion, as well as collective membrane fluctuations. Specifically, NSE and QENS enable measurements of membrane dynamics over a broad range of time scales at well defined length scales (Fig. 12). Combination with neutron contrast matching of specific chemical moieties in a sample enables these techniques to determine the hierarchy of dynamics in membranes and membrane-protein complexes.

Collective thermal fluctuations are dynamic modes intrinsic to self-assembled lipid membranes that are determined by their mechanical and viscoelastic properties. Such fluctuations are associated with important membrane properties, such as the repulsion between bilayers that prevents uncontrolled membrane fusion. They manifest themselves in two modes, specifically bending and thickness fluctuations. Thickness fluctuations, which were theoretically predicted in the 1980s, were seldom characterized prior to the advent of NSE and selective lipid deuteration. For example, with NSE, direct insights into stiffening/softening under the influence of drugs and changes in the membrane mechanical and viscoelastic properties with cholesterol content will be possible (Nagao *et al.*, 2017). These types of studies involving the mechanical properties of biological and bio-inspired membranes will be key in the development of functional synthetic membranes and drug-delivery methods.

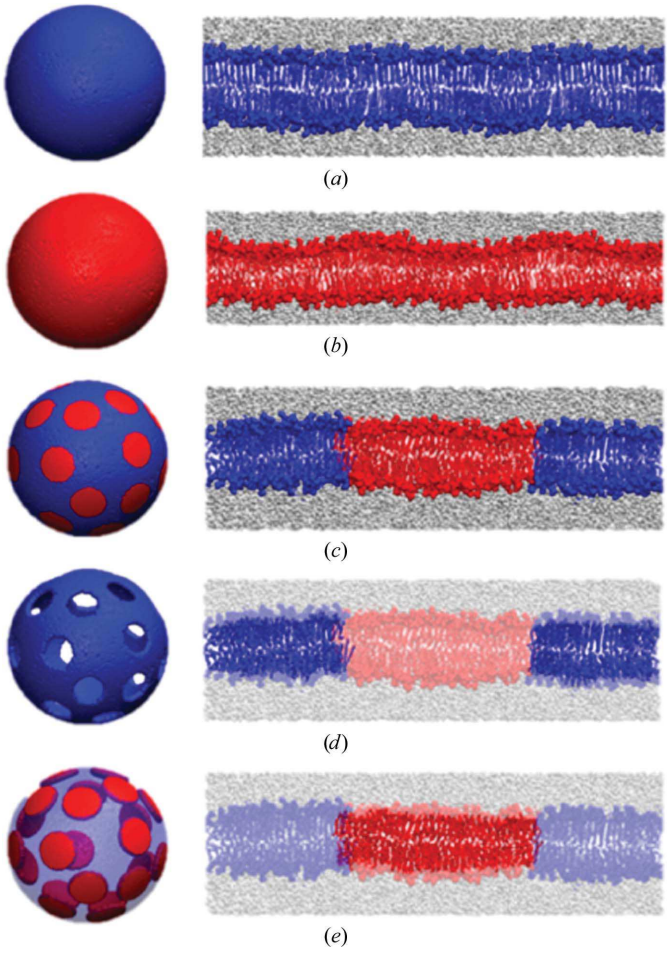

Figure 13
Difference contrast-matched ULVs. (*a*) L_O ULV. (*b*) L_D ULV. (*c*) L_O ULV with L_D nanodomains. (*d*) L_O ULV with contrast-matched L_D nanodomains. (*e*) L_D nanodomains with contrast-matched L_D surrounding (Nickels *et al.*, 2015)

Another notable example of neutron spectroscopy providing a unique and cutting-edge capability for understanding vital biological properties is the formation and the stability of lateral domains within phase-separating membranes. Among the contributions to the global free energy that drives phase separation is the difference in bending moduli between the L_O and L_D phases. NSE, selective deuteration and MD simulations are essential capabilities for determining the bending moduli of the different lipid phases in phase-separated membranes (Fig. 13). By combining these capabilities, it is possible to independently measure the bending modulus of L_O domains and the L_D lipid matrix in which they reside (Nickels *et al.*, 2015). When combined with all-atom MD simulations, molecular details of the domain interface can also be revealed, such as the preferential enrichment of a lipid species at the interface. Such studies can be extended to investigate the mechanical coupling between membrane compartments or individual bilayer leaflets in asymmetric membranes (Heberle *et al.*, 2016). However, to expand these types of membrane dynamics studies the following requirements must be met: (i) a more comprehensive catalog of deuterated biomolecules, (ii) improved all-atom MD simulations capable of addressing the current state-of-the-art NSE-accessible time scales (∼400 ns), such as might be achieved using Markov state modeling (Noé *et al.*, 2007), and (iii) NSE instrumentation capable of accessing time scales approaching 500 ns (Woodka *et al.*, 2012).

5.2.5. Next-generation force-field development and membrane dynamics. Because membranes are fluid and disordered, MD simulations have complemented experiments in understanding membrane structure, since structural measurements are limited in the detail that they can provide. However, when combined with scattering and spectroscopic techniques, MD simulations have revealed molecular details under physiologically relevant conditions that lead to observable structural features, such as the area per lipid, the membrane thickness, the compressibility and the chain order (Klauda *et al.*, 2010). Moreover, the same structural data have been used to refine the parameters (so-called 'force fields') that determine intramolecular and intermolecular interactions in MD simulations, with current efforts focused on improving transferability by including atomic polarizabilities and long-range dispersion interactions. This is currently an area of intense research that will continue into the foreseeable future.

The next generation of MD force fields will be tuned to reproduce the complex structure and dynamics of biomembranes discussed above. Because structural dynamics is intimately connected to understanding membrane signaling, its characterization represents a critical advance for the field. This is certainly true for the conformational transition rates of membrane-embedded signaling proteins, which are intimately coupled to membrane properties, and of the diffusive encounters of signaling partners, which are governed by

in-plane dynamics and lipid–protein interactions. Thus, measurements of lipid diffusion, the dynamics of membrane undulations and membrane viscosity will be targets for next-generation force fields.

On longer length scales other processes dominate. An emerging area of interest in cell biology is the maintenance of organelle structure and membrane composition. Most membranes found in the cell are asymmetric across the leaflets (see above) and include regions of high curvature [for example the Golgi and the endoplasmic reticulum (ER)]. Furthermore, the lipid composition differs dramatically across organelles: the ER contains very little cholesterol, while the plasma membrane contains up to 40 mol% cholesterol (Fig. 14). How are these differences maintained?

These areas of research are just now entering into the reach of MD simulation. A few asymmetric membrane simulations using all-atom models have been published (López Cascales *et al.*, 2006; He *et al.*, 2015), but there are very few experimental data to validate these simulations. Coarse-grained simulations of organelle structures (which resolve molecular interactions at reduced chemical accuracy) are beginning to appear (Perilla *et al.*, 2015). For the simulation field to advance and develop into a greatly anticipated highly predictive tool, new experimental measurements are needed. SANS is ideally suited to interrogate the structure of topologically complex organelles, as well as mimetic systems in which contrast is easily controlled. SANS from asymmetric vesicles is just beginning to reveal the molecular organization and balance of species across the bilayer leaflets (Eicher *et al.*, 2018). Time-resolved neutron scattering has recently revealed the dynamics of lipid transfer within and between membranes more directly than any previous measurement (Wah *et al.*, 2017). Acquiring such data from more complex systems will be essential for the development of the next generation of force fields.

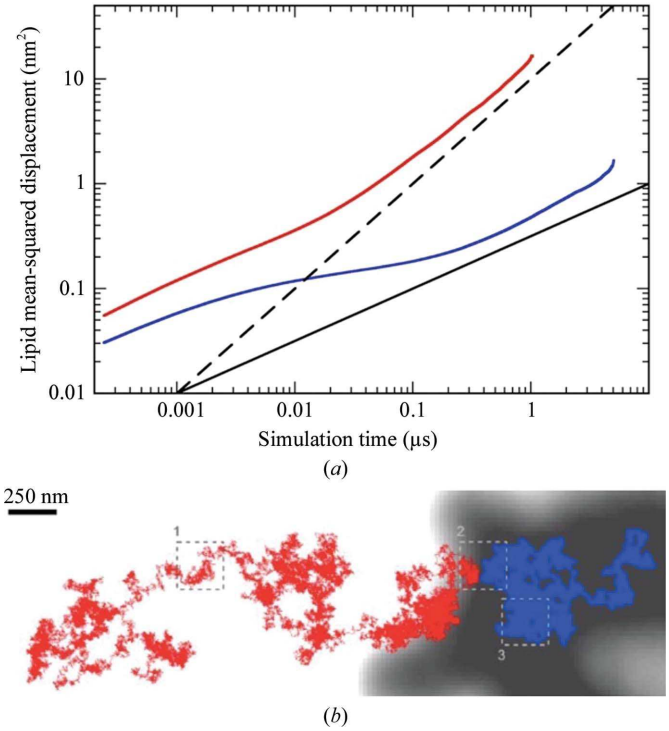

Figure 14
(*a*) Lipid mean-squared displacement scales sublinearly with time in cholesterol-rich membranes (red line) and linearly in more disordered membranes (blue). (*b*) A lipid trajectory as observed by iSCAT microscopy switches from normal diffusion (blue) to subdiffusion (red) when crossing a domain boundary into a cholesterol-rich phase (dark background).

5.3. Membranes and membrane proteins

Over one-third of the human genome is comprised of integral membrane proteins. These proteins mediate fundamental biological processes and represent a crucial class of drug targets. However, they remain underrepresented in the PDB. Study of these proteins by techniques such as MX, NMR and cryo-EM is confounded by an array of technical issues. However, SANS with contrast variation remains one of the most powerful techniques available to study the solution structures of protein–lipid and protein–detergent complexes.

There is broad overlap between the surface-sensitive scattering techniques described above and solution scattering techniques such as SANS and SAXS. SANS and neutron reflectometry (NR) can be used along with contrast variation to study the structures of both integral and peripheral membrane proteins, and their interactions with biomimetic membrane systems. However, while many structural biology researchers take advantage of complementary structural techniques, such as SAXS, they are often simply not aware of SANS or NR. SANS requires quantities of purified proteins comparable to those for crystallographic trials (1 mg per sample). Membrane-protein biochemists, biophysicists and structural biologists can readily take advantage of SANS and contrast variation to obtain coveted three-dimensional structural models of detergent-, vesicle-, bicelle- or nanodisc-stabilized membrane proteins (Bayburt *et al.*, 2002; Nath *et al.*, 2007; Ritchie *et al.*, 2009; Perera *et al.*, 2018) in solution and in complex with binding partners or substrates (Breyton *et al.*, 2013; Trewhella, 2006). The software required (Pérez & Koutsioubas, 2015) differs only slightly from the SAXS software that is familiar to structural biologists. The key in the experimental design is to ensure the proper use of contrast to obtain the signal from the membrane protein. The routine use of SANS to characterize membrane proteins would be transformative for the membrane-protein biochemistry field and have ripple effects from basic structure–function relationships to drug discovery and development.

To broaden the scope of membrane-protein determination by SANS, two technical improvements (Gimpl *et al.*, 2016; Oliver *et al.*, 2017; Midtgaard *et al.*, 2018) are needed.

(i) Deuterated lipids and detergents for precise contrast matching. Repositories of common deuterated detergents and lipids can accelerate the desired outcomes, and these repositories could include deuterated detergents or lipids commonly used to study membrane proteins (for example maltosides, glucosides of different alkyl-chain lengths and *N*,*N*-dimethyldodecylamine *N*-oxide, amongst others; Maric *et al.*, 2014). To achieve the true extinction of any scattering contribution from

detergents such as DDM, two refined approaches have very recently been developed and demonstrated on test cases involving different classes of membrane proteins. One method is to raise the CMP of the DDM micelle core to 48.5% D_2O to match the shell by precisely blending 44%(*w*/*v*) tail-deuterated DDM (d_{25}-DDM), which is commercially available (Anatrace), with regular DDM (Naing *et al.*, 2018; Oliver *et al.*, 2017). The second approach uses a single detergent species with partial deuterium substitutions on the alkyl chain and/or head group (Midtgaard Søren *et al.*, 2017). Under these complete matching conditions, scattering features from DDM micelles are rendered negligible

(ii) Nanodiscs. The characterization of protein-loaded lipid membrane nanodiscs bounded by hydrophobic membrane-scaffold proteins or synthetic polymers also has strong potential for synergistic studies. This novel class of membrane models is amenable to characterization by SANS but is currently under-utilized. There are established protocols to reconstitute transmembrane proteins into nanodiscs (Bayburt *et al.*, 2002; Nath *et al.*, 2007; Ritchie *et al.*, 2009), a protein class that is much more difficult to study in substrate-supported membranes, and owing to their small size and homogeneity these model systems are easily accessible to a large range of complementary methods, including solution NMR, cryo-EM and even all-atom MD simulations. So-called 'stealth' nanodiscs, prepared using both deuterated lipid and scaffold protein, are designed to be fully contrast-matched in 100% D_2O solvent (Maric *et al.*, 2014). This enables study of the membrane protein using the familiar data-analysis tools developed for soluble proteins. It is therefore expected that concentrated efforts on nanodisc-stabilized membrane-protein characterization in which SANS will play a leading role will significantly expand the reach of neutron-based methods in structural biology. The current under-utilization of these systems is mainly owing to the need for partially deuterated phospholipids in which the deuteration in the head and tail groups is carefully controlled to allow maximum contrast matching.

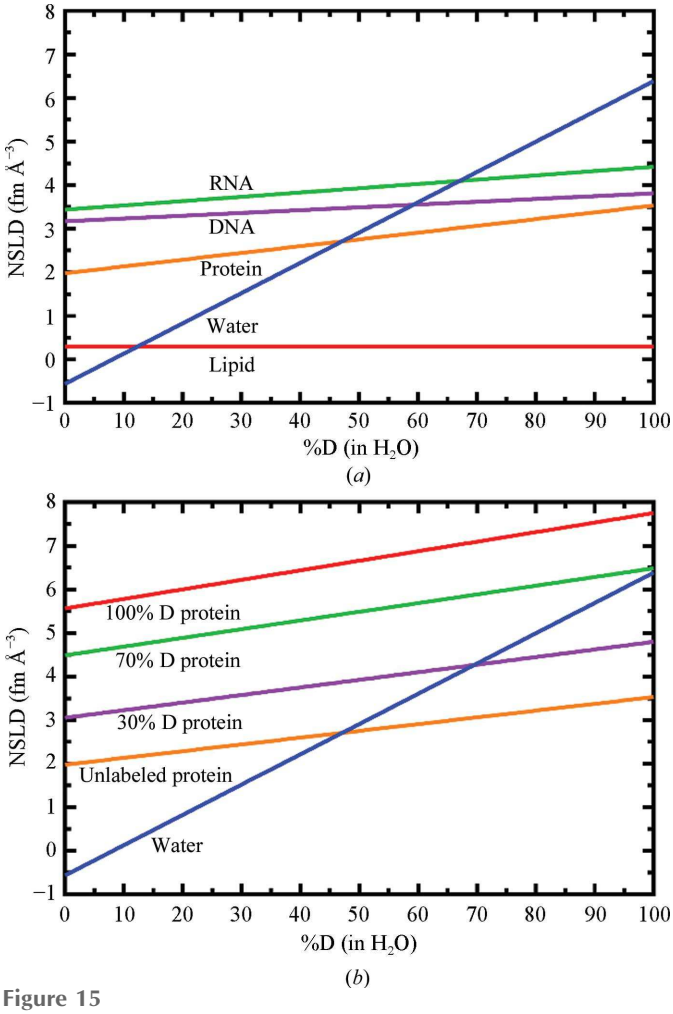

Figure 15
Neutron scattering-length density (NSLD) variation as a function of D_2O concentration in the aqueous phase. (*a*) The NSLDs of unlabeled biomolecules are such that significantly distinct contrast-match points exist for lipids, proteins and nucleic acids. (*b*) Uniform partial or total deuterium labeling of a protein increases the NSLD and allows selective matching of individual proteins with differing degrees of deuterium substitution.

6. Labeling

The marked differences between the interactions of neutrons with hydrogen and with its isotope deuterium (Sears, 1992; see Fig. 15) make H/D isotopic substitution a powerful tool for increasing the information content of biological neutron scattering studies across various techniques. The classic example of a small-angle neutron scattering (SANS) experiment with contrast variation readily demonstrates the power of H/D labeling. Fig. 15(*a*) shows how the neutron scattering-length densities (NSLDs) of different general classes of biomolecules vary as a function of D_2O concentration when the biomolecules are dissolved in an aqueous medium. The contribution of a biomolecule to the observed *q*-dependent scattering at small scattering angles is weighted by the difference between the NSLD of the molecule and the NSLD of the medium (also known as the contrast); therefore, the intersections of the NSLD curves in Fig. 15(*a*) indicate media conditions for which biomolecules are 'contrast-matched' and do not contribute to the measured *q*-dependent scattering from a sample. Multi-component samples comprising natural isotopic abundance (unlabeled) biomolecules from different classes, such as proteins within a lipid bilayer or protein–nucleic acid complexes, can be measured at different contrast-match points to observe the scattering arising from single components at a time or at various nonmatching contrasts to deconvolve the individual scattering contributions from each component and from the entire sample.

While the inherent NSLD contrast between different classes of biomolecules and aqueous media is sufficient to distinguish individual low-*q* scattering contributions without the use of H/D labeling, samples having multiple unique components from the same class of biomolecule require some degree of covalent deuterium labeling to increase the NSLD of one component to a distinct value. As shown in Fig. 15(*b*), uniform

covalent deuterium labeling of up to ∼70% total covalent hydrogens in a protein creates a contrast-match point distinct from the match point for unlabeled protein. Covalent labeling exceeding ∼70% deuterium increases the NSLD of the labeled protein to the point that its scattering can no longer be matched in aqueous media. The careful use of differing degrees of deuterium labeling, particularly in proteins, detergents and lipids, can enable sophisticated and tractable low-q scattering characterization of global protein conformation, protein–membrane interaction *etc.* in complex biological samples.

As discussed in the preceding sections, H/D labeling of biological molecules enables contrast-variation approaches for low-q scattering techniques, diffraction-signal enhancement for neutron protein crystallography (NPC) and dynamical signal enhancement (or masking) for quasi-elastic and inelastic neutron spectroscopies. In this section, various strategies for producing deuterium-labeled proteins, protein–detergent/lipid complexes, carbohydrate biopolymers and even entire bacterial cells for direct interrogation of biomolecular structure and dynamics *in vivo* using neutron scattering are discussed.

6.1. Protein-expression systems

6.1.1. Bacteria. Owing to its many advantages, *Escherichia coli* remains the primary host organism for heterologous protein production (Demain & Vaishnav, 2009). Heterologous protein-expression pipelines have been utilized for many years to accelerate production and testing in a variety of expression vectors (Peti & Page, 2007; Walhout *et al.*, 2000). This approach has allowed researchers to generate proteins with a variety of purification tags or fusion partners in a range of strains. Once a protein of interest has been selected for study by neutron scattering, cultivations typically need to be carried out on multi-litre scales to obtain sufficient material for scattering sample preparation. Traditional shake-flask methods can often be used, but the productivity of these cultures can occasionally limit their use (Rosano & Ceccarelli, 2014). This is especially true when deuterium-labeled protein is required. In such cases, minimal medium cultures are grown in various percentages of D_2O to control the deuterium-incorporation level of the expressed protein of interest (Hoopes *et al.*, 2015; Leiting *et al.*, 1998; Perkins, 1981). When high levels of deuteration are needed, the cells are first adapted to D_2O by subculturing into minimal medium with stepwise increases in the D_2O content (Paliy *et al.*, 2003). Once the cultures have adapted, fed-batch bioreactor cultivations are commonly used to overcome the limitations of shake-flask growth to generate sufficient quantities of deuterium-labeled biomass (Duff *et al.*, 2015; Haertlein *et al.*, 2016; Meilleur *et al.*, 2009).

Fed-batch cultivations produce adequate quantities of protein in many cases, but the inequivalence of cultivation parameters between the shaking incubator and the bioreactor can yield unpredictable results (Losen *et al.*, 2004). As the technologies continue to mature, there will be an opportunity to improve the protein-expression screening process. Micro-bioreactor systems have now been developed that possess a level of monitoring and process control that enables the rapid optimization of expression protocols (Funke, Buchenauer, Mokwa *et al.*, 2010; Funke, Buchenauer, Schnakenberg *et al.*, 2010). These microplate-based systems have been shown to be directly scalable to multi-litre culture volumes. Furthermore, the addition of microfluidics and automated liquid handling to a micro-bioreactor system creates a high-throughput platform that will allow the development of micro-scale screening protocols that can be rapidly translated to the production scale.

6.1.2. Yeast. Heterologous protein overexpression in deuterium-adapted *E. coli* has been an invaluable means of obtaining proteins with uniform or non-uniform partial covalent deuterium labeling or complete covalent deuterium labeling. However, prokaryotic expression hosts lack mechanisms for performing certain eukaryotic-like post-translational modifications (PTMs) such as N- and O-linked glycosylation. The results of high-throughput, genome-scale protein-expression efforts reflect the frequent unsuitability of *E. coli* as a host to express native-sequence, full-length and soluble eukaryotic proteins, with the success rates for eukaryotic proteins (satisfying the above three criteria) estimated to be ≤10%, while the success rates for bacterial and archeal proteins are estimated to be ≤50% (Braun & LaBaer, 2003; Gräslund *et al.*, 2008). *E. coli* strains engineered to overcome some challenges of heterologous eukaryotic protein expression (for example codon-usage bias, intracellular disulfide-bond formation, *etc.*) are available, as are characterized methods for solubilizing and even refolding *E. coli*-expressed proteins. Nonetheless, many eukaryotic proteins of interest for neutron scattering studies will be inaccessible without the continued development of methods for overexpressing D-labeled proteins in eukaryotic hosts.

Yeasts are appealing hosts for deuterium-labeled protein expression since they are eukaryotic microorganisms that can often be grown in defined inorganic media with minimal organic supplementation apart from the primary carbon source. As such, similar to deuterium labeling with *E. coli*, a majority of the required covalent deuterium label is incorporated from D_2O in the medium and the use of expensive deuterium-labeled medium supplements can be avoided. Yeasts are also biotechnologically relevant, with industrial-scale roles spanning from biofuel production to biopharmaceutical manufacturing (Steensels *et al.*, 2014). The long history of *Saccharomyces cerevisiae* research includes a report from 1962 of growth in 99.6% D_2O minimal medium supplemented with thiamine, inositol and pyridoxine derived from lysates of algae grown in D_2O medium (Mohan *et al.*, 1962). Shibata *et al.* (1995) successfully applied this approach to produce native *S. cerevisiae* phosphoglycerate kinase for study by nuclear magnetic resonance (NMR) spectroscopy. Despite this example from the early 1990s, there are few reported uses of *S. cerevisiae* as a host for producing deuterium-labeled protein for NMR studies and no examples for neutron scattering studies.

In contrast, the methylotrophic yeast *Pichia pastoris* (also known as *Komagataella pastoris* and *K. phaffii*) has been used to produce highly deuterium-enriched chitosan (Russell *et al.*, 2015), lipids (De Ghellinck *et al.*, 2014; Gerelli *et al.*, 2014; Luchini *et al.*, 2018) and cholesterol (Moulin *et al.*, 2018), and uniform partially deuterium-labeled heterologous eukaryotic proteins (Bodenheimer *et al.*, 2018; Dunne *et al.*, 2017) for neutron scattering studies. Each of the following is likely to have contributed to the choice of *P. pastoris* for producing deuterium-labeled materials: the high overexpression efficiencies of secreted and membrane-incorporated proteins per unit culture volume (Macauley-Patrick *et al.*, 2005), the low concentration of natively secreted proteins (Cregg *et al.*, 2000; Love *et al.*, 2016) and the ability to use relatively inexpensive D_4-labeled methanol as a carbon source. Progressive adaption of *P. pastoris* to >99% ^{2}H-enriched culture can yield a total cell mass comparable to that of unlabeled culture (De Ghellinck *et al.*, 2014), and the extracted components of the cell membrane and cell wall exhibit high deuterium incorporation (Russell *et al.*, 2015; De Ghellinck *et al.*, 2014). However, the overexpression yields of secreted heterologous proteins in partially deuterium-enriched conditions have typically not exceeded 10 mg protein per litre of culture, which contrasts strikingly with secreted protein yields, which often exceed 100 mg protein per litre of culture (and occasionally exceed 1 g protein per litre of culture) in unlabeled conditions (Macauley-Patrick *et al.*, 2005). [The singular report by Tomida *et al.* (2003) of secreted human serum albumin yields of 180 mg protein per litre of culture culture in 70% D_2O medium is a noteworthy exception.] The apparent disconnect between biomass accumulation and heterologous protein overexpression efficiencies warrants detailed investigation of deuterium-induced impediments to protein overexpression in *P. pastoris* as a possible path towards routinely obtaining hundreds of milligrams of recombinant deuterium-labeled proteins for neutron scattering within the constraints of laboratory production scales.

6.1.3. Eukaryotic cell lines. The high costs associated with formulating deuterated media suitable for mammalian cell cultures (Haertlein *et al.*, 2016; Takahashi & Shimada, 2010) coupled with the low (∼20–30%) level of D_2O enrichment tolerated by mammalian cell lines have prevented the production of deuterium-labeled protein for neutron scattering from mammalian expression hosts. Insect cell lines have been successfully employed as expression hosts to produce deuterium-labeled protein for NMR experiments. Kofuku *et al.* (2014) demonstrated that by formulating amino-acid-deficient media with a combination of unlabeled amino acids, deuterium-labeled amino acids (Ala, Tyr and Cys) and deuterium-enriched algal lysate yielded some deuterium incorporation in all residues of *E. coli* thioredoxin except Asn, Asp, Gln, Glu, His and Met. This success inspired other groups to demonstrate that highly deuterium-enriched algal or yeast lysates alone are sufficient to introduce a deuterium label into insect-cell-expressed proteins at sites and in quantities useful for NMR spectroscopy (Opitz *et al.*, 2015; Sitarska *et al.*, 2015).

6.2. *In vitro* approaches for protein labeling

6.2.1. Segmental labeling. The classical approach in SANS of using deuteration in combination with solvent-contrast variation (H_2O/D_2O exchange) has been to reconstitute macromolecular complexes from unlabeled and deuterium-labeled building blocks to characterize inter-subunit interactions. A textbook example are the ribosomal subunits (Capel *et al.*, 1987; Nierhaus *et al.*, 1983). However, many important biological proteins, in particular in eukaryotic systems, consist of multiple domains that are covalently connected by flexible linkers. As these proteins are expressed as single polypeptide chains, a simple labeling and reconstitution approach cannot be applied to interrogate inter-domain interactions. However, so-called 'segmental' labeling, in which individual domains within a single polypeptide chain are uniquely deuterium-labeled, is a labeling strategy that can enable studies of inter-domain interactions.

Segmental labeling requires that individual protein-domain constructs, including cognate terminal amino-acid sequences facing the linker region(s), are expressed separately with appropriate deuterium-label incorporation. Known ligating enzymes (for example sortase A; Freiburger *et al.*, 2015) are then used to fuse the distinct polypeptides into a single chain. Segmental labeling has been used for many years in NMR for the study of large multi-domain proteins (Xu *et al.*, 1999; Yamazaki *et al.*, 1998), but has only very recently been applied for the first time to provide information on relative domain arrangements in a binary protein–RNA complex involved in alternative splicing (Sonntag *et al.*, 2017). In this study, differently segmentally labeled proteins were bound to RNA and the constructs were measured by SAXS and SANS. The differently labeled constructs could be easily distinguished by their pair distribution function at the contrast-match point of the unlabeled protein component (*i.e.* 42% D_2O; Fig. 15). Moreover, it was shown that the differently labeled proteins allowed the conformational degrees of freedom to be restricted significantly and a clustered family of structures to be selected as the final model (Fig. 15). The SANS and segmental deuteration approach provides a powerful tool for the structural investigation of protein–protein or protein–RNA/DNA complexes when proteins are comprised of several domains connected by flexible linkers.

6.2.2. Residue-selective labeling. Similar to segmental labeling, amino-acid residue-selective deuterium-labeling schemes also afford novel neutron scattering experiments. In particular, SANS measurements of these labeled proteins can explore region-specific protein structure, which is fortuitous given the current growing interest in flexible and intrinsically disordered domains. Selective labeling combined with SANS can determine the localized conformational ensemble of such flexible regions within the context of the global structure of a protein. This represents an advancement over SAXS and SANS studies of isolated protein fragments, since the connection to the full-length protein can now be discerned. There have been only a few demonstrations of residue-selective labeling for scattering. A SANS study of maltose-binding protein with deuterium labels primarily served as a

feasibility study, with limited analysis being performed (Laux *et al.*, 2008). It mainly demonstrated that with a sufficient number of deuterated residues, the correlations between these labeled residues can be detected. An analogous type of selective labeling experiment with SAXS has also recently been shown. This X-ray specific labeling strategy has proved to be useful in an elastic incoherent neutron scattering experiment to specifically probe and compare the dynamics of the inner and outer regions of the calbindin-D9k protein (Wood *et al.*, 2013).

Looking forward, there is a great potential for selective labeling and SANS experiments to provide more useful distance constraints within protein structures. One simple application of residue-selective deuterium labeling for SANS would be to target protein regions enriched in certain residues. This is the case for many disordered proteins with domains of low sequence complexity. Labeling these amino acids throughout the protein would effectively yield a segmental label of the protein region where the residues are enriched and may be easier to achieve than true segmental labeling.

A more advanced application of the selective labeling technology is to provide correlations between multiple, specifically deuterated residues to yield more precise distance constraints on a structure. This can be especially valuable for challenging, flexible systems that exist as an ensemble. SANS contrast matching and variation on a selectively deuterated system can provide data sets that serve as additional structural constraints on these systems. The new information obtained is most powerful when combined with computations. Computations can be used to generate atomic models to compare with the SANS data, along with information from other biophysical techniques. The computational methods can then be refined, as needed, to accurately reproduce the experimental data. Ultimately, these refined atomic models may assist in understanding the molecular basis for many functions of disordered proteins.

6.3. Membranes and membrane-protein labeling

Biological neutron scattering studies of model lipid membrane systems are well established (Braun & LaBaer, 2003; Majkrzak *et al.*, 2006; Lakey, 2009; Fragneto & Gabel, 2013). Other than the ubiquitous variation of contrast using H_2O/D_2O media, until recently isotopic labeling had played only a minor role in low-q neutron scattering studies of membranes. The scattering contrast between protein (NSLD $\simeq 2 \times 10^{-6}$ Å^{-2}) and the hydrocarbon core of the lipid bilayer (NSLD $\simeq -0.5 \times 10^{-6}$ Å^{-2}) is sufficient to differentiate unlabeled proteinaceous material penetrating the lipid bilayer. Lipid deuteration therefore mostly finds applications in studies probing the bilayer structure itself (Vacklin *et al.*, 2005; Callow *et al.*, 2005) or involving small molecules and polymers that more closely match the NSLD of the hydrocarbons (Benedetto *et al.*, 2014). Lipid head-group regions contain ~50%(*v*/*v*) solvent, and any additional material in this region is readily distinguished using bulk-solvent NSLD variation. Using lipid molecules with deuterated tails (NSLD $\simeq 6 \times 10^{-6}$ Å^{-2}) doubles the contrast between unlabeled protein and lipid tails, yielding better characterization of transmembrane protein regions. However, the cost and effort of obtaining tail-deuterated lipids are prohibitive in most cases since most biomimetic membranes contain mixtures of mostly unsaturated lipids that are difficult to synthesize in their deuterated forms. Rather than synthesizing those lipids, some facilities consequently engage in the extraction of lipids from bacteria or yeasts grown in deuterated media (De Ghellinck *et al.*, 2014; Gerelli *et al.*, 2014).

Given the general difficulty of obtaining deuterium-labeled lipid and the general amenability of recombinant proteins to deuterium labeling, protein deuteration continues to dominate the applications of isotopic labeling to the study of membrane proteins and protein–lipid interactions. Increasing the number of known structures of solubilized membrane proteins is a substantial unmet need in structural biology. As discussed for lipids, unlabeled protein NSLDs differ significantly from the NSLDs of detergent aliphatic regions, providing contrast without the use of deuterium labeling. Unfortunately, also like lipids, detergents are typically comprised of chemically distinct tail- and head-group regions and self-assemble to form micelles or other structures with volumes equal to or greater than the molecular volume of the protein of interest. The chemical differences result in significantly different tail- and head-group NSLDs so that the detergent cannot be fully contrast-matched, and the large volume of the detergent aggregates allows the detergent to contribute substantially to the observed q-dependent scattering even under very low but nonzero contrast conditions. As such, even with average NSLD contrast matching using ~15–20% deuterated media, residual scattering from the detergent micelles can overwhelm the scattering from the protein of interest. Uniform deuterium labeling of the protein can increase the contribution of the protein to the observed scattering, but residual detergent scattering arising from both the protein–detergent complex and any remaining 'empty' detergent micelles would persist.

Recently, two sophisticated approaches to studying protein–detergent systems have been developed and demonstrated with test cases involving different classes of membrane protein to achieve precise contrast-matching of detergent scattering. One method is to raise the contrast-match point of the *n*-dodecyl-β-D-maltopyranoside (dodecyl maltoside; DDM) tail to equal that of the head group by precisely blending 44% (by mole) commercially available fully tail-deuterated DDM (d_{25}-DDM) into unlabeled DDM (Naing *et al.*, 2018; Oliver *et al.*, 2017). This mixture produces a detergent micelle for which both the core and shell can be contrast-matched by 48% deuterated aqueous medium. In this case, the NSLD of the H/D micelle nearly equals that of unlabeled protein, and using deuterium-labeled protein is necessary to measure protein scattering. The second approach uses a single detergent species, either DDM or octyl-β-D-glucopyranoside, with distinct amounts of partial deuterium labeling on the alkyl chain and on the head group to produce a detergent molecule with both tail- and head-group NSLDs equivalent to that of D_2O (Midtgaard *et al.*, 2018). In 100% deuterium buffers,

scattering from the detergent micelles is precisely contrast-matched, leaving only the q-dependent scattering contribution from unlabeled protein.

Protein-loaded, lipid membrane nanodiscs, bounded by either hydrophobic membrane-scaffold proteins or synthetic polymers, are model protein-containing membrane systems (Bayburt *et al.*, 2002; Nath *et al.*, 2007; Ritchie *et al.*, 2009) that are suitable for study not only by SANS but also by complementary methods, including NMR spectroscopy, cryo-electron microscopy and even all-atom molecular-dynamics simulations. So-called 'stealth' nanodiscs, prepared using both deuterium-labeled lipid and scaffold protein, are designed to be fully contrast-matched in 100% deuterated medium (Maric *et al.*, 2014) and can enable the study of a membrane protein using familiar data-analysis tools developed for soluble proteins since the 'membrane' has no q-dependent scattering contribution. Nanodisc systems are currently rarely used for SANS studies owing to the need for partially deuterated phospholipids in which the tail- and head-groups are carefully labeled to allow precise nanodisc contrast matching. Nonetheless, it is likely that SANS studies of 'stealth' nanodisc-stabilized membrane proteins will play an important role in expanding the reach of neutron scattering methods in structural biology.

6.4. Labeling for in-cell scattering studies

Examining the fundamental structure and processes of living cells at the nanoscale poses a unique analytical challenge, as cells are dynamic, chemically diverse and fragile (Nickels *et al.*, 2017). To overcome this, most investigators isolate single components, perform experiments *ex vivo* or resort to exogenous labels to enhance contrast and impart specificity. Neutron scattering provides some unique possibilities to undertake nanoscale investigations on intact living systems. Through genetic and chemical manipulation of some organisms, it is possible to specifically label individual cellular components with hydrogen and deuterium to extents that are detectable *via* neutron scattering without fatally altering the chemical composition of the cell.

This concept has been used to study the cell membrane and its organization in the bacterium *B. subtilis* (Nickels *et al.*, 2017). The cell membrane is a great example of nanoscale structure in a biological system: it is too small to be seen directly by optical microscopy and provides little observational contrast for other methods. *B. subtilis* is in turn an ideal *in vivo* model system for the application of neutron contrast-variation strategies. *B. subtilis* has a well studied lipid metabolism, is highly amenable to genetic manipulation and tolerates highly deuterium-enriched growth conditions. Through specific growth conditions and selected genotypes, it was possible to homogenize and match the cellular contrast globally and to precisely reintroduce contrast into the membrane. With the ability to control both the chemical and the isotopic properties of the membrane lipids, it was possible to interrogate both transverse and lateral membrane structure. The lamellar structure of the *B. subtilis* membrane was confirmed and an average hydrophobic thickness of 23.9 $\pm$ 0.9 Å was determined. This approach also revealed nanoscopic lateral membrane structures consistent with the notion of lipid domains or rafts. This definitively demonstrated the existence of lipid rafts based on the emergence of neutron contrast and was arguably the first observation of nanoscale lipid rafts in a microorganism.

The same general approach to selective contrast can potentially be extended to other biomolecules and other model organisms for applications outside the membrane arena. For instance, stable isotope labeling was used to overexpress protiated GroEL in deuterated *E. coli* cells, making it possible to study the dynamics of the protein *in cellulo* using quasi-elastic neutron scattering (QENS). QENS shows that the in-cell diffusion coefficient of GroEL was a factor of four slower than its diffusion coefficient in buffer solution and, importantly, the internal protein dynamics showed a relaxation time that was a factor of two slower compared with the protein in solution (Anunciado *et al.*, 2017). The *in vivo* experimental platform can be used to investigate the response of the plasma membrane to a diverse range of physical, chemical, genetic and environmental stimuli. Such a capability is likely to prove valuable in many areas, such as antibiotic development, biofuel production and membrane-protein function, and in understanding the interplay between the membrane, cytoskeleton and cell wall in creating a protective, adaptable and multifunctional interface.

Having said this, whole-cell labeling approaches must be undertaken with great care. *In vivo* measurements present unique challenges for establishing, proving and preserving the quality of scattering samples. The maintenance of the cells over the course of an experiment is not trivial. Neutron measurements are long, typically of the order of hours. Yet living cells are dynamic and change (or die) if placed in stressful environments such as oxygen deprivation or starvation. Parallel offline experiments can be a useful guide for determining valid experimental conditions. Also, it is likely to be best practice to use orthogonal methods to quantitatively verify the degree and location of labeling. Mass spectrometry is an ideal technique for such verification because the mass change associated with deuteration is readily detected. Verification might need to be repeated at time points throughout data collection to ensure that the labeling remains consistent, since the resulting ability to hold constant NSLDs for certain structures is an invaluable constraint in the modeling of data.

Finally, a comment regarding the choice of labeling targets. SANS samples in which the majority of the sample (calculated on the basis of volume fraction) is contrast-matched generally exhibit weak scattering intensity above background. Despite the capabilities of current SANS instruments, accurately measuring such weak scattering may require difficult or infeasible measurement times, sample volumes *etc.* A reasoned estimate of the expected scattering intensity would seem to be a very good step before undertaking the work of a complex labeling strategy on a living organism. Questions of how the desired structure will stand out from the rest of the cellular milieu in terms of the scattering profile and to what

degree the cell background can be minimized should be considered. (As an example, *B. subtilis* was used in part because it is a Gram-positive bacterium with only one cell membrane.) Experimental planning based upon such forward-looking considerations is vital for subsequent data analyses and, in the end, for drawing meaningful conclusions from the scattering experiment.

6.5. Polymer systems

There have been several reports of the biosynthesis of deuterium-labeled native biopolymers in bacteria and yeasts (Russell *et al.*, 2015). Deuterated cellulose from *Gluconacetobacter xylinus* has been studied to understand the fundamental properties of cellulose and for the development of composite materials to investigate polymer–polymer interactions (Bali *et al.*, 2013; He *et al.*, 2014; Martínez-Sanz, Gidley *et al.*, 2016; Martínez-Sanz *et al.*, 2015, 2017; Martínez-Sanz, Mikkelsen *et al.*, 2016; Raghuwanshi *et al.*, 2017; O'Neill *et al.*, 2017). Deuterated chitosan has been produced in *P. pastoris* for the characterization of chitosan blended with other carbohydrate molecules to enhance contrasting deuterated chitosan against the other components in the blend (Russell *et al.*, 2014). In other work, deuterated polyhydroxyalkanoate biopolyesters such as poly(3-hydroxybutyrate) poly(3-hydroxyoctanoate) have been synthesized by bacteria such as *Cupriavidus necator* (Yoshie *et al.*, 1992) and *Pseudomonas oleovorans* (Russell *et al.*, 2015). These labeled polymers can create structural contrast in polymer blends and composites and can also provide insight into the biosynthetic pathways.

Another area of interest that impacts biology-related neutron scattering experiments is the availability of deuterated synthetic polymers. Water-soluble polymers are excellent candidates for medical and environmental applications and for fundamental studies of polymer properties, enabling an understanding of the nanoscale to macroscale properties of these systems (Zhang & Hoogenboom, 2015; Kufelt *et al.*, 2015; Kozlovskaya *et al.*, 2015). Furthermore, understanding the interactions of synthetic polymers with biomolecules is of interest for applications such as the development of novel biohybrid materials and drug-delivery systems.

Currently, the synthesis of hydrophilic deuterated polymers is achieved by the synthesis of deuterated monomers followed by polymerization or post-polymerization H/D exchange. However, only a few deuterated monomers are currently commercially available. In addition, converting hydrogenated polymers requires harsh conditions and a transition-metal catalyst in deuterated solvents; this risks undesired changes to the polymer structure and necessitates secondary purification. Similar to the above, the availability of deuterated cross-linkers [such as glutaraldehyde (Linden *et al.*, 2016; Barbosa *et al.*, 2014) or ethylenediamine (Meng *et al.*, 2018; Zhang *et al.*, 2014)] are not available, which may limit neutron investigations of cross-linked structures or hydrophilic gel fabrication.

7. Neutron imaging

Neutron imaging provides a direct visualization of the distribution of protons in a sample owing to the penetrating power of neutrons in samples and the large variation of neutron absorptivity between protons and D atoms. This imaging is nondestructive and has provided insight into water–plant interactions, soil–water dynamics and plant–microbe interactions. Neutron radiography (nR) and computed tomography (nCT) provide a mesoscale imaging capability with a broad temporal range (from seconds to days) for biological applications (see below). Current attenuation-based imaging capabilities include a field of view of several square centimetres with a spatial resolution of approximately 50 µm at reactor sources. Most present research is focused on the below-ground soil–root interactions and the understanding of the rhizosphere water dynamics in two dimensions (Oswald *et al.*, 2008; Dhiman *et al.*, 2018), although there have been reports of medical applications such as bone–metal interfaces (Isaksson *et al.*, 2017) and soft-tissue imaging (Anderson *et al.*, 2009). Compared with engineering applications neutron imaging is underused in biology, although the potential impact of this technique in biology is immense.

7.1. Overview

nR and nCT are direct imaging methods that allow two-dimensional (and three-dimensional) visualization and quantification of features inside a biological system. This contrasts with, for example, small-angle neutron scattering (SANS), which can reconstruct the shape of biological molecules but in an indirect manner. Although the neutron imaging technique has seen a tremendous increase in use in materials science and engineering applications (Anderson *et al.*, 2009), it is seldom utilized for biology apart from root–soil interactions in plant physiology and a handful of biomedical applications. This is mostly owing to its limited achievable spatial resolution, which is only of the order of tens of micrometres. However, owing to their high sensitivity to light elements such as hydrogen (H), which is the principal contributor to neutron contrast in biological tissues, neutrons are well suited for biological and medical applications. Similarly to SANS, contrast enhancement can be applied in an area of the image or simply to increase transmission through a biological sample.

Recently, improvements in spatial resolution (in certain instances below 10 µm) and novel methods, such as neutron phase-contrast imaging, which measures the neutron phase shift in presence of a sample, have opened up capabilities that could potentially impact the field of biology (Allman *et al.*, 2000; Pfeiffer *et al.*, 2006; Pushin *et al.*, 2018).

7.2. Recent advances

In the past decades, neutron imaging has been extensively used by plant physiologists to study *in situ* below-ground plant behavior nondestructively, compared with previous endeavors which required destructive sampling or sensor utilization in the surrounding soil. Since the morphological development of a plant can be assessed by its tissue water distribution, nR and nCT can provide unique water-distribution maps in and around a plant root system at a spatial resolution of approximately 50–100 µm. Areas of research include root–soil

interaction (in and close to the rhizosphere; Carminati *et al.*, 2010; Moradi *et al.*, 2011), root growth (Nakanishi *et al.*, 2003; Oswald *et al.*, 2008), redistribution of water within roots (Warren *et al.*, 2013), the effect of mucilage on water flow (Kroener *et al.*, 2014), drought events (see Fig. 16; Holz *et al.*, 2018; Dhiman *et al.*, 2018) and root response to soil poisoning (Furukawa *et al.*, 1999).

Compared with nCT, nR is capable of acquiring radiographs in seconds and thus can be used to investigate rapid processes such as water uptake in a root. In contrast, nCT can provide the three-dimensional mapping capability needed for complex root systems. However, nCTs usually require a few hours of exposure, and thus any real-time observation of water movement is difficult without sacrificing spatial resolution for flux, as recently reported (Tötzke *et al.*, 2017).

Similarly to magnetic resonance imaging (MRI), neutrons are ideally suited to measure hydrogen-rich biological tissues, with the advantage that higher spatial resolution can be achieved with neutrons. In theory, MRI can reach a similar spatial resolution as nCT, but this requires magnets that are capable of producing magnetic fields of several tesla, which represents a technical challenge for medical imaging devices. Human exposure to high magnetic fields is also not well understood. A recent medical application focuses on understanding studies of lung physiology and respiratory therapy. *Ex situ* inflated rat lungs were measured in three dimensions without the need for tissue preparation or contrast media (Metzke *et al.*, 2011). Lung structures such as lobes and distal airways were visible in the nCT, as illustrated in Fig. 17. Another recent medical application studied the hydration mechanism involved in the setting of glass ionomer cements (GICs), which are promising materials for dental restoration. The role of water in the formation of a hydrated inorganic network needs to be understood to improve the strength of these cements. Multimodal CT scans using X-rays and neutrons were used to study the relationship between micrometre-sized pores/cracks and water. During the aging of the cement, the presence of water measured using neutrons was observed in these microstructures mapped with X-rays. Indeed, water is absorbed in the GIC and expands the material, creating cracks and thus reducing the strength of the material (Benetti *et al.*, 2015).

Bone–metal interfaces are difficult to measure with X-ray computed tomography (xCT). X-rays are highly attenuated by metals and thus xCT suffers from strong metal artifacts that mask the bone–metal interface (Isaksson *et al.*, 2017), as

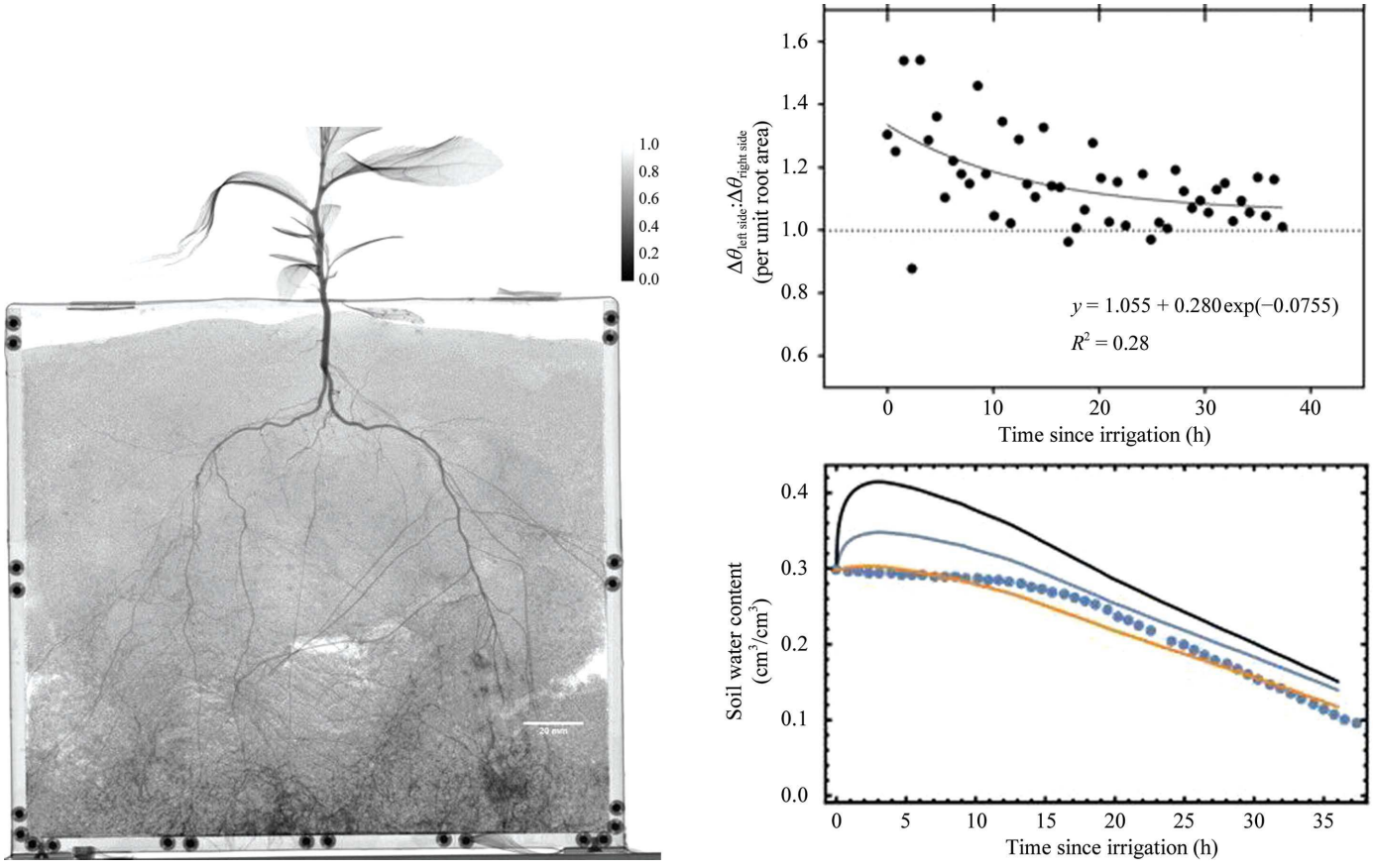

Figure 16
Left: 11-week-old poplar seedling in sand. The intensity indicates the water content. Greater initial water uptake per unit root area is observed for the left side (of the chamber), which has younger, finer diameter roots. Right: water content based on measured NR (circles) or forward modeling using measured (black) or alternate (blue, orange) soil saturated hydraulic conductivities (Dhiman *et al.*, 2018). In these studies, nR links root water uptake to characteristic root traits and can assess the performance of common water-uptake models.

illustrated in Fig. 18. The microstructure bone ingrowth was quantified using nCT in the peri-implant region, where the bone volume fraction (BVF) was 38% compared with the tracebular bone region.

Manufacturing processes in the biopharmaceutical industry can also benefit from neutron imaging capabilities, as demonstrated by De Bardi *et al.* (2018). Pre-filled syringes (PFS) are used as the primary container for drug products (DP) such as in auto-injectors and vaccines. Neutron imaging provided information on the interaction of high concentrations of DP and PFS during accelerated storage conditions with temperatures above the recommended storage temperature and with selected relative humidity values. Water vapor outgassing from DP and through the rigid needle shield resulted in a progressive loss of water from the DP solution and thus clogging within the needle.

7.3. Innovative opportunities

7.3.1. High spatial resolution. Although neutron imaging surpasses medical imaging modalities in spatial resolution, it is still behind xCT for pathology applications. Dedicated efforts are needed to obtain a high-resolution detector (less than 5 µm) with a reasonable field of view (∼1 × 1 cm). Recently, a detector design that comprises a fiber-optic taper oriented such that it provides magnification power has been published (Morgano *et al.*, 2018). The team were able to obtain a spatial resolution of 11 µm over a field of view of 5.5 × 6.5 mm and a limited dynamic range using a gadolinium-based scintillator. The acquisition time was 300 s over this field of view. However, this is a one-off system and efforts are required to enable routine high-resolution measurements at worldwide user facilities with a higher dynamic range or grayscale sensitivity.

7.3.2. Multimodal imaging. There is an untapped potential to use neutron imaging techniques for large-scale biological systems such as the examples listed in the section above. Because radiography is capable of mapping *in situ* kinetic changes in biological systems nondestructively, the technique can provide unique insight into organism interactions such as the bacterial colonization of a plant root network, subsurface water resource competition between different plant species or with fungi, nutrient fluxes *etc.* However, the present spatial resolution of neutron imaging is a limiting factor. Thus, there is a clear advantage to combining neutrons with other non-destructive techniques such as X-ray imaging, which can provide root morphology at the micrometre scale. Combined

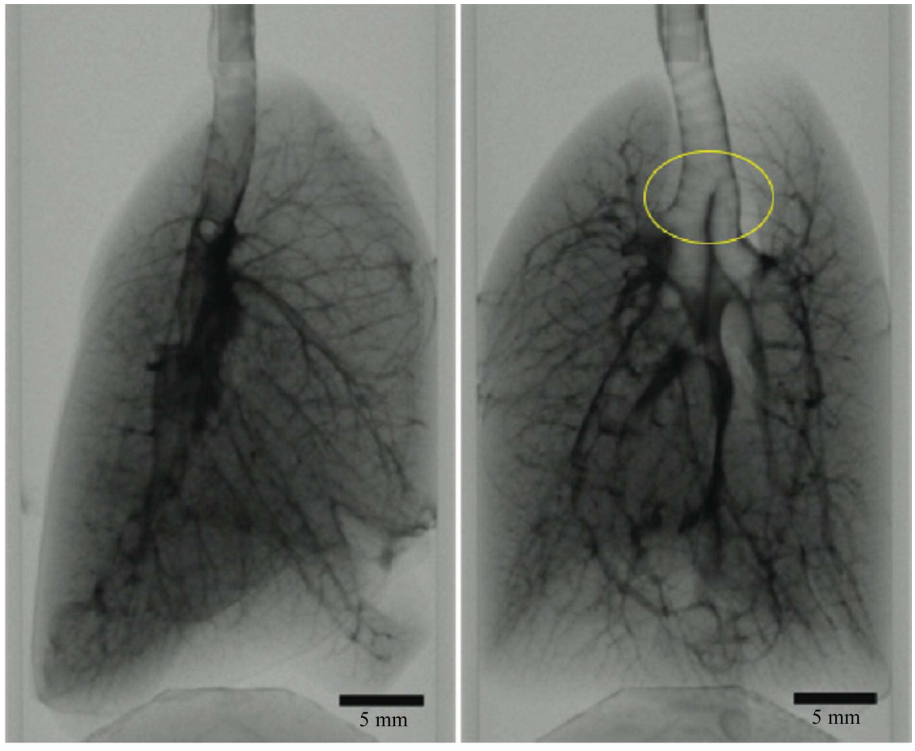

Figure 17
Left: photograph of a rat lung at the neutron beamline. Right: lateral and frontal neutron radiographs of the lung showing the lung physiology such as the trachea, lobes and airways (Metzke *et al.*, 2011). The spatial resolution was approximately 50–60 µm. The yellow ellipse indicates the first bifurcation. Videos of the nCT data are available at http://iopscience.iop.org/article/10.1088/0031-9155/56/1/N01/data#.

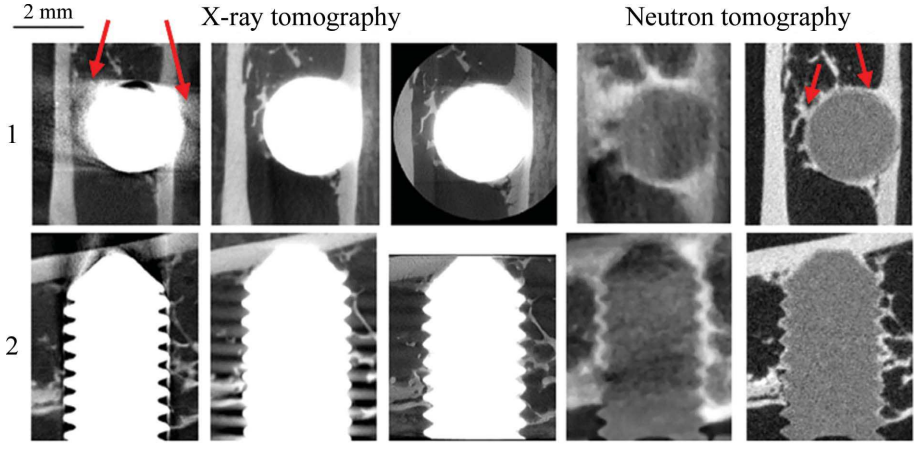

Figure 18
Comparison between xCT and nCT. In xCT the interface between bone and metal is masked by strong artifacts owing to metal attenuation (red arrows, left side). On the contrary, nCT is able to visualize the thin interface between bone and metal (red arrows, right side).

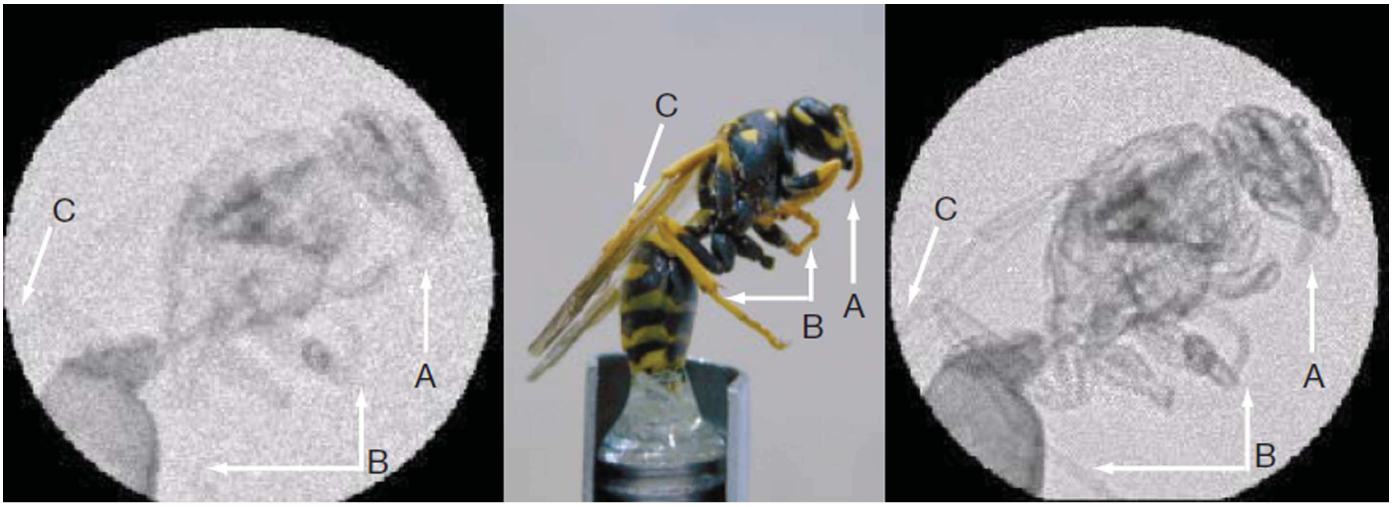

(*a*) (*b*) (*c*)

Figure 19
(*a*) Conventional neutron radiograph of the wasp displayed in (*b*). In comparison, the phase-contrast imaging in (*c*) shows significantly increased contrast and edge/interface details such as the antenna (labeled A), leg (labeled B) and wing (labeled C) (Allman *et al.*, 2000).

multimodal imaging has had a significant impact on the field of medical research with, for example, PET-CT and its capability to scan both bones and soft tissue or to provide combined anatomical and functional capabilities for clinical oncology (Beyer *et al.*, 2000).

7.3.3. Contrast and labeling. There is a great and largely untapped potential for the use of neutrons in biomedical imaging using isotopically labeled marker compounds. Medical compounds incorporating neutron-absorbing isotopes can be targeted to specific organs, such as the heart, to enable neutron imaging of anatomical structure and organ function as well as to deliver radiation doses specifically to tumor sites. Such a system could provide higher resolution images than PET and more precision in targeting disease. Neutrons may also be used with water-stable small-particulate gadolinium oxide nanoparticles (SPGOs) for targeted or nontargeted contrast enhancement. Neutron imaging through metal, for example stents and other metallic objects used for biological purposes, is possible. Small-animal imaging studies, isotopic imaging and targeted contrast-enhanced imaging are all potential applications.

7.3.4. Neutron phase and dark-field imaging. A technique that can provide significant impact in the field of biology is incontestably neutron phase imaging. Neutron phase imaging is based on measurement of the real part of the refraction index of the sample. This is enabled by creating a highly coherent source and increasing the distance between the defining beam aperture and the detector where the radiograph is formed (Beyer *et al.*, 2000). This can also be achieved by using a grating interferometry system. In the past few years, European facilities have implemented grating interferometry systems at their neutron imaging beamlines, but the focus has mostly been on materials science and engineering, and sometimes physics-based applications. The results are an enhanced contrast of biological tissues, as illustrated in Fig. 19.

The grating interferometry system also provides high angular resolution, which can be exploited to detect ultrasmall angular scattering (USANS) effects. This technique, called dark-field imaging (DFI), measures structures of between ∼500 nm and a few micrometres. Combining neutron imaging with SANS and DFI can offer unprecedented multi-length scales from the molecular to the system level.

7.3.5. Multi-spectral imaging. Neutron energies higher than the typical thermal neutrons from reactor sources will be required to image larger biological specimens. The range of a neutron is determined by the mean free path. For example, the mean free path for a thermal neutron in human brain tissue is 0.46 cm, whereas the mean free path for a 10 MeV neutron is 10.8 cm. Spallation sources provide a uniquely easily 'tuned' neutron source for tissues, eliminating the need for only thin slices as now required by reactor neutron sources. Preliminary dose estimates would indicate doses for *in vivo* animal imaging that would be comparable to those for xCT.

8. Conclusions

As quantitative research in the biological sciences continues to break barriers at a blistering pace, the amount and variety of data being produced has lead to calls to resort to machine-learning and data-driven methods to move forward. However, biology can only be understood when it is seen in three dimensions and as a function of time, and it is here where the relatively low throughput of neutron scattering techniques will occupy a distinctive niche in the future. Neutrons, being nondestructive, reach the parts that other radiations cannot reach, and by providing label-induced information on the location of specific types of atom, molecule and domain can help piece together the jigsaws of structure needed to understand function. Moreover, by the exchange of thermal energies being close to the incident energies of neutrons, dynamic neutron scattering has few competitors as a direct probe of global atomic and molecular motions.

Some of the machinery needed to stimulate future advances may, at first sight, appear to be rather mundane. For example,

innovations that reduce sample requirements are needed. Many of the most interesting model systems rely upon challenging expression systems, limiting the quantity of sample available and the ability to deuterate sufficient quantities. The broadcast of best practices would benefit both the existing larger community and inexperienced users. While the X-ray community has matured considerably in recent years with published guidance on best experimental practices, including publication standards, similar guidelines have not been published for neutrons. This would help to elevate the quality and reproducibility of neutron studies. Also, there is a varied understanding of the requirements for sample management among the neutron community. Specific guidelines could be established and published to guide the resources made available to experimentalists at general user facilities. This includes standards for adjoining wet laboratory facilities, sample-storage requirements (*i.e.* refrigeration), sample preparation, quantitation and quality-control requirements (*i.e.* FPLCs, UV–Vis spectrophotometers, light scattering, SEC-MALS, centrifugation), and sample management immediately after completion of the experiment. Finally, while publications have recently established guidelines for the presentation of coarse-grained and atomistic modeling of single models against neutron data, fewer best-practice guidelines are available for newer computational techniques, such as ensemble modeling of SAS data, especially when experimental contrast is available. As these analytical approaches continue to mature and become more sophisticated (for example the use of MD simulations), dissemination of best practices and procedures will be important to the development of neutron scattering.

Notwithstanding, the progress of biological neutron scattering over the past years has been remarkable. Neutron crystallography, combined with quantum-mechanics/molecular-mechanics (QM/MM) simulations, is providing answers to detailed questions on binding and reaction mechanisms. Solution scattering is deriving configurational distributions of flexible systems, which themselves have assumed increased importance in assessments of biological function. Membrane work has provided the first direct detection of lipid rafts in a living cell, and dynamic studies have probed global protein motions in detail. In parallel, a highly significant development is the integration of molecular-simulation tools to interpret neutron scattering profiles. Additional improvements in instrumental capabilities include dynamic nuclear polarization, which offers a sample environment that improves the ratio of coherent to incoherent scattering, machine learning is being paired with Rietveld analysis, and computer modeling that is combined with X-ray and neutron data provides more effective and efficient structure refinement. New phasing methods are being developed, such as the use of anomalous dispersion to determine experimental phases of protein crystal structures. New beamlines at the European Spallation Source and the planned second target station at the Spallation Neutron Source (SNS) also offer new capabilities, including improved structural and time resolution. The ability to selectively deuterate segments ('segmental labeling') of complexes is a powerful new tool for neutron scattering that provides insights that are difficult to obtain using other methods. Additional promising capabilities include multimodal sample environments that enable the simultaneous measurement of neutron scattering and complementary experimental techniques, and combined small-angle, wide-angle and grazing-incidence neutron scattering on a single sample. Time-resolved and neutron scattering studies coupled with molecular-dynamics simulation and Markov state modeling have potential for understanding the allosteric and kinetic pathways of complexes and provide a basis for the predictive modeling of larger living systems. *In vivo* neutron scattering studies of living organisms and cells, using genetic manipulation to create deuterated specific components, and macroscopic imaging are exciting developments that provide a completely new platform for structural and dynamic studies of components and processes.

Mathematical and computational approaches, software and new neutron technologies will fuel the continued expansion of neutron scattering in biology. We expect that neutrons will play a role in addressing many of the future challenges in understanding complex biological systems as part of a larger integrated structural biology approach that involves the seamless integration of information from different experimental techniques across length and time scales, and across different information types. This information will then couple with the dynamic visualization and multi-scale simulation of complete living cells and microorganisms. Having the best tools, used by excellent scientists, to tackle the largest problems will enable neutrons to be used in a transformative way to unify the structural and dynamical description of biological systems across a broad range of length and time scales. We expect this approach to transition the concept of a predictive understanding of biological systems to reality.

Acknowledgements

The authors thank the National Science Foundation for funding the workshop that led to this article. The workshop was chaired by Jeremy C. Smith and Mark Dadmun. The attendees thank Adam Green and Lora Davis for logistical support. This manuscript has been authored by UT-Battelle LLC under Contract No. DE-AC05-00OR22725 with the US Department of Energy. The United States Government retains and the publisher, by accepting the article for publication, acknowledges that the United States Government retains a non-exclusive, paid-up, irrevocable, worldwide license to publish or reproduce the published form of this manuscript, or allow others to do so, for United States Government purposes. The Department of Energy will provide public access to these results of federally sponsored research in accordance with the DOE Public Access Plan (http://energy.gov/downloads/doe-public-access-plan).

References

Abragam, A. & Goldman, M. (1978). *Rep. Prog. Phys.* **41**, 395–467.
Adams, P. D., Afonine, P. V., Bunkóczi, G., Chen, V. B., Echols, N., Headd, J. J., Hung, L. W., Jain, S., Kapral, G. J., Grosse-Kunstleve,

R. W., McCoy, A. J., Moriarty, N. W., Oeffner, R. D., Read, R. J., Richardson, D. C., Richardson, J. S., Terwilliger, T. C. & Zwart, P. H. (2011). *Methods*, **55**, 94–106.
Adams, P. D., Mustyakimov, M., Afonine, P. V. & Langan, P. (2009). *Acta Cryst.* D**65**, 567–573.
Afonine, P. V., Mustyakimov, M., Grosse-Kunstleve, R. W., Moriarty, N. W., Langan, P. & Adams, P. D. (2010). *Acta Cryst.* D**66**, 1153–1163.
Agapov, A. L., Kolesnikov, A. I., Novikov, V. N., Richert, R. & Sokolov, A. P. (2015). *Phys. Rev. E Stat. Nonlin. Soft Matter Phys.* **91**, 022312.
Aggarwal, M., Kovalevsky, A. Y., Velazquez, H., Fisher, S. Z., Smith, J. C. & McKenna, R. (2016). *IUCrJ*, **3**, 319–325.
Al-Ayoubi, S. R., Schummel, P. H., Golub, M., Peters, J. & Winter, R. (2017). *Phys. Chem. Chem. Phys.* **19**, 14230–14237.
Alberts, B. (2011). *Science*, **333**, 1200.
Allman, B. E., McMahon, P. J., Nugent, K. A., Paganin, D., Jacobson, D. L., Arif, M. & Werner, S. A. (2000). *Nature (London)*, **408**, 158–159.
Alongi, K. S. & Shields, G. C. (2010). *Annu. Rep. Comput. Chem.* **6**, 113–138.
Anderson, I. S., McGreevy, R. L. & Bilheux, H. Z. (2009). Editors. *Neutron Imaging and Applications*, pp. 987–980. New York: Springer.
Anunciado, D. B., Nyugen, V. P., Hurst, G. B., Doktycz, M. J., Urban, V., Langan, P., Mamontov, E. & O'Neill, H. (2017). *J. Phys. Chem. Lett.* **8**, 1899–1904.
Armstrong, C. L., Häussler, W., Seydel, T., Katsaras, J. & Rheinstädter, M. C. (2014). *Soft Matter*, **10**, 2600–2611.
Artero, J.-B., Härtlein, M., McSweeney, S. & Timmins, P. (2005). *Acta Cryst.* D**61**, 1541–1549.
Arzt, S., Campbell, J. W., Harding, M. M., Hao, Q. & Helliwell, J. R. (1999). *J. Appl. Cryst.* **32**, 554–562.
Azadmanesh, J., Trickel, S. R., Weiss, K. L., Coates, L. & Borgstahl, G. E. O. (2017). *Acta Cryst.* F**73**, 235–240.
Bacik, J.-P., Mekasha, S., Forsberg, Z., Kovalevsky, A. Y., Vaaje-Kolstad, G., Eijsink, V. G. H., Nix, J. C., Coates, L., Cuneo, M. J., Unkefer, C. J. & Chen, J. C.-H. (2017). *Biochemistry*, **56**, 2529–2532.
Bai, X.-C., McMullan, G. & Scheres, S. H. W. (2015). *Trends Biochem. Sci.* **40**, 49–57.
Bali, G., Foston, M. B., O'Neill, H. M., Evans, B. R., He, J. & Ragauskas, A. J. (2013). *Carbohydr. Res.* **374**, 82–88.
Ball, P. (2011). *Nature (London)*, **474**, 272–274.
Balog, E., Becker, T., Oettl, M., Lechner, R., Daniel, R., Finney, J. & Smith, J. C. (2004). *Phys. Rev. Lett.* **93**, 028103.
Bancaud, A., Huet, S., Daigle, N., Mozziconacci, J., Beaudouin, J. & Ellenberg, J. (2009). *EMBO J.* **28**, 3785–3798.
Banco, M. T., Mishra, V., Ostermann, A., Schrader, T. E., Evans, G. B., Kovalevsky, A. & Ronning, D. R. (2016). *Proc. Natl Acad. Sci. USA*, **113**, 13756–13761.
Barbosa, O., Ortiz, C., Berenguer-Murcia, A., Torres, R., Rodrigues, R. C. & Fernandez-Lafuente, R. (2014). *RSC Adv.* **4**, 1583–1600.
Barrett, A. B., Murphy, M., Bruno, M. A., Noirhomme, Q., Boly, M., Laureys, S. & Seth, A. K. (2012). *PLoS One*, **7**, e29072.
Barros, M., Heinrich, F., Datta, S. A. K., Rein, A., Karageorgos, I., Nanda, H. & Lösche, M. (2016). *J. Virol.* **90**, 4544–4555.
Bashford, D. & Karplus, M. (1990). *Biochemistry*, **29**, 10219–10225.
Bayburt, T. H., Grinkova, Y. V. & Sligar, S. G. (2002). *Nano Lett.* **2**, 853–856.
Beaucage, G. (1996). *J. Appl. Cryst.* **29**, 134–146.
Beck, M. & Baumeister, W. (2016). *Trends Cell Biol.* **26**, 825–837.
Benedetto, A., Heinrich, F., Gonzalez, M. A., Fragneto, G., Watkins, E. & Ballone, P. (2014). *J. Phys. Chem. B*, **118**, 12192–12206.
Benetti, A. R., Jacobsen, J., Lehnhoff, B., Momsen, N. C., Okhrimenko, D. V., Telling, M. T., Kardjilov, N., Strobl, M., Seydel, T., Manke, I. & Bordallo, H. N. (2015). *Sci. Rep.* **5**, 8972.
Bennett, B., Langan, P., Coates, L., Mustyakimov, M., Schoenborn, B., Howell, E. E. & Dealwis, C. (2006). *Proc. Natl Acad. Sci. USA*, **103**, 18493–18498.
Beyer, T., Townsend, D. W., Brun, T., Kinahan, P. E., Charron, M., Roddy, R., Jerin, J., Young, J., Byars, L. & Nutt, R. (2000). *J. Nucl. Med.* **41**, 1369–1379.
Blakeley, M. P. (2009). *Crystallogr. Rev.* **15**, 157–218.
Bodenheimer, A. M., O'Dell, W. B., Oliver, R. C., Qian, S., Stanley, C. B. & Meilleur, F. (2018). *Biochim. Biophys. Acta*, **1862**, 1031–1039.
Bodenheimer, A. M., O'Dell, W. B., Stanley, C. B. & Meilleur, F. (2017). *Carbohydr. Res.* **448**, 200–204.
Boura, E., Rózycki, B., Herrick, D. Z., Chung, H. S., Vecer, J., Eaton, W. A., Cafiso, D. S., Hummer, G. & Hurley, J. H. (2011). *Proc. Natl Acad. Sci. USA*, **108**, 9437–9442.
Braun, P. & LaBaer, J. (2003). *Trends Biotechnol.* **21**, 383–388.
Breidigan, J. M., Krzyzanowski, N., Liu, Y., Porcar, L. & Perez-Salas, U. (2017). *J. Lipid Res.* **58**, 2255–2263.
Breyton, C., Gabel, F., Lethier, M., Flayhan, A., Durand, G., Jault, J.-M., Juillan-Binard, C., Imbert, L., Moulin, M., Ravaud, S., Härtlein, M. & Ebel, C. (2013). *Eur. Phys. J. E*, **36**, 71.
Brunger, A. T. (2007). *Nature Protoc.* **2**, 2728–2733.
Brünger, A. T., Adams, P. D., Clore, G. M., DeLano, W. L., Gros, P., Grosse-Kunstleve, R. W., Jiang, J.-S., Kuszewski, J., Nilges, M., Pannu, N. S., Read, R. J., Rice, L. M., Simonson, T. & Warren, G. L. (1998). *Acta Cryst.* D**54**, 905–921.
Bu, Z., Biehl, R., Monkenbusch, M., Richert, R. & Callaway, D. J. E. (2005). *Proc. Natl Acad. Sci. USA*, **102**, 17646–17651.
Calandrini, V., Hamon, V., Hinsen, K., Calligari, P., Bellissent-Funel, M.-C. & Kneller, G. R. (2008). *Chem. Phys.* **345**, 289–297.
Callow, P., Fragneto, G., Cubitt, R., Barlow, D., Lawrence, M. & Timmins, P. (2005). *Langmuir*, **21**, 7912–7920.
Campbell, J. W., Hao, Q., Harding, M. M., Nguti, N. D. & Wilkinson, C. (1998). *J. Appl. Cryst.* **31**, 496–502.
Capel, M., Engelman, D., Freeborn, B., Kjeldgaard, M., Langer, J., Ramakrishnan, V., Schindler, D., Schneider, D., Schoenborn, B. & Sillers, I. (1987). *Science*, **238**, 1403–1406.
Carminati, A., Moradi, A. B., Vetterlein, D., Vontobel, P., Lehmann, E., Weller, U., Vogel, H.-J. & Oswald, S. E. (2010). *Plant Soil*, **332**, 163–176.
Casadei, C. M., Gumiero, A., Metcalfe, C. L., Murphy, E. J., Basran, J., Concilio, M. G., Teixeira, S. C. M., Schrader, T. E., Fielding, A. J., Ostermann, A., Blakeley, M. P., Raven, E. L. & Moody, P. C. E. (2014). *Science*, **345**, 193–197.
Chen, J. C.-H., Hanson, B. L., Fisher, S. Z., Langan, P. & Kovalevsky, A. Y. (2012). *Proc. Natl Acad. Sci. USA*, **109**, 15301–15306.
Cherhal, F., Cousin, F. & Capron, I. (2015). *Langmuir*, **31**, 5596–5602.
Chevrot, G., Hinsen, K. & Kneller, G. R. (2013). *J. Chem. Phys.* **139**, 154110.
Christensen, A. S., Kubař, T., Cui, Q. & Elstner, M. (2016). *Chem. Rev.* **116**, 5301–5337.
Chu, X.-Q., Mamontov, E., O'Neill, H. & Zhang, Q. (2012). *J. Phys. Chem. Lett.* **3**, 380–385.
Coates, L., Cuneo, M. J., Frost, M. J., He, J., Weiss, K. L., Tomanicek, S. J., McFeeters, H., Vandavasi, V. G., Langan, P. & Iverson, E. B. (2015). *J. Appl. Cryst.* **48**, 1302–1306.
Coates, L., Erskine, P. T., Wood, S. P., Myles, D. A. A. & Cooper, J. B. (2001). *Biochemistry*, **40**, 13149–13157.
Coates, L. & Robertson, L. (2017). *J. Appl. Cryst.* **50**, 1174–1178.
Cobo, I., Li, M., Sumerlin, B. S. & Perrier, S. (2015). *Nature Mater.* **14**, 143–159.
Coskun, Ü. & Simons, K. (2011). *Structure*, **19**, 1543–1548.
Cregg, J. M., Cereghino, J. L., Shi, J. & Higgins, D. R. (2000). *Mol. Biotechnol.* **16**, 23–52.
Curtis, J. E., Nanda, H., Khodadadi, S., Cicerone, M., Lee, H. J., McAuley, A. & Krueger, S. (2012). *J. Phys. Chem. B*, **116**, 9653–9667.
Curtis, J. E., Raghunandan, S., Nanda, H. & Krueger, S. (2012). *Comput. Phys. Commun.* **183**, 382–389.

Cuypers, M. G., Mason, S. A., Blakeley, M. P., Mitchell, E. P., Haertlein, M. & Forsyth, V. T. (2013). *Angew. Chem. Int. Ed.* **52**, 1022–1025.
Cuypers, M. G., Mason, S. A., Mossou, E., Haertlein, M., Forsyth, V. T. & Mitchell, E. P. (2016). *Sci. Rep.* **6**, 31487.
Dajnowicz, S., Johnston, R. C., Parks, J. M., Blakeley, M. P., Keen, D. A., Weiss, K. L., Gerlits, O., Kovalevsky, A. & Mueser, T. C. (2017). *Nature Commun.* **8**, 955.
Dante, S., Hauss, T., Brandt, A. & Dencher, N. A. (2008). *J. Mol. Biol.* **376**, 393–404.
Datta, S. A. K., Heinrich, F., Raghunandan, S., Krueger, S., Curtis, J. E., Rein, A. & Nanda, H. (2011). *J. Mol. Biol.* **406**, 205–214.
Deacon, A., Gleichmann, T. J., Kalb (Gilboa), A. J., Price, H., Raftery, J., Bradbrook, G., Yariv, J. & Helliwell, R. (1997). *Faraday Trans.* **93**, 4305–4312.
De Bardi, M., Müller, R., Grünzweig, C., Mannes, D., Rigollet, M., Bamberg, F., Jung, T. & Yang, K. (2018). *Eur. J. Pharm. Biopharm.* **127**, 104–111.
Demain, A. L. & Vaishnav, P. (2009). *Biotechnol. Adv.* **27**, 297–306.
Dhiman, I., Bilheux, H., DeCarlo, K., Painter, S. L., Santodonato, L. & Warren, J. M. (2018). *Plant Soil*, **424**, 73–89.
Dhindsa, G. K., Bhowmik, D., Goswami, M., O'Neill, H. M., Mamontov, E., Sumpter, B. G., Hong, L., Ganesh, P. & Chu, X.-Q. (2016). *J. Phys. Chem. B*, **120**, 10059.
Dhindsa, G., Tyagi, M. S. & Chu, X.-Q. (2014). *J. Phys. Chem. B*, **118**, 10821–10829.
Di Costanzo, L., Moulin, M., Haertlein, M., Meilleur, F. & Christianson, D. W. (2007). *Arch. Biochem. Biophys.* **465**, 82–89.
Dixit, M., Das, S., Mhashal, A. R., Eitan, R. & Major, D. T. (2016). *Methods Enzymol.* **577**, 251–286.
Doktorova, M., Heberle, F. A., Dzikovski, B., Chandrasekaran, S., Katsaras, J., Feigenson, G. & Weinstein, H. (2018). *Biophys. J.* **114**, 604a.
Doster, W., Cusack, S. & Petry, W. (1989). *Nature (London)*, **337**, 754–756.
Duff, A. P., Wilde, K. L., Rekas, A., Lake, V. & Holden, P. J. (2015). *Methods Enzymol.* **565**, 3–25.
Dunne, O., Weidenhaupt, M., Callow, P., Martel, A., Moulin, M., Perkins, S., Haertlein, M. & Forsyth, V. (2017). *Eur. Biophys. J.* **46**, 425–432.
Eells, R., Barros, M., Scott, K. M., Karageorgos, I., Heinrich, F. & Lösche, M. (2017). *Biointerphases*, **12**, 02D408.
Eicher, B., Marquardt, D., Heberle, F. A., Letofsky-Papst, I., Rechberger, G. N., Appavou, M.-S., Katsaras, J. & Pabst, G. (2018). *Biophys. J.* **114**, 146–157.
Englander, S. W., Sosnick, T. R., Englander, J. J. & Mayne, L. (1996). *Curr. Opin. Struct. Biol.* **6**, 18–23.
Erlkamp, M., Marion, J., Martinez, N., Czeslik, C., Peters, J. & Winter, R. (2015). *J. Phys. Chem. B*, **119**, 4842–4848.
Farago, B., Li, J., Cornilescu, G., Callaway, D. J. & Bu, Z. (2010). *Biophys. J.* **99**, 3473–3482.
Fenimore, P. W., Frauenfelder, H., McMahon, B. H. & Parak, F. G. (2002). *Proc. Natl Acad. Sci. USA*, **99**, 16047–16051.
Fernandez-Castanon, J., Bomboi, F., Rovigatti, L., Zanatta, M., Paciaroni, A., Comez, L., Porcar, L., Jafta, C. J., Fadda, G. C., Bellini, T. & Sciortino, F. (2016). *J. Chem. Phys.* **145**, 084910.
Fisher, S. J. & Helliwell, J. R. (2008). *Acta Cryst.* A**64**, 359–367.
Fisher, S. J., Wilkinson, J., Henchman, R. H. & Helliwell, J. R. (2009). *Crystallogr. Rev.* **15**, 231–259.
Fisher, S. Z., Kovalevsky, A. Y., Domsic, J. F., Mustyakimov, M., McKenna, R., Silverman, D. N. & Langan, P. A. (2010). *Biochemistry*, **49**, 415–421.
Fisher, S. Z., von Schantz, L., Håkansson, M., Logan, D. T. & Ohlin, M. (2015). *Biochemistry*, **54**, 6435–6438.
Fitter, J., Gutberlet, T. & Katsaras, J. (2006). *Neutron Scattering in Biology: Techniques and Applications.* Berlin, Heidelberg: Springer-Verlag.
Fragneto, G. & Gabel, F. (2013). *Eur. Phys. J. E*, **86**, 81.
Frauenfelder, H., Chen, G., Berendzen, J., Fenimore, P. W., Jansson, H., McMahon, B. H., Stroe, I. R., Swenson, J. & Young, R. D. (2009). *Proc. Natl Acad. Sci. USA*, **106**, 5129–5134.
Frauenfelder, H., Young, R. D. & Fenimore, P. W. (2017). *Proc. Natl Acad. Sci. USA*, **114**, 5130–5135.
Freiburger, L., Sonntag, M., Hennig, J., Li, J., Zou, P. & Sattler, M. (2015). *J. Biomol. NMR*, **63**, 1–8.
Funke, M., Buchenauer, A., Mokwa, W., Kluge, S., Hein, L., Müller, C., Kensy, F. & Büchs, J. (2010). *Microb. Cell Fact.* **9**, 86.
Funke, M., Buchenauer, A., Schnakenberg, U., Mokwa, W., Diederichs, S., Mertens, A., Müller, C., Kensy, F. & Büchs, J. (2010). *Biotechnol. Bioeng.* **107**, 497–505.
Furukawa, J., Nakanishi, T. & Matsubayashi, M. (1999). *Nucl. Instrum. Methods Phys. Res. A*, **424**, 116–121.
Gainaru, C., Agapov, A. L., Fuentes-Landete, V., Amann-Winkel, K., Nelson, H., Köster, K. W., Kolesnikov, A. I., Novikov, V. N., Richert, R., Böhmer, R., Loerting, T. & Sokolov, A. P. (2014). *Proc. Natl Acad. Sci. USA*, **111**, 17402–17407.
Gao, M., Arns, L. & Winter, R. (2017). *Angew. Chem.* **56**, 2302–2306.
Garg, S., Porcar, L., Woodka, A. C., Butler, P. D. & Perez-Salas, U. (2011). *Biophys. J.* **101**, 370–377.
Gaspar, A. M., Busch, S., Appavou, M. S., Haeussler, W., Georgii, R., Su, Y. & Doster, W. (2010). *Biochim. Biophys. Acta*, **1804**, 76–82.
Gaus, M., Cui, Q. & Elstner, M. (2012). *J. Chem. Theory Comput.* **7**, 931–948.
Gerelli, Y., de Ghellinck, A., Jouhet, J., Laux, V., Haertlein, M. & Fragneto, G. (2014). *Acta Cryst.* D**70**, 3167–3176.
Gerlits, O., Campbell, J. C., Blakeley, M. P., Kim, C. & Kovalevsky, A. (2018). *Biochemistry*, **57**, 1833–1837.
Gerlits, O., Keen, D. A., Blakeley, M. P., Louis, J. M., Weber, I. T. & Kovalevsky, A. (2017). *J. Med. Chem.* **60**, 2018–2025.
Gerlits, O., Wymore, T., Das, A., Shen, C. H., Parks, J. M., Smith, J. C., Weiss, K. L., Keen, D. A., Blakeley, M. P., Louis, J. M., Langan, P., Weber, I. T. & Kovalevsky, A. (2016). *Angew. Chem. Int. Ed.* **55**, 4924–4927.
Gerlits, O. O., Coates, L., Woods, R. J. & Kovalevsky, A. (2017). *Biochemistry*, **56**, 4747–4750.
Ghellinck, A. de, Schaller, H., Laux, V., Haertlein, M., Sferrazza, M., Maréchal, E., Wacklin, H., Jouhet, J. & Fragneto, G. (2014). *PLoS One*, **9**, e92999.
Gimpl, K., Klement, J. & Keller, S. (2016). *Biol. Proced. Online*, **18**, 4.
Goh, G. B., Hulbert, B. S., Zhou, H. & Brooks, C. L. (2014). *Proteins*, **82**, 1319–1331.
Golden, E., Yu, L.-J., Meilleur, F., Blakeley, M. P., Duff, A. P., Karton, A. & Vrielink, A. (2017). *Sci. Rep.* **7**, 40517.
Goupil-Lamy, A. V., Smith, J. C., Yunoki, J., Parker, S. F. & Kataoka, M. (1997). *J. Am. Chem. Soc.* **119**, 9268–9273.
Gräslund, S., Nordlund, P., Weigelt, J., Hallberg, B. M., Bray, J., Gileadi, O., Knapp, S., Oppermann, U., Arrowsmith, C., Hui, R., Ming, J., dhe-Paganon, S., Park, H. W., Savchenko, A., Yee, A., Edwards, A., Vincentelli, R., Cambillau, C., Kim, R., Kim, S. H., Rao, Z., Shi, Y., Terwilliger, T. C., Kim, C. Y., Hung, L. W., Waldo, G. S., Peleg, Y., Albeck, S., Unger, T., Dym, O., Prilusky, J., Sussman, J. L., Stevens, R. C., Lesley, S. A., Wilson, I. A., Joachimiak, A., Collart, F., Dementieva, I., Donnelly, M. I., Eschenfeldt, W. H., Kim, Y., Stols, L., Wu, R., Zhou, M., Burley, S. K., Emtage, J. S., Sauder, J. M., Thompson, D., Bain, K., Luz, J., Gheyi, T., Zhang, F., Atwell, S., Almo, S. C., Bonanno, J. B., Fiser, A., Swaminathan, S., Studier, F. W., Chance, M. R., Sali, A., Acton, T. B., Xiao, R., Zhao, L., Ma, L. C., Hunt, J. F., Tong, L., Cunningham, K., Inouye, M., Anderson, S., Janjua, H., Shastry, R., Ho, C. K., Wang, D., Wang, H., Jiang, M., Montelione, G. T., Stuart, D. I., Owens, R. J., Daenke, S., Schütz, A., Heinemann, U., Yokoyama, S., Büssow, K. & Gunsalus, K. C. (2008). *Nature Methods*, **5**, 135.
Gruene, T., Hahn, H. W., Luebben, A. V., Meilleur, F. & Sheldrick, G. M. (2014). *J. Appl. Cryst.* **47**, 462–466.

Guogui, L., Xiaodong, Z. & Qiang, C. (2003). *J. Phys. Chem. B*, **107**, 8643–8653.
Habash, J., Raftery, J., Nuttall, R., Price, H. J., Wilkinson, C., Kalb (Gilboa), A. J. & Helliwell, J. R. (2000). *Acta Cryst.* D**56**, 541–550.
Habash, J., Raftery, J., Weisgerber, S., Cassetta, A., Lehmann, M. S., Høghøj, P., Wilkinson, C., Campbell, J. W. & Helliwell, J. R. (1997). *Faraday Trans.* **93**, 4313–4317.
Haertlein, M., Moulin, M., Devos, J. M., Laux, V., Dunne, O. & Forsyth, V. T. (2016). *Methods Enzymol.* **566**, 113–157.
Harms, M. J. & Thornton, J. W. (2013). *Nature Rev. Genet.* **14**, 559–571.
Harris, R. J., Shire, S. J. & Winter, C. (2004). *Drug Dev. Res.* **61**, 137–154.
Haupt, M., Blakeley, M. P., Fisher, S. J., Mason, S. A., Cooper, J. B., Mitchell, E. P. & Forsyth, V. T. (2014). *IUCrJ*, **1**, 429–438.
Hazemann, I., Dauvergne, M. T., Blakeley, M. P., Meilleur, F., Haertlein, M., Van Dorsselaer, A., Mitschler, A., Myles, D. A. A. & Podjarny, A. (2005). *Acta Cryst.* D**61**, 1413–1417.
He, J., Pingali, S. V., Chundawat, S. P. S., Pack, A., Jones, A. D., Langan, P., Davison, B. H., Urban, V., Evans, B. & O'Neill, H. (2014). *Cellulose*, **21**, 927–936.
He, X., Lin, M., Sha, B., Feng, S., Shi, X., Qu, Z. & Xu, F. (2015). *Sci. Rep.* **5**, 12808.
Heberle, F. A., Doktorova, M., Goh, S. L., Standaert, R. F., Katsaras, J. & Feigenson, G. W. (2013). *J. Am. Chem. Soc.* **135**, 14932–14935.
Heberle, F. A., Marquardt, D., Doktorova, M., Geier, B., Standaert, R. F., Heftberger, P., Kollmitzer, B., Nickels, J. D., Dick, R. A., Feigenson, G. W., Katsaras, J., London, E. & Pabst, G. (2016). *Langmuir*, **32**, 5195–5200.
Heinrich, F. (2016). *Methods Enzymol.* **566**, 211–230.
Heinrich, F. & Lösche, M. (2014). *Biochim. Biophys. Acta*, **1838**, 2341–2349.
Heinrich, F., Nanda, H., Goh, H. Z., Bachert, C., Lösche, M. & Linstedt, A. D. (2014). *J. Biol. Chem.* **289**, 9683–9691.
Helliwell, J. R. (1997). *Nature Struct. Biol.* **4**, 874–876.
Helliwell, J. R., Habash, J., Cruickshank, D. W. J., Harding, M. M., Greenhough, T. J., Campbell, J. W., Clifton, I. J., Elder, M., Machin, P. A., Papiz, M. Z. & Zurek, S. (1989). *J. Appl. Cryst.* **22**, 483–497.
Hinsen, K. & Kneller, G. R. (2016). *J. Chem. Phys.* **145**, 151101.
Hinsen, K., Pellegrini, E., Stachura, S. & Kneller, G. R. (2012). *J. Comput. Chem.* **33**, 2043–2048.
Hiromoto, T., Meilleur, F., Shimizu, R., Shibazaki, C., Adachi, M., Tamada, T. & Kuroki, R. (2017). *Protein Sci.* **26**, 1953–1963.
Holz, M., Zarebanadkouki, M., Kaestner, A., Kuzyakov, Y. & Carminati, A. (2018). *Plant Soil*, **423**, 429–442.
Hong, L., Jain, N., Cheng, X., Bernal, A., Tyagi, M. & Smith, J. (2016). *Sci. Adv.* **2**, e1600886.
Hong, L., Smolin, N. & Smith, J. C. (2014). *Phys. Rev. Lett.* **112**, 158102.
Hoogerheide, D. P., Noskov, S. Y., Jacobs, D., Bergdoll, L., Silin, V., Worcester, D. L., Abramson, J., Nanda, H., Rostovtseva, T. K. & Bezrukov, S. M. (2017). *Proc. Natl Acad. Sci. USA*, **114**, E3622–E3631.
Hoopes, J. T., Elberson, M. A., Preston, R. J., Reddy, P. T. & Kelman, Z. (2015). *Methods Enzymol.* **565**, 27–44.
Howard, E. I., Guillot, B., Blakeley, M. P., Haertlein, M., Moulin, M., Mitschler, A., Cousido-Siah, A., Fadel, F., Valsecchi, W. M., Tomizaki, T., Petrova, T., Claudot, J. & Podjarny, A. (2016). *IUCrJ*, **3**, 115–126.
Ibrahim, Z., Martel, A., Moulin, M., Kim, H. S., Härtlein, M., Franzetti, B. & Gabel, F. (2017). *Sci. Rep.* **7**, 40948.
Ikeda, M., Kihara, A. & Igarashi, Y. (2006). *Biol. Pharm. Bull.* **29**, 1542–1546.
Ingham, B., Erlangga, G. D., Smialowska, A., Kirby, N. M., Wang, C., Matia-Merino, L., Haverkamp, R. G. & Carr, A. J. (2015). *Soft Matter*, **11**, 2723–2725.
Isaksson, H., Le Cann, S., Perdikouri, C., Turunen, M. J., Kaestner, A., Tägil, M., Hall, S. A. & Tudisco, E. (2017). *Bone*, **103**, 295–301.
Jelsch, C., Teeter, M. M., Lamzin, V., Pichon-Pesme, V., Blessing, R. H. & Lecomte, C. (2000). *Proc. Natl Acad. Sci. USA*, **97**, 3171–3176.
Jones, E. M., Dubey, M., Camp, P. J., Vernon, B. C., Biernat, J., Mandelkow, E., Majewski, J. & Chi, E. Y. (2012). *Biochemistry*, **51**, 2539–2550.
Junghans, A., Waltman, M. J., Smith, H. L., Pocivavsek, L., Zebda, N., Birukov, K., Viapiano, M. & Majewski, J. (2014). *Mod. Phys. Lett. B Condens. Matter Phys. Stat. Phys. Appl. Phys.* **28**, 1430015.
Katz, A. K., Li, X., Carrell, H. L., Hanson, B. L., Langan, P., Coates, L., Schoenborn, B. P., Glusker, J. P. & Bunick, G. J. (2006). *Proc. Natl Acad. Sci. USA*, **103**, 8342–8347.
Kent, M. S., Murton, J. K., Sasaki, D. Y., Satija, S., Akgun, B., Nanda, H., Curtis, J. E., Majewski, J., Morgan, C. R. & Engen, J. R. (2010). *Biophys. J.* **99**, 1940–1948.
Khodadadi, S., Pawlus, S. & Sokolov, A. P. (2008). *J. Phys. Chem. B*, **112**, 14273–14280.
Khoshouei, M., Radjainia, M., Baumeister, W. & Danev, R. (2017). *Nature Commun.* **8**, 16099.
Kita, A. & Morimoto, Y. (2016). *Mol. Biotechnol.* **58**, 130–136.
Klauda, J. B., Venable, R. M., Freites, J. A., O'Connor, J. W., Tobias, D. J., Mondragon-Ramirez, C., Vorobyov, I., MacKerell, A. D. Jr & Pastor, R. W. (2010). *J. Phys. Chem. B*, **114**, 7830–7843.
Klinman, J. P. & Kohen, A. (2013). *Annu. Rev. Biochem.* **82**, 471–496.
Kneller, G. R. (1994). *Mol. Phys.* **83**, 63–87.
Kneller, G. R. (2005). *Phys. Chem. Chem. Phys.* **7**, 2641–2655.
Kneller, G. R. (2018). *Proc. Natl Acad. Sci. USA*, **115**, 9450–9455.
Kneller, G. R. & Chevrot, G. (2012). *J. Chem. Phys.* **137**, 225101.
Kneller, G. R. & Hinsen, K. (2015). *Acta Cryst.* D**71**, 1411–1422.
Knight, J. L. & Brooks, C. L. (2011). *J. Comput. Chem.* **32**, 2909–2923.
Knihtila, R. (2016). PhD Dissertation, Northeastern University. http://hdl.handle.net/2047/D20211606.
Knihtila, R., Holzapfel, G., Weiss, K., Meilleur, F. & Mattos, C. (2015). *J. Biol. Chem.* **290**, 31025–31036.
Kofuku, Y., Ueda, T., Okude, J., Shiraishi, Y., Kondo, K., Mizumura, T., Suzuki, S. & Shimada, I. (2014). *Angew. Chem. Int. Ed.* **53**, 13376–13379.
König, S., Bayerl, T. M., Coddens, G., Richter, D. & Sackmann, E. (1995). *Biophys. J.* **68**, 1871–1880.
Kossiakoff, A. A. & Spencer, S. A. (1980). *Nature (London)*, **288**, 414–416.
Kovalevsky, A., Aggarwal, M., Velazquez, H., Cuneo, M. J., Blakeley, M. P., Weiss, K. L., Smith, J. C., Fisher, S. Z. & McKenna, R. (2018). *Structure*, **26**, 383–390.
Kovalevsky, A. Y., Hanson, B. L., Mason, S. A., Yoshida, T., Fisher, S. Z., Mustyakimov, M., Forsyth, V. T., Blakeley, M. P., Keen, D. A. & Langan, P. (2011). *Angew. Chem. Int. Ed.* **50**, 7520–7523.
Kovalevsky, A. Y., Katz, A. K., Carrell, H. L., Hanson, L., Mustyakimov, M., Fisher, S. Z., Coates, L., Schoenborn, B. P., Bunick, G. J., Glusker, J. P. & Langan, P. (2008). *Biochemistry*, **47**, 7595–7597.
Kozlovskaya, V., Zavgorodnya, O., Ankner, J. F. & Kharlampieva, E. (2015). *Macromolecules*, **48**, 8585–8593.
Kroener, E., Zarebanadkouki, M., Kaestner, A. & Carminati, A. (2014). *Water Resour. Res.* **50**, 6479–6495.
Krueger, S., Meuse, C. W., Majkrzak, C. F., Dura, J. A., Berk, N. F., Tarek, M. & Plant, A. L. (2001). *Langmuir*, **17**, 511–521.
Kučerka, N., Nieh, M.-P. & Katsaras, J. (2011). *Biochim. Biophys. Acta*, **1808**, 2761–2771.
Kufelt, O., El-Tamer, A., Sehring, C., Meissner, M., Schlie-Wolter, S. & Chichkov, B. N. (2015). *Acta Biomater.* **18**, 186–195.
Kumar, P., Serpersu, E. H. & Cuneo, M. J. (2018). *Sci. Adv.* **4**, eaas8667.
Kurihara, K., Hirano, Y., Oikawa, K., Harada, M., Nakamura, T. & Tamada, T. (2018). *J. Appl. Cryst.* **51**, 596–605.
Kwon, H., Basran, J., Casadei, C. M., Fielding, A. J., Schrader, T. E., Ostermann, A., Devos, J. M., Aller, P., Blakeley, M. P., Moody, P. C. E. & Raven, E. L. (2016). *Nature Commun.* **7**, 13445.

Kwon, H., Langan, P. S., Coates, L., Raven, E. L. & Moody, P. C. E. (2018). *Acta Cryst.* D**74**, 792–799.
Lakey, J. H. (2009). *J. R. Soc. Interface*, **6**, S567–S573.
Langan, P. & Greene, G. (2004). *J. Appl. Cryst.* **37**, 253–257.
Langan, P., Petridis, L., O'Neill, H. M., Pingali, S. V., Foston, M., Nishiyama, Y., Schulz, R., Lindner, B., Hanson, B. L., Harton, S., Heller, W. T., Urban, V., Evans, B. R., Gnanakaran, S., Ragauskas, A. J., Smith, J. C. & Davison, B. H. (2014). *Green Chem.* **16**, 63–68.
Langan, P. S., Close, D. W., Coates, L., Rocha, R. C., Ghosh, K., Kiss, C., Waldo, G., Freyer, J., Kovalevsky, A. & Bradbury, A. R. (2016). *J. Mol. Biol.* **428**, 1776–1789.
Langan, P. S., Vandavasi, V. G., Cooper, S. J., Weiss, K. L., Ginell, S. L., Parks, J. M. & Coates, L. (2018). *ACS Catal.* **8**, 2428–2437.
Laux, V., Callow, P., Svergun, D. I., Timmins, P. A., Forsyth, V. T. & Haertlein, M. (2008). *Eur. Biophys. J.* **37**, 815–822.
Leiting, B., Marsilio, F. & O'Connell, J. F. (1998). *Anal. Biochem.* **265**, 351–355.
Li, L., Shukla, S., Meilleur, F., Standaert, R. F., Pierce, J., Myles, D. A. A. & Cuneo, M. J. (2017). *Protein Sci.* **26**, 2098–2104.
Liakos, D. G. & Neese, F. (2015). *J. Chem. Theory Comput.* **11**, 4054–4063.
Liebschner, D., Elias, M., Moniot, S., Fournier, B., Scott, K., Jelsch, C., Guillot, B., Lecomte, C. & Chabrière, E. (2009). *J. Am. Chem. Soc.* **131**, 7879–7886.
Linden, J. B., Larsson, M., Kaur, S., Nosrati, A. & Nyden, M. (2016). *J. Appl. Polym. Sci.* **133**, 43954.
Lindner, B. & Smith, J. C. (2012). *Comput. Phys. Commun.* **183**, 1491–1501.
Lindner, B., Yi, Z., Prinz, J. H., Smith, J. C. & Noé, F. (2013). *J. Chem. Phys.* **139**, 175101.
Liu, Y., Chen, C.-Y., Chen, H.-L., Hong, K., Shew, C.-Y., Li, X., Liu, L., Melnichenko, Y. B., Smith, G. S., Herwig, K. W., Porcar, L. & Chen, W.-R. (2010). *J. Phys. Chem. Lett.* **1**, 2020–2024.
López Cascales, J. J., Otero, T. F., Smith, B. D., González, C. & Márquez, M. (2006). *J. Phys. Chem. B*, **110**, 2358–2363.
Losen, M., Frölich, B., Pohl, M. & Büchs, J. (2004). *Biotechnol. Prog.* **20**, 1062–1068.
Love, K. R., Shah, K. A., Whittaker, C. A., Wu, J., Bartlett, M. C., Ma, D., Leeson, R. L., Priest, M., Borowsky, J., Young, S. K. & Love, J. C. (2016). *BMC Genomics*, **17**, 550.
Lu, X., Fang, D., Ito, S., Okamoto, Y., Ovchinnikov, V. & Cui, Q. (2016). *Mol. Simul.* **42**, 1056–1078.
Luchini, A., Delhom, R., Demé, B., Laux, V., Moulin, M., Haertlein, M., Pichler, H., Strohmeier, G. A., Wacklin, H. & Fragneto, G. (2018). *Colloids Surf. B Biointerfaces*, **168**, 126–133.
Macauley-Patrick, S., Fazenda, M. L., McNeil, B. & Harvey, L. M. (2005). *Yeast*, **22**, 249–270.
Majewski, J., Wong, J. Y., Park, C. K., Seitz, M., Israelachvili, J. N. & Smith, G. S. (1998). *Biophys. J.* **75**, 2363–2367.
Majkrzak, C., Berk, N., Krueger, S. & Perez-Salas, U. (2006). *Neutron Scattering in Biology: Techniques and Applications*, edited by J. Fitter, T. Gutberlet & J. Katsaras, pp. 225–263. Berlin, Heidelberg: Springer-Verlag.
Mamontov, E. (2017). *Biochim. Biophys. Acta*, **1861**, 2382–2390.
Mamontov, E. (2018). *Sci. Rep.* **8**, 4190.
Mamontov, E. & Chu, X. (2012). *Phys. Chem. Chem. Phys.* **14**, 11573–11588.
Manzoni, F., Wallerstein, J., Schrader, T. E., Ostermann, A., Coates, L., Akke, M., Blakeley, M. P., Oksanen, E. & Logan, D. T. (2018). *J. Med. Chem.* **61**, 4412–4420.
Maric, S., Skar-Gislinge, N., Midtgaard, S., Thygesen, M. B., Schiller, J., Frielinghaus, H., Moulin, M., Haertlein, M., Forsyth, V. T., Pomorski, T. G. & Arleth, L. (2014). *Acta Cryst.* D**70**, 317–328.
Martinez, N., Michoud, G., Cario, A., Ollivier, J., Franzetti, B., Jebbar, M., Oger, P. & Peters, J. (2016). *Sci. Rep.* **6**, 32816.
Martínez-Sanz, M., Gidley, M. J. & Gilbert, E. P. (2016). *Soft Matter*, **12**, 1534–1549.
Martínez-Sanz, M., Lopez-Sanchez, P., Gidley, M. J. & Gilbert, E. P. (2015). *Cellulose*, **22**, 1541–1563.
Martínez-Sanz, M., Mikkelsen, D., Flanagan, B. M., Gidley, M. J. & Gilbert, E. P. (2017). *Polymer*, **124**, 1–11.
Martínez-Sanz, M., Mikkelsen, D., Flanagan, B. M., Rehm, C., de Campo, L., Gidley, M. J. & Gilbert, E. P. (2016). *Polymer*, **105**, 449–460.
McGillivray, D. J., Valincius, G., Heinrich, F., Robertson, J. W. F., Vanderah, D. J., Febo-Ayala, W., Ignatjev, I., Lösche, M. & Kasianowicz, J. J. (2009). *Biophys. J.* **96**, 1547–1553.
McGillivray, D. J., Valincius, G., Vanderah, D. J., Febo-Ayala, W., Woodward, J. T., Heinrich, F., Kasianowicz, J. J. & Löscheb, M. (2007). *Biointerphases*, **2**, 21–33.
McVey, C. E., Walsh, M. A., Dodson, G. G., Wilson, K. S. & Brannigan, J. A. (2001). *J. Mol. Biol.* **313**, 139–150.
Meilleur, F., Dauvergne, M.-T., Schlichting, I. & Myles, D. A. A. (2005). *Acta Cryst.* D**61**, 539–544.
Meilleur, F., Munshi, P., Robertson, L., Stoica, A. D., Crow, L., Kovalevsky, A., Koritsanszky, T., Chakoumakos, B. C., Blessing, R. & Myles, D. A. A. (2013). *Acta Cryst.* D**69**, 2157–2160.
Meilleur, F., Myles, D. A. A. & Blakeley, M. P. (2006). *Eur. Biophys. J.* **35**, 611–620.
Meilleur, F., Snell, E. H., van der Woerd, M. J., Judge, R. A. & Myles, D. A. A. (2006). *Eur. Biophys. J.* **35**, 601–609.
Meilleur, F., Weiss, K. L. & Myles, D. A. A. (2009). *Micro and Nano Technologies in Bioanalysis: Methods and Protocols*, edited by R. S. Foote & J. W. Lee, pp. 281–292. Totowa: Humana Press.
Meinhold, L., Clement, D., Tehei, M., Daniel, R., Finney, J. L. & Smith, J. C. (2008). *Biophys. J.* **94**, 4812–4818.
Meinhold, L., Merzel, F. & Smith, J. C. (2007). *Phys. Rev. Lett.* **99**, 138101.
Meng, N., Zhao, W., Shamsaei, E., Wang, G., Zeng, X. K., Lin, X. C., Xu, T. W., Wang, H. T. & Zhang, X. W. (2018). *J. Membr. Sci.* **548**, 363–371.
Merkl, R. & Sterner, R. (2016). *Biol. Chem.* **397**, 1–21.
Merzel, F. & Smith, J. C. (2002). *Proc. Natl Acad. Sci. USA*, **99**, 5378–5383.
Metzke, R. W., Runck, H., Stahl, C. A., Schillinger, B., Calzada, E., Muhlbauer, M., Schulz, M., Schneider, M., Priebe, H. J., Wall, W. A. & Guttmann, J. (2011). *Phys. Med. Biol.* **56**, N1–N10.
Mezei, F. (1972). *Z. Phys.* **255**, 146–160.
Miao, Y., Yi, Z., Cantrell, C., Glass, D. C., Baudry, J., Jain, N. & Smith, J. C. (2012). *Biophys. J.* **103**, 2167–2176.
Midtgaard, S. R., Darwish, T. A., Pedersen, M. C., Huda, P., Larsen, A. H., Jensen, G. V., Kynde, S. A. R., Skar-Gislinge, N., Nielsen, A. J. Z., Olesen, C., Blaise, M., Dorosz, J. J., Thorsen, T. S., Venskutonytė, R., Krintel, C., Møller, J. V., Frielinghaus, H., Gilbert, E. P., Martel, A., Kastrup, J. S., Jensen, P. E., Nissen, P. & Arleth, L. (2018). *FEBS J.* **285**, 357–371.
Miller, C. E., Majewski, J., Faller, R., Satija, S. & Kuhl, T. L. (2004). *Biophys. J.* **86**, 3700–3708.
Miller, C. E., Majewski, J., Gog, T. & Kuhl, T. L. (2005). *Phys. Rev. Lett.* **94**, 238104.
Mohan, V. S., Crespi, H. L. & Katz, J. J. (1962). *Nature (London)*, **193**, 189–190.
Moradi, A. B., Carminati, A., Vetterlein, D., Vontobel, P., Lehmann, E., Weller, U., Hopmans, J. W., Vogel, H. J. & Oswald, S. E. (2011). *New Phytol.* **192**, 653–663.
Morgano, M., Trtik, P., Meyer, M., Lehmann, E., Hovind, J. & Strobl, M. (2018). *Opt. Express*, **26**, 1809–1816.
Moulin, M., Strohmeier, G. A., Hirz, M., Thompson, K. C., Rennie, A. R., Campbell, R. A., Pichler, H., Maric, S., Forsyth, V. T. & Haertlein, M. (2018). *Chem. Phys. Lipids*, **212**, 80–87.
Munshi, P., Chung, S.-L., Blakeley, M. P., Weiss, K. L., Myles, D. A. A. & Meilleur, F. (2012). *Acta Cryst.* D**68**, 35–41.
Munshi, P., Snell, E. H., van der Woerd, M. J., Judge, R. A., Myles, D. A. A., Ren, Z. & Meilleur, F. (2014). *Acta Cryst.* D**70**, 414–420.

Mustyakimov, M. & Langan, P. (2007). *nCNS: An Open Source Distribution Patch for CNS for Macromolecular Structure Refinement*. Los Alamos National Laboratory.
Nagao, M., Kelley, E. G., Ashkar, R., Bradbury, R. & Butler, P. D. (2017). *J. Phys. Chem. Lett.* **8**, 4679–4684.
Nagata, Y., Nishikawa, T., Suginome, M., Sato, S., Sugiyama, M., Porcar, L., Martel, A., Inoue, R. & Sato, N. (2018). *J. Am. Chem. Soc.* **140**, 2722–2726.
Naing, S.-H., Oliver, R. C., Weiss, K. L., Urban, V. S. & Lieberman, R. L. (2018). *Biophys. J.* **114**, 602–608.
Nakamura, A., Ishida, T., Kusaka, K., Yamada, T., Fushinobu, S., Tanaka, I., Kaneko, S., Ohta, K., Tanaka, H., Inaka, K., Higuchi, Y., Niimura, N., Samejima, M. & Igarashi, K. (2015). *Sci. Adv.* **1**, e1500263.
Nakanishi, T., Okuni, Y., Furukawa, J., Tanoi, K., Yokota, H., Ikeue, N., Matsubayashi, M., Uchida, H. & Tsiji, A. (2003). *J. Radioanal. Nucl. Chem.* **255**, 149–153.
Nakano, M., Fukuda, M., Kudo, T., Endo, H. & Handa, T. (2007). *Phys. Rev. Lett.* **98**, 238101.
Nanda, H., Datta, S. A. K., Heinrich, F., Lösche, M., Rein, A., Krueger, S. & Curtis, J. E. (2010). *Biophys. J.* **99**, 2516–2524.
Nanda, H., Heinrich, F. & Lösche, M. (2015). *Methods*, **77–78**, 136–146.
Natali, F., Dolce, C., Peters, J., Gerelli, Y., Stelletta, C. & Leduc, G. (2013). *J. Phys. Soc. Jpn*, **82**, SA017.
Nath, A., Atkins, W. M. & Sligar, S. G. (2007). *Biochemistry*, **46**, 2059–2069.
Neumann, P. & Tittmann, K. (2014). *Curr. Opin. Struct. Biol.* **29**, 122–133.
Nickels, J. D., Chatterjee, S., Stanley, C. B., Qian, S., Cheng, X., Myles, D. A. A., Standaert, R. F., Elkins, J. G. & Katsaras, J. (2017). *PLoS Biol.* **15**, e2002214.
Nickels, J. D., Cheng, X., Mostofian, B., Stanley, C., Lindner, B., Heberle, F. A., Perticaroli, S., Feygenson, M., Egami, T., Standaert, R. F., Smith, J. C., Myles, D. A. A., Ohl, M. & Katsaras, J. (2015). *J. Am. Chem. Soc.* **137**, 15772–15780.
Nickels, J. D., O'Neill, H., Hong, L., Tyagi, M., Ehlers, G., Weiss, K. L., Zhang, Q., Yi, Z., Mamontov, E., Smith, J. C. & Sokolov, A. P. (2012). *Biophys. J.* **103**, 1566–1575.
Nickels, J. D., Perticaroli, S., O'Neill, H., Zhang, Q., Ehlers, G. & Sokolov, A. P. (2013). *Biophys. J.* **105**, 2182–2187.
Nierhaus, K. H., Lietzke, R., May, R. P., Nowotny, V., Schulze, H., Simpson, K., Wurmbach, P. & Stuhrmann, H. B. (1983). *Proc. Natl Acad. Sci. USA*, **80**, 2889–2893.
Niimura, N., Chatake, T., Ostermann, A., Kurihara, K. & Tanaka, I. (2003). *Z. Kristallogr.* **218**, 96–107.
Nishiyama, Y., Langan, P. & Chanzy, H. (2002). *J. Am. Chem. Soc.* **124**, 9074–9082.
Noé, F., Horenko, I., Schütte, C. & Smith, J. C. (2007). *J. Chem. Phys.* **126**, 155102.
Novikov, V. N. & Sokolov, A. P. (2013). *Phys. Rev. Lett.* **110**, 065701.
O'Dell, W. B., Agarwal, P. K. & Meilleur, F. (2017). *Angew. Chem.* **129**, 785–788.
O'Dell, W. B., Bodenheimer, A. M. & Meilleur, F. (2016). *Arch. Biochem. Biophys.* **602**, 48–60.
Ohhara, T., Kusaka, K., Hosoya, T., Kurihara, K., Tomoyori, K., Niimura, N., Tanaka, I., Suzuki, J., Nakatani, T., Otomo, T., Matsuoka, S., Tomita, K., Nishimaki, Y., Ajima, T. & Ryufuku, S. (2009). *Nucl. Instrum. Methods Phys. Res. A*, **600**, 195–197.
Oliver, R. C., Pingali, S. V. & Urban, V. S. (2017). *J. Phys. Chem. Lett.* **8**, 5041–5046.
O'Neil, L., Andenoro, K., Pagano, I., Carroll, L., Langer, L., Dell, Z., Perera, D., Treece, B. W., Heinrich, F., Lösche, M., Nagle, J. F. & Tristram-Nagle, S. (2016). *Biochim. Biophys. Acta*, **1858**, 3071–3081.
O'Neill, H., Pingali, S. V., Petridis, L., He, J. H., Mamontov, E., Hong, L., Urban, V., Evans, B., Langan, P., Smith, J. C. & Davison, B. H. (2017). *Sci. Rep.* **7**, 11840.
Opitz, C., Isogai, S. & Grzesiek, S. (2015). *J. Biomol. NMR*, **62**, 373–385.
Oswald, S. E., Menon, M., Carminati, A., Vontobel, P., Lehmann, E. & Schulin, R. (2008). *Vadose Zone J.* **7**, 1035–1047.
Otwinowski, Z. & Minor, W. (1997). *Methods Enzymol.* **276**, 307–326.
Paliy, O., Bloor, D., Brockwell, D., Gilbert, P. & Barber, J. (2003). *J. Appl. Microbiol.* **94**, 580–586.
Paul, F., Wehmeyer, C., Abualrous, E. T., Wu, H., Crabtree, M. D., Schöneberg, J., Clarke, J., Freund, C., Weikl, T. R. & Noé, F. (2017). *Nature Commun.* **8**, 1095.
Perera, S. M. D. C., Chawla, U., Shrestha, U. R., Bhowmik, D., Struts, A. V., Qian, S., Chu, X.-Q. & Brown, M. F. (2018). *J. Phys. Chem. Lett.* **9**, 7064–7071.
Pérez, J. & Koutsioubas, A. (2015). *Acta Cryst.* D**71**, 86–93.
Perilla, J. R., Goh, B. C., Cassidy, C. K., Liu, B., Bernardi, R. C., Rudack, T., Yu, H., Wu, Z. & Schulten, K. (2015). *Curr. Opin. Struct. Biol.* **31**, 64–74.
Perkins, S. J. (1981). *Biochem. J.* **199**, 163–170.
Perkins, S. J., Wright, D. W., Zhang, H., Brookes, E. H., Chen, J., Irving, T. C., Krueger, S., Barlow, D. J., Edler, K. J., Scott, D. J., Terrill, N. J., King, S. M., Butler, P. D. & Curtis, J. E. (2016). *J. Appl. Cryst.* **49**, 1861–1875.
Perticaroli, S., Ehlers, G., Stanley, C. B., Mamontov, E., O'Neill, H., Zhang, Q., Cheng, X., Myles, D. A. A., Katsaras, J. & Nickels, J. D. (2017). *J. Am. Chem. Soc.* **139**, 1098–1105.
Perticaroli, S., Nickels, J. D., Ehlers, G., O'Neill, H., Zhang, Q. & Sokolov, A. P. (2013). *Soft Matter*, **9**, 9548–9556.
Peters, J. & Kneller, G. R. (2013). *J. Chem. Phys.* **139**, 165102.
Peti, W. & Page, R. (2007). *Protein Expr. Purif.* **51**, 1–10.
Pfefferkorn, C. M., Heinrich, F., Sodt, A. J., Maltsev, A. S., Pastor, R. W. & Lee, J. C. (2012). *Biophys. J.* **102**, 613–621.
Pfeiffer, F., Grunzweig, C., Bunk, O., Frei, G., Lehmann, E. & David, C. (2006). *Phys. Rev. Lett* **96**, 215505.
Pflugrath, J. W. (1999). *Acta Cryst.* D**55**, 1718–1725.
Pushin, D. A., Sarenac, D., Hussey, D. S., Miao, H., Arif, M., Cory, D. G., Huber, M. G., Jacobson, D. L., LaManna, J. M., Parker, J. D., Shinohara, T., Ueno, W. & Wen, H. (2018). *Phys. Rev. A*, **95**, 043637.
Quesne, M. G., Borowski, T. & de Visser, S. P. (2016). *Chem. Eur. J.* **22**, 2562–2581.
Raghuwanshi, V. S., Su, J. L., Garvey, C. J., Holt, S. A., Raverty, W., Tabor, R. F., Holden, P. J., Gillon, M., Batchelor, W. & Garnier, G. (2017). *Cellulose*, **24**, 11–20.
Reiter, G., Burnham, C., Homouz, D., Platzman, P. M., Mayers, J., Abdul-Redah, T., Moravsky, A. P., Li, A. P., Loong, J. C. & Kolesnikov, C.-K. (2006). *Phys. Rev. Lett.* **97**, 247801.
Rheinstädter, M. C., Häussler, W. & Salditt, T. (2006). *Phys. Rev. Lett.* **97**, 048103.
Richter, D., Frick, B. & Farago, B. (1988). *Phys. Rev. Lett.* **61**, 2465–2468.
Ritchie, T. K., Grinkova, Y. V., Bayburt, T. H., Denisov, I. G., Zolnerciks, J. K., Atkins, W. M. & Sligar, S. G. (2009). *Methods Enzymol.* **484**, 211–231.
Roberts, C. J. (2014). *Curr. Opin. Biotechnol.* **30**, 211–217.
Róg, T., Murzyn, K., Hinsen, K. & Kneller, G. R. (2003). *J. Comput. Chem.* **24**, 657–667.
Roosen-Runge, F., Hennig, M., Zhang, F., Jacobs, R. M., Sztucki, M., Schober, H., Seydel, T. & Schreiber, F. (2011). *Proc. Natl Acad. Sci. USA*, **108**, 11815–11820.
Rosano, G. L. & Ceccarelli, E. A. (2014). *Front. Microbiol.* **5**, 172.
Roy, R., Hohng, S. & Ha, T. (2008). *Nature Methods*, **5**, 507–516.
Russel, D., Lasker, K., Webb, B., Velázquez-Muriel, J., Tjioe, E., Schneidman-Duhovny, D., Peterson, B. & Sali, A. (2012). *PLoS Biol.* **10**, e1001244.
Russell, R. A., Darwish, T. A., Puskar, L., Martin, D. E., Holden, P. J. & Foster, L. J. R. (2014). *Biomacromolecules*, **15**, 644–649.
Russell, R. A., Garvey, C. J., Darwish, T. A., Foster, L. J. R. & Holden, P. J. (2015). *Methods Enzymol.* **565**, 97–121.

Sanz, A., Hansen, H. W., Jakobsen, B., Pedersen, I. H., Capaccioli, S., Adrjanowicz, K., Paluch, M., Gonthier, J., Frick, B., Lelièvre-Berna, E., Peters, J. & Niss, K. (2018). *Rev. Sci. Instrum.* **89**, 023904.
Schaffner, I., Mlynek, G., Flego, N., Pühringer, D., Libiseller-Egger, J., Coates, L., Hofbauer, S., Bellei, M., Furtmüller, P. G., Battistuzzi, G., Smulevich, G., Djinović-Carugo, K. & Obinger, C. (2017). *ACS Catal.* **7**, 7962–7976.
Schiebel, J., Gaspari, R., Sandner, A., Ngo, K., Gerber, H. D., Cavalli, A., Ostermann, A., Heine, A. & Klebe, G. (2017). *Angew. Chem.* **56**, 4887–4890.
Schirò, G., Fichou, Y., Gallat, F. X., Wood, K., Gabel, F., Moulin, M., Härtlein, M., Heyden, M., Colletier, J.-P., Orecchini, A., Paciaroni, A., Wuttke, J., Tobias, D. J. & Weik, M. (2015). *Nature Commun.* **6**, 6490.
Schröder, G. C., O'Dell, W. B., Myles, D. A. A., Kovalevsky, A. & Meilleur, F. (2018). *Acta Cryst.* D**74**, 778–786.
Schrödinger, E. (1944). *What Is Life? The Physical Aspect of the Living Cell*. Cambridge University Press.
Schroer, M. A. & Svergun, D. I. (2018). *Emerg. Top. Life Sci.* **2**, 69–79.
Schultz, A. J., Jørgensen, M. R. V., Wang, X., Mikkelson, R. L., Mikkelson, D. J., Lynch, V. E., Peterson, P. F., Green, M. L. & Hoffmann, C. M. (2014). *J. Appl. Cryst.* **47**, 915–921.
Schultz, A. J., Thiyagarajan, P., Hodges, J. P., Rehm, C., Myles, D. A. A., Langan, P. & Mesecar, A. D. (2005). *J. Appl. Cryst.* **38**, 964–974.
Sears, V. F. (1992). *Neutron News*, **3**(3), 26–37.
Sharma, V., Chotia, C., Tarachand, T., Ganesan, V. & Okram, G. (2017). *Phys. Chem. Chem. Phys.* **19**, 14096–14106.
Shekhar, P., Nanda, H., Lösche, M. & Heinrich, F. (2011). *J. Appl. Phys.* **110**, 102216–10221612.
Sheldrick, G. M. (2015). *Acta Cryst.* C**71**, 3–8.
Shen, H.-H., Leyton, D. L., Shiota, T., Belousoff, M. J., Noinaj, N., Lu, J., Holt, S. A., Tan, K., Selkrig, J., Webb, C. T., Buchanan, S. K., Martin, L. L. & Lithgow, T. (2014). *Nature Commun.* **5**, 5078.
Shenoy, S., Shekhar, P., Heinrich, F., Daou, M.-C., Gericke, A., Ross, A. H. & Lösche, M. (2012). *PLoS One*, **7**, e32591.
Shenoy, S. S., Nanda, H. & Lösche, M. (2012). *J. Struct. Biol.* **180**, 394–408.
Shibata, C. G., Gregory, J. D., Gerhardt, B. S. & Serpersu, E. H. (1995). *Arch. Biochem. Biophys.* **319**, 204–210.
Shrestha, U. R., Bhowmik, D., Copley, J. R. D., Tyagi, M. S., Leão, J. B. & Chu, X.-Q. (2015). *Proc. Natl Acad. Sci. USA*, **112** 13886–13891.
Shrestha, U. R., Perera, S. M. D. C., Bhowmik, D., Chawla, U., Mamontov, E., Brown, M. F. & Chu, X.-Q. (2916). *J. Phys. Chem. Lett.* **7**, 4130–4136.
Sitarska, A., Skora, L., Klopp, J., Roest, S., Fernández, C., Shrestha, B. & Gossert, A. D. (2015). *J. Biomol. NMR*, **62**, 191–197.
Smith, J. C., Merzel, F., Bondar, A.-N., Tournier, A. & Fischer, S. (2004). *Philos. Trans. R. Soc. B Biol. Sci.* **359**, 1181–1190.
Smith, J. C. & Roux, B. (2013). *Structure*, **21**, 2102–2105.
Smith, J. C., Tan, P., Petridis, L. & Hong, L. (2018). *Annu. Rev. Biophys.* **47**, 335–354.
Smith, M. D., Mostofian, B., Cheng, X., Petridis, L., Cai, C. M., Wyman, C. E. & Smith, J. C. (2015). *Green Chem.* **18**, 1268–1277.
Sonntag, M., Jagtap, P., Simon, B., Appavou, M.-S., Geerlof, A., Stehle, R., Gabel, F., Hennig, J. & Sattler, M. (2017). *Angew. Chem. Int. Ed.* **56**, 9322–9325.
Stachowiak, J. C., Schmid, E. M., Ryan, C. J., Ann, H. S., Sasaki, D. Y., Sherman, M. B., Geissler, P. L., Fletcher, D. A. & Hayden, C. C. (2012). *Nature Cell Biol.* **14**, 944–949.
Steensels, J., Snoek, T., Meersman, E., Picca Nicolino, M., Voordeckers, K. & Verstrepen, K. J. (2014). *FEMS Microbiol. Rev.* **38**, 947–995.
Stingaciu, L. R., O'Neill, H., Liberton, M., Urban, V. S., Pakrasi, H. B. & Ohl, M. (2016). *Sci. Rep.* **6**, 19627.
Stuhrmann, H. B. (2004). *Rep. Prog. Phys.* **67**, 1073–1115.
Svergun, D. I., Richard, S., Koch, M. H., Sayers, Z., Kuprin, S. & Zaccai, G. (1998). *Proc. Natl Acad. Sci. USA*, **95**, 2267–2272.
Takahashi, H. & Shimada, I. (2010). *J. Biomol. NMR*, **46**, 3–10.
Tarek, M. & Tobias, D. J. (2002). *Phys. Rev. Lett.* **88**, 138101.
Tehei, M., Franzetti, B., Wood, K., Gabel, F., Fabiani, E., Jasnin, M., Zamponi, M., Oesterhelt, D., Zaccai, G., Ginzburg, M. & Ginzburg, B. (2007). *Proc. Natl Acad. Sci. USA*, **104**, 766–771.
Tomanicek, S. J., Standaert, R. F., Weiss, K. L., Ostermann, A., Schrader, T. E., Ng, J. D. & Coates, L. (2013). *J. Biol. Chem.* **288**, 4715–4722.
Tomida, M., Kimura, M., Kuwata, K., Hayashi, T., Okano, Y. & Era, S. (2003). *Jpn J. Physiol.* **53**, 65–69.
Toppozini, L., Roosen-Runge, F., Bewley, R. I., Dalgliesh, R. M., Perring, T., Seydel, T., Glyde, H. R., García Sakai, V. & Rheinstädter, M. C. (2015). *Soft Matter*, **11**, 8354–8371.
Tötzke, C., Kardjilov, N., Manke, I. & Oswald, S. E. (2017). *Sci. Rep.* **7**, 6192.
Trewhella, J. (2006). *Physica B*, **385–386**, 825–830.
Tronin, A. Y., Nordgren, C. E., Strzalka, J. W., Kuzmenko, I., Worcester, D. L., Lauter, V., Freites, J. A., Tobias, D. J. & Blasie, J. K. (2014). *Langmuir*, **30**, 4784–4796.
Unno, M., Ishikawa-Suto, K., Kusaka, K., Tamada, T., Hagiwara, Y., Sugishima, M., Wada, K., Yamada, T., Tomoyori, K., Hosoya, T., Tanaka, I., Niimura, N., Kuroki, R., Inaka, K., Ishihara, M. & Fukuyama, K. (2015). *J. Am. Chem. Soc.* **137**, 5452–5460.
Vacklin, H. P., Tiberg, F., Fragneto, G. & Thomas, R. K. (2005). *Langmuir*, **21**, 2827–2837.
Valincius, G., Heinrich, F., Budvytyte, R., Vanderah, D. J., McGillivray, D. J., Sokolov, Y., Hall, J. E. & Lösche, M. (2008). *Biophys. J.* **95**, 4845–4861.
Van Hove, L. (1954). *Phys. Rev.* **95**, 249–262.
Van Hove, L. (1958). *Physica*, **24**, 404–408.
Vauclare, P., Marty, V., Fabiani, E., Martinez, N., Jasnin, M., Gabel, F., Peters, J., Zaccai, G. & Franzetti, B. (2015). *Extremophiles*, **19**, 1099–1107.
Vojtěchovský, J., Chu, K., Berendzen, J., Sweet, R. M. & Schlichting, I. (1999). *Biophys. J.* **77**, 2153–2174.
Vural, D., Hong, L., Smith, J. C. & Glyde, H. R. (2015). *Phys. Rev. E*, **91**, 052705.
Wah, B., Breidigan, J. M., Adams, J., Horbal, P., Garg, S., Porcar, L. & Perez-Salas, U. (2017). *Langmuir*, **33**, 3384–3394.
Walhout, A. J. M., Temple, G. F., Brasch, M. A., Hartley, J. L., Lorson, M. A., van den Heuvel, S. & Vidal, M. (2000). *Methods Enzymol.* **328**, 575–592.
Wan, Q., Parks, J. M., Hanson, B. L., Fisher, S. Z., Ostermann, A., Schrader, T. E., Graham, D. E., Coates, L., Langan, P. & Kovalevsky, A. (2015). *Proc. Natl Acad. Sci. USA*, **112**, 12384–12389.
Wang, M., Lu, Z. & Yang, W. (2006). *J. Chem. Phys.* **124**, 124516.
Ward, J. J., Sodhi, J. S., McGuffin, L. J., Buxton, B. F. & Jones, D. T. (2004). *J. Mol. Biol.* **337**, 635–645.
Warren, J. M., Bilheux, H., Kang, M., Voisin, S., Cheng, C.-L., Horita, J. & Perfect, E. (2013). *Plant Soil*, **366**, 683–693.
Wilkinson, C. & Lehmann, M. S. (1991). *Nucl. Instrum. Methods Phys. Res. A*, **310**, 411–415.
Winn, M. D., Ballard, C. C., Cowtan, K. D., Dodson, E. J., Emsley, P., Evans, P. R., Keegan, R. M., Krissinel, E. B., Leslie, A. G. W., McCoy, A., McNicholas, S. J., Murshudov, G. N., Pannu, N. S., Potterton, E. A., Powell, H. R., Read, R. J., Vagin, A. & Wilson, K. S. (2011). *Acta Cryst.* D**67**, 235–242.
Wlodawer, A. & Hendrickson, W. A. (1982). *Acta Cryst.* A**38**, 239–247.
Wong, J. Y., Majewski, J., Seitz, M., Park, C. K., Israelachvili, J. N. & Smith, G. S. (1999). *Biophys. J.* **77**, 1445–1457.
Wood, K., Gallat, F. X., Otten, R., van Heel, A. J., Lethier, M., van Eijck, L., Moulin, M., Haertlein, M., Weik, M. & Mulder, F. A. (2013). *Angew. Chem. Int. Ed.* **52**, 665–668.
Woodka, A. C., Butler, P. D., Porcar, L., Farago, B. & Nagao, M. (2012). *Phys. Rev. Lett.* **109**, 058102.

Wright, P. E. & Dyson, H. J. (2015). *Nature Rev. Mol. Cell Biol.* **16**, 18–29.
Wymore, T., Field, M. J., Langan, P., Smith, J. C. & Parks, J. M. (2014). *J. Phys. Chem. B*, **118**, 4479–4489.
Xu, R., Ayers, B., Cowburn, D. & Muir, T. W. (1999). *Proc. Natl Acad. Sci. USA*, **96**, 388–393.
Yamazaki, T., Otomo, T., Oda, N., Kyogoku, Y., Uegaki, K., Ito, N., Ishino, Y. & Nakamura, H. (1998). *J. Am. Chem. Soc.* **120**, 5591–5592.
Yang, S., Blachowicz, L., Makowski, L. & Roux, B. (2010). *Proc. Natl Acad. Sci. USA*, **107**, 15757–15762.
Yap, T. L., Jiang, Z., Heinrich, F., Gruschus, J. M., Pfefferkorn, C. M., Barros, M., Curtis, J. E., Sidransky, E. & Lee, J. C. (2015). *J. Biol. Chem.* **290**, 744–754.
Yee, A. W., Blakeley, M. P., Moulin, M., Haertlein, M., Mitchell, E. & Forsyth, V. T. (2017). *J. Appl. Cryst.* **50**, 660–664.
Yi, Z., Miao, Y., Baudry, J., Jain, N. & Smith, J. C. (2012). *J. Phys. Chem. B*, **116**, 5028–5036.
Yokoyama, T., Mizuguchi, M., Ostermann, A., Kusaka, K., Niimura, N., Schrader, T. E. & Tanaka, I. (2015). *J. Med. Chem.* **58**, 7549–7556.
Yonezawa, K., Shimizu, N., Kurihara, K., Yamazaki, Y., Kamikubo, H. & Kataoka, M. (2017). *Sci. Rep.* **7**, 9361.
Yong, W., Lomakin, A., Kirkitadze, M. D., Teplow, D. B., Chen, S.-H. & Benedek, G. B. (2002). *Proc. Natl Acad. Sci. USA*, **99**, 150–154.
Yoshie, N., Goto, Y., Sakurai, M., Inoue, Y., Chûjô, R. & Doi, Y. (1992). *Int. J. Biol. Macromol.* **14**, 81–86.
Zaccai, G. (2000). *Science*, **288**, 1604–1607.
Zanotti, J., Bellissent-Funel, M. C. & Parello, J. (1999). *Biophys. J.* **76**, 2390–2411.
Zarychta, B., Lyubimov, A., Ahmed, M., Munshi, P., Guillot, B., Vrielink, A. & Jelsch, C. (2015). *Acta Cryst.* D**71**, 954–968.
Zhang, C. D., Wu, S. H. & Qin, X. H. (2014). *Mater. Lett.* **132**, 393–396.
Zhang, Q. L. & Hoogenboom, R. (2015). *Prog. Polym. Sci.* **48**, 122–142.
Zhao, J., Pierce, J., Myles, D., Robertson, J. L., Herwig, K. W., Standaert, B., Cuneo, M., Li, L. & Meilleur, F. (2016). *J. Phys. Conf. Ser.* **746**, 012008.
Zhao, J. K., Robertson, L., Herwig, K. & Crabb, D. (2013). *Phys. Procedia*, **42**, 39–45.
Zimmermann, K., Eells, R., Heinrich, F., Rintoul, S., Josey, B., Shekhar, P., Lösche, M. & Stern, L. J. (2017). *J. Biol. Chem.* **292**, 17746–17759.